MULTISCALE STUDY OF THE INTERACTIONS BETWEEN CLIMATE, LAND USE, AND AGRICULTURAL PRODUCTIVITY IN WESTERN SAHEL: A CASE STUDY OF CHAD

A THESIS IN

Environmental and Urban Geosciences

Presented to the Faculty of the University
Of Missouri – Kansas City in partial fulfillment of
The requirements for the degree

MASTER OF SCIENCE

BY

KIM-NDOR DJIMADOUMNGAR

Specialized Master in Computer & Geomatics, International Institute for Water and Environmental Engineering, 2007, Ouagadougou - Burkina Faso

Kansas City, Missouri
2014

MULTISCALE STUDY OF THE INTERACTIONS BETWEEN CLIMATE, LAND USE, AND AGRICULTURAL PRODUCTIVITY IN WESTERN SAHEL: A CASE STUDY OF CHAD

KIM-NDOR DJIMADOUMNGAR, Candidate for the Master of Science Degree

University Of Missouri – Kansas City, 2014

ABSTRACT

This study employed an integrated approach to investigate drivers and impacts of environmental change from the 1980s to 2012 using geospatial and statistical analyses of atmospheric, climate, land use land cover, and socio-economic data.

The atmospheric and climate data were obtained from the NASA Giovanni web-portal (GES DISC) for area covering all of Southern Chad and extending to the neighboring countries of Cameroon, Central African Republic, Niger, Nigeria, and Sudan. The geographic coordinates of that area are: North 14.403, West 10.815, East 24.219, and South 7.328. Agricultural productivity country summary data for Chad was obtained from the Food and Agriculture Organization (FAO) of the United Nations. Other data sets, including the Landsat imagery used for deriving land use and land cover information focusing on the transition areas between desert in the Northern Chad and Sahel/Savanna areas to the South. These transition areas are ecologically sensitive and especially vulnerable to changes in climate variables.

The geostatistical analyses revealed gradients of precipitation, soil moisture, and NDVI that are positively highly correlated with each other and negatively correlated with the

temperature. Cloud fraction amounts, specific humidity, aerosol optical depth, soil moisture, and NDVI values are higher in wetter years than in dryer years; in contrary, wind speeds and surface air temperature are lower during wetter years.

The land use land cover analysis of the lake Fitri region shows that the areas covered by natural vegetation such as forest, savanna, and steppe has been decreasing since 1986. Alongside, farm and grasslands have been increasing during that same period of time.

In multiple linear regression analysis, it has been shown a positive correlation between precipitation and crops such as sorghum (0.53), maize (0.5), and rice paddy (0.54) and livestock such as sheep (0.43), goat (0.5), and cattle (0.40). But these correlations are higher with population than with precipitation.

Keywords: Multiscale, Climate, Variability, Land use Land cover, Agricultural Productivity, Chad**.**

APPROVAL PAGE

The faculty listed below, appointed by the Dean of the College of Arts and Sciences have examined a thesis titled "Multiscale Study of the Interactions between Climate, Land Use, and Agricultural Productivity in Western Sahel: A Case Study of Chad," presented by Kim-Ndor Djimadoumngar, candidate for the Master of Science degree, and certify that in their opinion it is worthy of acceptance.

Supervisory Committee

Jimmy O. Adegoke, Ph.D., Committee Chair
Department of Geosciences

Jejung Lee, Ph.D.
Department of Geosciences

Wei Ji, Ph.D.
Department of Geosciences

CONTENTS

ABSTRACT iii

LIST OF ILLUSTRATIONS x

LIST OF TABLES xiii

ACKNOWLEDGEMENTS xvii

Chapter

1. OVERVIEW 1

1.1 Climate – Land Use-Land Cover Interactions 2

1.2. Climate – Water Interactions 4

1.3. Socio-economic Consequences of Climate Change 5

1.4. Problem Statement and Objectives 6

1.5. Definition of the Study Area 7

2. LITERATURE REVIEW 9

2.1. Background of the Meteorology of West Africa 9

2.1.1. Rain Producing Systems and the Intertropical Convergence Zone (ITCZ) 9

2.1.2 West African Monsoon 11

2.1.3. Rainfall over West Africa and Seasonal Forecasting 14

2.1.4. Factors Influencing Rainfall Variability in the Sahel 17

2.2. Climate and Socio-economic Impacts 23

3. DATA AND METHODOLOGY 28

3.1.Data 29

3.1.1. Climate Data 29

3.1.2. Land Use Land Cover Data 31

3.1.3. Socio-economic Data 32

3.2. Data Sources and Platforms 32

3.2.1. Giovanni (GES-DISC) 32

3.2.2. Global Visualization (GloVis) Viewer 33

3.2.3. FAOSTAT 34

3.2.4. Global Historical Climatology Network (GHCN) 34

3.3. Software Platforms 35

3.3.1. Erdas Imagine 2013 35

3.3.2. ArcGIS 10.1 37

3.3.3. IBM SPSS 21 38

3.4. Analytical Methods 40

3.4.1. Climate Data Analytical Method 40

3.4.2. Land Use Land Cover Data Analytical Method 42

3.4.3. Socio-economic Data Analytical Method 45

4. DATA ANALYSIS AND RESULTS 49

4.1. Atmospheric Parameters 49
4.1.1. GPCP 50
4.1.2. Aerosol Optical Depth 65
4.1.3. Surface Air Temperature 67
4.2. Land Parameters 74
4.2.1. Evapotranspiration 76
4.2.2. Soil Moisture 78
4.2.3. Normalized Difference Vegetation Index, NDVI. 81
4.3. Atmospheric - Land Parameters Correlation 87
4.4. Land Use Land Cover Analysis: Case Study of Lake Fitri 88
4.4.1. Land Use Land Cover Analysis 1986 – 2003 89
4.4.2. Land Use Land Cover Analysis 2003 – 2013 91
4.4.3. Land Use Land Cover Rate of Change 98
4.5. Socio-Economic Data Evolution 99
4.5.1. Population and Agricultural Land Trends 99
4.5.2. Agricultural Production 100
4.5.3. Commercial and Industrial Production 100
4.5.4. Livestock 102
4. 6. Socio-economic Data Multiple Linear Regression Analysis 103

4.6.1. Cereals Multiple Linear Regression Analysis 103

4.6.2. Commercial and Industrial Crops Multiple Linear Regression Analysis 105

4.6.3. Livestock Multiple Linear Regression Analysis 107

5. DISCUSSION 110

5.1 Atmospheric Parameters 110

5.2. Land Parameters 114

5.2.1. Land Use Land Cover Analysis and Trends 116

5.3. Socio-economic Data 117

5.4. Multiple Linear Regression Analysis 118

5.4.1. Cereals Multiple Linear Regression Analysis 119

5.4.2. Commercial and Industrial Crops Multiple Linear Regression Analysis 119

5.4.3. Livestock Multiple Linear Regression Analysis 120

6. CONCLUSION 122

ANNEXES: Accuracy Assessment Tables 126

A. Accuracy Assessment 1986 126

B. Accuracy Assessment 2003 126

C. Accuracy Assessment 2013 126

REFERENCES 127

VITA ..... **Error! Bookmark not defined.**

LIST OF ILLUSTRATIONS

Figure Page

Figure 1. Area of Study Map 8

Figure 2. Picture of the West African Monsoon 14

Figure 3. Flow Diagram of the Research Protocol 28

Figure 4. Research Design Data Flow Diagram 40

Figure 5. Climate Data Processing Flow Chart Diagram 42

Figure 6. LULC Data Processing Flow Chart Diagram 45

Figure 7. Socio-economic Data Processing Flow Chart Diagram 48

Figure 8. Atmospheric Parameters Graph from 2003 to 2012 50

Figure 9. Global Precipitation and Anomaly Trends from 1980 to 2012 51

Figure 10. Global Precipitation Annual Cycle from 1980 to 2012 52

Figure 11. Global Precipitation Distribution Map 53

Figure 12. Weather Stations Locations maps 54

Figure 13. Monthly Rainfall in Weather Stations 55

Figure 14. Global Precipitation Wetter and Dryer Years Graph 55

Figure 15. Cloud Fraction - Precipitation Annual Cycle 56

Figure 16. Cloud Fraction Composite Analysis Graph 57

Figure 17. V250 & U250 Winds Composite Analysis Graphs 60

Figure 18. V850 & U850 Winds Composite Analysis Graphs 61

Figure 19. 500 & 850 Specific Humidity – Precipitation Trends 1980 to 2012 63

Figure 20. Specific Humidity Composite Analysis Graph 64
Figure 21. Aerosol Optical Depth Distribution Map 65
Figure 22. Cloud Fraction - Aerosol Optical Depth Trend 66
Figure 23. Aerosol Optical Depth Composite Analysis 67
Figure 24. Surface Air Temperature Mean (2003-2012) 68
Figure 25. Surface Air Temperature Annual Cycle (2003-2012) 69
Figure 26. Surface Air Temperature Distribution Map 70
Figure 27. Surface Air Temperature Composite Analysis 71
Figure 28. Soil Moisture – Precipitation Trend 75
Figure 29. Land Parameters Annual Cycle 75
Figure 30. Total Evapotranspiration Distribution Map 76
Figure 31. Total Evapotranspiration Composite Analysis Graph 77
Figure 32. Soil Moisture Distribution Graph 79
Figure 33. Soil Moisture Composite Analysis graph 80
Figure 34. NDVI Distribution Maps 83
Figure 35. NDVI Composite Analysis Location Map 84
Figure 36. Dryer and Wetter NDVIs in the Center 84
Figure 37. Dryer and Wetter NDVIs in the South 85
Figure 38. Land Use Land Cover in 1986 90
Figure 39. Land Use Land Cover in 2003 91
Figure 40. Land Use Land Cover in 2013 92
Figure 41. Water Bodies Changes 93
Figure 42. Wetland Changes 94
Figure 43. Forest-Savanna-Steppe Changes 95

Figure 44. Grassland-Farmland Changes 96
Figure 45. Bare Soils Changes 97
Figure 46. Population and Agricultural Area Trend Graph 99
Figure 47. Cereals – Precipitation Trend Graph 100
Figure 48. Commercial and Industrial Crops – Precipitation Trend Graph 101
Figure 49. Livestock – Precipitation Trend Graph 102

LIST OF TABLES

Table		Page
1.	Cloud Fractions Percent Change from Dryer to Wetter Years	58
2.	Q500 & Q850 Composite Analysis Percent Change	64
3.	AOD Composite Analysis Values and Percent Change	67
4.	Surface Air Temperature Composite Analysis Values and Percent Change	71
5.	Total Evapotranspiration Percent change	78
6.	Soil Moisture Composite Analysis Values and Percent Change	80
7.	NDVI Composite Percent Change in Center and South	86
8.	NDVI Composite Analysis Center Vs South	86
9.	Atmospheric and Land parameters Correlations	88
10.	Land Use Land Cover Change from 1986 to 2003	89
11.	Land Use Land Cover Change from 2003 to 2013	92
12.	Land Use Land Cover Rate of Change	98
13.	Predictive variables Tolerance and VIF Table	103
14.	Cereals' Statistical Characteristics	105
15.	Commercial and Industrial Crops' Statistical Characteristics	107
16.	Livestock's Statistical Characteristics	109

LIST OF ABBREVIATIONS

ABL	Atmospheric Boundary Layer
AEJ	African Easterly Jet
AOD	Aerosol Optical Depth
ASCII	American Standard Code for Information Interchange
ASTER	Advanced Space-borne Thermal Emission and Reflection Radiometer
AT	Air Temperature
AVHRR	Advanced Very High Resolution Radiometer
AWJ	African Westerly Jet
CCN	Cloud Condensation Nuclei
CO2	Carbon dioxide
DKRZ	Deutshes Klimarechenzentrum - German Center of Climatic Computations
DO	Dissolved Oxygen
EC	Electrical Conductivity
EROS	Earth Resources Observation and Science
ET	Total Evapotranspiration
ETM+	Thematic Mapper Plus
FAO	Food and Agriculture Organization of the United Nations
FAOSTAT	FAO Statistics
GCM	General Circulation Model
GDP	Gross Domestic Product
GES	DISC Goddard Earth Sciences Data and Information Services Center

GHGs	Greenhouse Gases
GLM	General Linear Models
GloVis	Global Visualization
GPCP	Global Precipitation Climatology Project
GWT	Groundwater Temperature
hPa	Hectopascal
IBM SPSS	International Business Machine – Statistical Package for the Social Sciences
IPCC	Intergovernmental Panel on Climate Change
ITCZ	Intertropical Convergence Zone
ITF	Intertropical Front
JAS	July-August-September
LCC	Land Cover Changes
LULC	Land Use land Cover
MLR	Multiple Linear Regression
MODIS	Moderate Resolution Imaging Spectroradiometer
MRLC	Multi-Resolution Land Characteristics
MSS	Multispectral Scanner
NDVI	Normalized Difference Vegetation Index
NIR	Near Infrared
NSSA	Non-sub-Saharan Africa developing countries
OLI_TIRS	OLI (Operational Land Imager) and TIRS (Thermal Infrared Sensor)
PRD	Population Reference Bureau
RA	Rainfall Amount

SAT	Surface Air Temperature
SD	Standard Deviation
SPOT	Satellite Pour l'Observation de la Terre
SSA	Sub-Saharan Africa
SWL	Static Water Level
TDS	Total Dissolved Solids
TEJ	Tropical Easterly Jet
TM	Thematic Mapper
UMKC	University of Missouri – Kansas City
UNDP	United Nations Development Programme
UNEP	United Nations Environmental Programme
UNFCCC	United Nations Framework Convention on Climate Change
USGS	United States Geological Survey
VIF	Variance Inflexion Factor
VIS	Visible
VPMs	Vegetation Phonological Metrics

ACKNOWLEDGEMENTS

I owe my most heartfelt gratitude to a lot of institutions and people for their contributions to my beginning and accomplishing this study.

First, I express my sincere and cordial gratitude to the Institute of International Education through the Fulbright Program for its financial support, and to the Department of Geosciences (UMKC) for accepting my application.

I am especially thankful to Dr. Jimmy Adegoke, my Academic Advisor and Chair of my Master Degree Thesis Committee, Dr. Jejung Lee and Dr. Wei Ji for their tireless guidance, advice encouragement, and multiform supports. Their helpful and endless comments, support, and pragmatic suggestions have led to the successful fulfillment of this work.

I also express my deep and heartfelt thanks to all the Department of Geosciences Faculty especially Dr. Raymond Coveney, Dr. James Murowchick, and Dr. Tina Niemi for their fruitful encouragement and advice.

Finally, my thanks go to all of the Department of Geosciences Staff and fellow students for their multiform and considerable assistance.

DEDICATION

"My soul proclaims the greatness of the Lord and my spirit rejoices in God my Savior; because he has looked upon the humiliation of his servant." Luke 46 – 48.

Thank you Blessed Virgin Mary for your intercessions and actions in my life.

CHAPTER 1

OVERVIEW

According to IPCC (2007), the world's environment has been influenced by climate change, compositions of greenhouse gases (GHGs) and land use. Environmental change and human disturbances have altered global and regional water cycles in many parts of the world. Globally, there is an overall net negative impact of climate change on water resources and freshwater ecosystems (Kundzewicz et al., 2007). Oki and Kanae (2006) indicated that the impacts of climate change on water resources and their integrated management and sustainable usage are critical because of the importance of water for sustaining livelihoods and almost all human being activities. GHGs Emissions and human activities such as population change, life style, economy and food demand are some of the many pressures applied on water systems.

Compared to many other regions of the world, Africa is particularly vulnerable to the effects of climate change and variability. Widespread poverty, an extensive disease burden, and pockets of political instability across the continent have resulted in a low resilience and limited adaptive capacity of many African societies to climate related shocks and stresses (Williams & Kniveton, 2011). According to the United Nations Framework Convention on Climate Change (UNFCCC), documented decreases in annual rainfall and increases in frequency and intensity of extreme events are worsening food insecurity and increasing water stress for many countries in Africa. These events can lead to famine and widespread disruption of socio-economic well-being; for instance, one third of African people already live in drought-prone areas and 220 million are exposed to drought each year.

Several recent studies on interactions between land use, water, and climate change have been conducted throughout the world, with many focusing on Africa. Some of the more pertinent studies are highlighted in the sections below.

1.1 Climate – Land Use-Land Cover Interactions

Conversion of natural ecosystems to other uses can have a strong effect on GHG emissions and albedo, and thus, climate change. Weather and climate can be dramatically altered by slight changes in atmospheric conditions (Pielke et al., 1998), such as those associated with particular land use practices and patterns.

Land use and land cover interact with atmospheric conditions to determine current climate conditions, as well as, the impact of climate change and environmental variability on ecological systems. Such interactions are ubiquitous. LULC has the potential to compound, confound, or even contradict changes expected from GHG induced climate change alone. These properties give LULC the possibility to be considered as powerful tools capable of modifying local climate conditions and significantly contributing to the net global impact of climate change. Management practices based modifications of LULC patterns and processes could be applied strategically to increase the resilience of vulnerable ecological systems and facilitate climate adaptation (Pyke & Andelman, 2007).

Land cover and land cover changes (LCC) affect the moisture and temperature states as well as the composition of the atmospheric boundary layer (ABL). The often-unpleasant conditions in cities during the summer are some of the most obvious examples of how land use which is the realization of the actual land-cover affects local weather and climate. Land cover only affects the local atmospheric conditions, but it also is itself affected by local weather and depends on the local climate. Consequently, land cover may change naturally in

response to extreme weather events causing wildfires, lasting flooding, or multiple-year droughts. Land cover changes in response to climate include rising sea-levels, invasion of non-native plants and shifts in ecosystem boundaries (Molders, 2012).

A study focusing on the Sahel, (Taylor, Lambin, Stephenne, Harding., & Essery, 2002), used a general circulation model (GCM) to show the impact of changes in vegetation on rainfall. Their hypothesis was that recent changes in land use were strong enough to provoke the observed drought. The land use model used generated realistic maps of vegetation changes linked to land use. Their findings indicated that cropland coverage in the Sahel had risen from 5% to 14% in the 35 years prior to 1996. It was estimated that this process of agricultural intensification, coupled with deforestation and other land use changes, translated to a conversion of 4% of the land from tree to bare soil over that period. They concluded that the impact of land use on rainfall is likely to increase.

Similarly, Lambin, Geist, and Lepers (2003) studied the dynamics of land use and land cover change in tropical regions. Their work was based on summarizing recent estimates on changes in cropland, agricultural intensification, tropical deforestation, pasture expansion, and urbanization, and identifying the still unmeasured land cover changes. They found that climate-driven land cover modifications interact with land use changes. Land use change is shown to be driven by synergic factor combinations of resource scarcity leading to an increase in the pressure of production on resources, changing opportunities created by markets, outside policy intervention, loss of adaptive capacity, and changes in social organization and attitudes. They concluded that a systematic analysis of local-scale land use change studies, conducted over a range of timescales, helps uncover general principles that provide an explanation and prediction of new land use changes.

1.2. Climate – Water Interactions

Mercier, Cazenave, and Maheu (2002) studied African lake level variations by using a satellite altimetry technique. They concluded that water level fluctuations of continental lakes are related to regional and global scale climate changes. In fact, among the twelve African lakes presented in their study, nine were sensitive indicators of the climate evolution over Africa during the 1990s. Clear correlated regional variations were reported among African lakes; several exhibited a regular level decrease between 1993 and 1997, probably due to intense drought. Their study also showed that some African lakes can constitute sensitive proxies to remote large scale climate perturbation inside and above the Indian Ocean.

The relationship between some groundwater physical properties and climate variability indicators using statistical methods has also been used to assess the impact of climate variability on the quantity and quality of groundwater in Nigeria (Edet, Ukpong, & Ekwere, 2011). Their findings showed that irrespective to the geologic units and seasons, the static water level (SWL), groundwater temperature (GWT), pH and dissolved oxygen (DO) had been in stable state conditions based on low standard deviation (SD) values. They also found that the amount of rainfall (RA) and air temperature (AT) had showed significant correlation with the SWL, GWT, pH, electrical conductivity (EC), and total dissolved solids (TDS). They concluded that the fluctuations observed in groundwater properties (SWL, GWT) were attributed to the amount of rainfall and temperature. Likewise, Ojo, Oni, and Ogunkunle (2003) used climatic index method to investigate the implications of climate change on water resource availability and management, groundwater variations; rainfall trends, river flows and discharges, and climatic events like droughts and floods in West Africa. Their findings showed that significant spatial and temporal variations occur regionally and locally, but

generally there had been downward trends in rainfall and increases in water deficit and drought events.

Haas, Bartholome, Lambin,, & Vanacker (2011) studied the relationship between remotely sensed data and changes in eco-hydrological processes in sub-Saharan West Africa by analyzing time series of remotely sensed vegetation (SPOT Vegetation) cover, rainfall and surface water for the period extending from 1999 to 2008. Their findings suggested that vegetation cover is positively correlated to the amount of available surface water for catchment mainly covered by annual plants. The observed relationships between remotely sensed variables allow developing ecological indicators that can indicate short-term changes in arid and semi-arid ecosystems from local to regional scales.

1.3. Socio-economic Consequences of Climate Change

During the last 4 million years, the tropical African climate has oscillated between markedly wetter and drier conditions. These changes occurred on an all time scale; high-amplitude climate changes induced biome shifts, species migrations, community reorganizations, and changes in water resources of great importance for human beings. Recently, catastrophic rainfall events in equatorial East Africa, the drastic Sahel drought in the 1970s-1980s, and -rapid lake-level fluctuations illustrated the large inter-annual-/decadal rainfall variability and its serious impacts on societies (Gasse, 2005).

Conway and Schipper (2011) assessed the risks associated with future climate changes in Ethiopia and identified low-regret actions for their incorporation within development practice and policy. They examined the changing nature of climate risks using analysis of recent climate variability, future climate scenarios and their secondary impacts. They also assessed the effects of climate variability on agriculture production and national gross domestic

product (GDP) and identified entry points and knowledge gaps in relation to mainstreaming climate risks in Ethiopia using the Government's plan for poverty reduction. Their results suggested that rainfall dependent activities and sectors should consider, at very least, recent variability (last 20-30 years) as a guide to planning and resource management. Where long-term decisions are involved (such as for water infrastructure), they recommended considering a greater range of variability.

Such an approach could be complemented by using recent rainfall trends related with large-scale factors that might be associated with anthropogenic climate change and could therefore be extrapolated to inform climate risk assessments.

1.4. Problem Statement and Objectives

Despite the fact that a lot of studies on global environmental change and its consequences have been done in Africa, many questions remain unresolved. In particular, we do not yet fully understand how regional scale processes link to the local impact on water resources availability and related activities like agriculture, livestock, and human well-being. This study is therefore focused on interactions between climate variability, land use and agricultural productivity in at sub-regional and subnational levels over a forty-year period (1980-2012) using observational, satellite, and model-output data.

The general objective of the study is the evaluation of cross-scale impacts of environmental change indicators in West Sahel with an emphasis on southern Chad.

Specifically, the objectives of this study include the following:

1. To understand changes in key atmospheric and land surface parameters associated with environmental conditions in the study area from 1980s to 2010s;

2. To analyze land use changes within the study area using multi-temporal Landsat satellite data of Lake Fitri.
3. To investigate linkages between agricultural productivity, land use, and climate variability in Southern Chad from 1980 to 2012 using geostatistical methods.

1.5. Definition of the Study Area

There are three spatial scales used for the present study:

- The first, focusing on atmospheric and land parameters includes the whole southern Chad, extending to northeast Nigeria, center - east Niger, northeast Cameroun, and north Central African Republic. The area of interest geographic coordinates are: North 14.403, West 10.815, East 24.219, and South 7.328. This is the shaded area shown in figure 1.
- The second, mainly socio-economic, focuses on southern Chad. It describes the relationships between population, precipitation, and agricultural production
- The third, on land use and land cover changes, focuses on the transition zone between the desert and the Sahel/savanna zone with the particular emphasis on the Lake Fitri area.

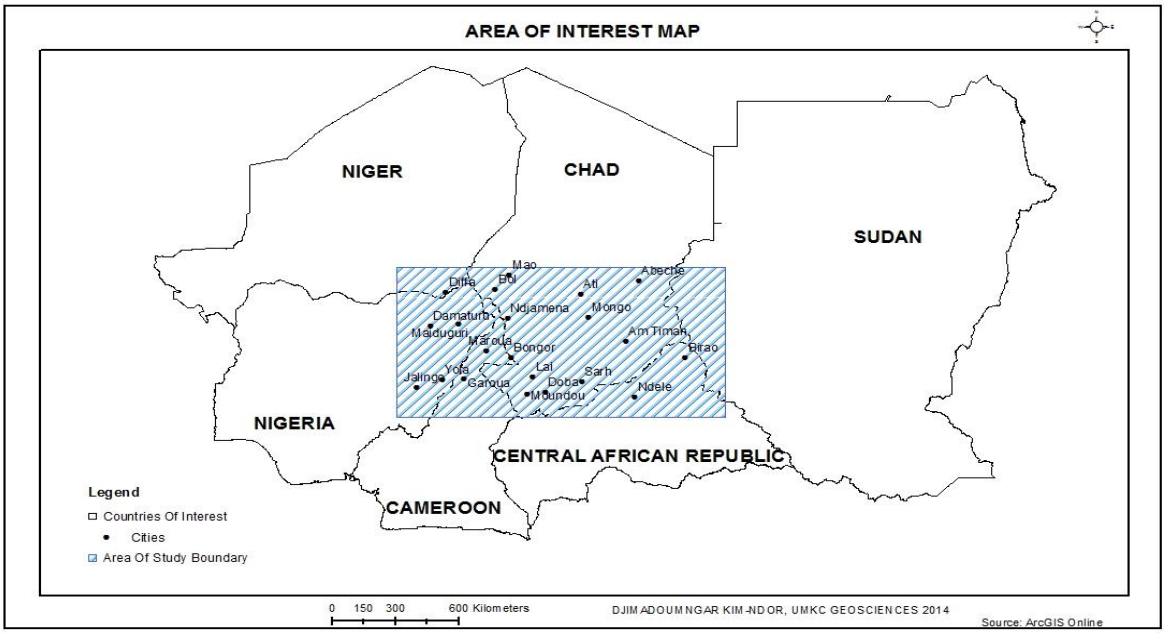

Figure 1. Area of Study Map

CHAPTER 2

LITERATURE REVIEW

2.1. Background of the Meteorology of West Africa

2.1.1. Rain Producing Systems and the Intertropical Convergence Zone (ITCZ)

The West African Sahel region is a semi-arid expanse of grassland, shrubs, and small, thorny trees lying just to the south of the Sahara desert. The term is often applied to the general region extending some 5000 km across the east-west extent of Africa and from the Sahara to the humid savanna at approximately 10^0 North. More properly, 'Sahel' applies to a smaller region between the latitudes of around 14^0 N and 18^0 N and includes the countries such as Mauritania, Senegal, Mali, Niger, Chad, the Sudan, and the northern fringes of Burkina Faso and Nigeria. Mean annual rainfall in the Sahel is one of the order of 100 to 200 mm in the north, towards the desert, and 500 to 600 mm in the south. Rainfall is generally limited to the boreal summer months, with maximum rainfall occurring in August. The rainy season length ranges from 1 to 2 months in the north and 4 to 5 months in the south. Occasional winter rains of extra-tropical origin can occur with less than 25 mm of rainfall. Within the region there is a strong east-west uniformity of climate and vegetation conditions of which the Sahel region is often considered as one entity in the meteorological context (Nicholson, 2013).

The Intertropical Convergence Zone (ITCZ) is a fundamental feature of the atmospheric circulation over West Africa. It separates the wedge of warm, moist, southwesterly, monsoon flow off the tropical Atlantic from much hotter and very dry northeasterly winds from the Sahara Desert (Lele & Lamb, 2010). The classical definition of the Intertropical Convergence

Zone is the convergence of the trade winds of the two hemispheres. This zone is characterized by low pressure, rising motion, clouds, and precipitation. From the global atmosphere point of view, the ITCZ forms the ascending branch of the Hadley circulation. The point of view is oversimplified regionally, especially over the land. Over West Africa, the prevailing image of the ITCZ is based on an outdated 1950s model and is erroneous. There is need to distinguish between ITCZ as the zone of convergence and the feature "Tropical Rainbelt". So, the term ITCZ itself is ambiguous for it sometimes refers to a surface wind and sometimes to the zone of maximum precipitation (Nicholson, 2009; Sultan & Janicot, 2000; Sultan, Janicot, & Diedhiou, 2003; Zhang, Woodworth, & Gu, 2006).

The ITCZ over Africa is conceptualized as a band of rainfall that "follows the sun", advancing into the northern hemisphere in boreal summer and retreating into the southern hemisphere in austral summer. The length of rainy season is equivalent to the length of ITCZ's influence and maximum precipitation occurs with its passage. A zone of wind convergence develops where the southwest "monsoon" flows into the center of the Saharan heat low and meets the dry desert air. A marked discontinuity in temperature and dew point also occurs at the point of convergence.

This classical picture shows the ITCZ sloping toward the equator with height, so that the depth of the moist layer rapidly increases equatorward. Accordingly, convergence and uplift occur all along this zone, but strong precipitation occurs only where the moist layer is sufficiently thick to support deep clouds and convection. This puts the cloudiness and precipitation maxima well equator ward of the surface convergence in contrast to the idealized "classical" picture of ITCZ in which they coincide (Nicholson, 2009).

The classical picture of the ITCZ has some weakness. The surface patterns do fit. The meridional (north – south) component of the wind converge at the latitude of the Saharan heat low. This surface convergence is the true ITCZ over Africa. However, it extends well to the east of the Saharan heat low so that the two are not synonymous. The convergence also marks the transition in the zonal winds from the easterly flow of the Harmattan to the westerly flow of the low-level monsoon. Relative humidity, specific humidity, and dew point at the surface increase rapidly equatorward from the surface position of the ITCZ. In contrast, the situation aloft gives a very different structure. Notable difference includes the depth of the moist layer, the role of the upper-level flow in producing the structure of the monsoon layer, and the relationship between the surface convergence and the rainfall maximum (Nicholson, 2009; Peyrille Lafore, & Redelsperger, 2007; Thorncroft, Nguyen, Zhang, & Peyrille, 2011).

An important point of the new picture of the ITCZ over West Africa is that ITCZ is dissociated from the main region of precipitation. A region of moderate subsidence separates the cell of ascent linked to the ITCZ from the cell associated with the maximum rainfall. In contrast, the ascent linked to the tropical rainbelt is coupled with low-level ascent near the coast, suggesting that the Mesoscale processes associated with the sea-breeze circulation have some influence on the larger-scale dynamics and rainfall formation (Nicholson, 2009).

2.1.2 West African Monsoon

The southwesterly monsoon flow is associated with the equatorial crossing of the southeast trade winds that arise on the equatorward flank of the subtropical high. So, the monsoon flow is distinguished by a clear southerly component. The vertical cross-section of the meridional winds suggests that the monsoon flow is confined to the lowest levels of the

troposphere. The southerly component decreases rapidly above 900 hPa, generally disappearing by 850 hPa. In opposition, the westerly component of the flow has a maximum at 850 hPa, where the southerly component approaches zero. There, the westerly speed reaches 6 m/s in the long-term.

A key component of the monsoon flow (figure 2) is the African westerly jet (AWJ) with strongly developed core speeds at 850 hPa as high as 10 m/s. Its development appears to be controlled by the surface pressure gradient over the tropical Atlantic, as a strong cross-equatorial gradient is needed to produce inertial stability. There is a strong correlation between the surface pressure gradient within 20°N and 20°S and the speed of the jet. The weak gradients occurred without exception during the relatively dry years and the strong gradients occurred primary during the wet years. Thus the speed of the westerly jet is also well correlated with rainfall in the Sahel.

Other major components of the monsoon flow include the African easterly jet (AEJ) with its maximum near 600 hPa in the mid-troposphere and the Tropical easterly jet (TEJ), with its maximum near 150 hPa in the upper-troposphere (Laux, Kunstmann, & Bardossy, 2008; Nicholson, 2009; Sultan & Janicot, 2003; Thorncroft & Hodges, 2000).

The meridional winds associated with the AEJ and TEJ, together with the surface convergence zone, produce a divergence field that is considerably complex. At 650 hPa, near the AEJ level, the ITCZ convergence is replaced by weak divergence. This suggest a cell of meridional overturning extending from the surface ITCZ to the anti-cyclonic side of the AEJ in the mid-troposphere. Just to the south is weak convergence, centered near 5 - 10°N on the cyclonic side of the AEJ. At the TEJ level of the 150 hPa, the picture is reversed. Divergence prevails over West Africa from about 15 – 5°N, while convergence prevail near 15 – 25°N.

This suggests a second cell of meridional overturning that links the mid- and upper troposphere. Lying just to the south of the lower meridional cell, this cell extends from the cyclonic side of the AEJ to the anti-cyclonic poleward flank of the TEJ. The associated patterns of convergence and divergence are evident in the meridional flow fields associated with these jets (Nicholson, 2009).

The most striking feature is the deep core of moist air extending from the surface to the upper troposphere and centered at about 8 – 10°N. In this core relative humidity is more than 60% all over the troposphere; it is less than 40% over the Sahara and most of the southern Africa. This core coincides with the region of strong ascent lying between the axes of the AEJ and TEJ and the very humid air is essentially limited to the region of ascent.

The specific humidity shows that the actual amount of vapor in the atmosphere is relatively constant with latitude between about 5 and 18°N. So, the moisture convergence essentially reflect the winds convergence. The relatively small moisture gradients seem counter-intuitive, in view of the strong precipitation gradient in the region. This implies that atmospheric dynamics rather than low-level moisture control the precipitation regime over West Africa. Specific humidity decreases quickly to the north, closer to the Sahara and gradually equatorward, in progressing from the continent to the ocean. This suggest that much of the moisture in the monsoon layer is recycled water deriving from local evaporation over the continent, rather than transport from Atlantic (Nicholson, 2009).

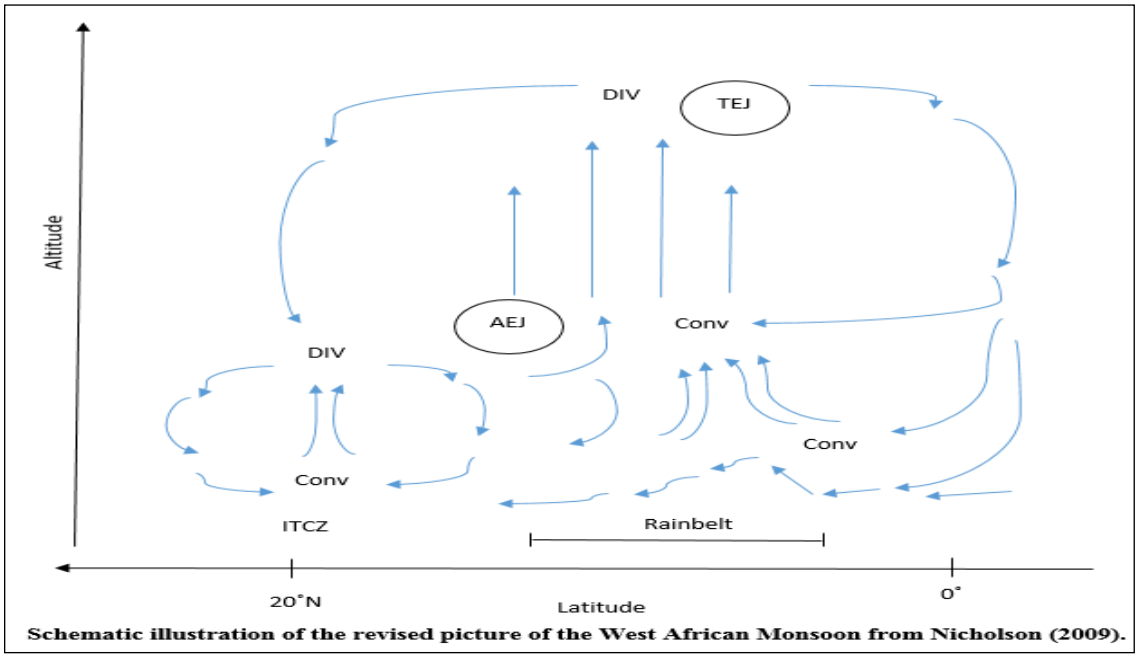

Figure 2. Picture of the West African Monsoon

2.1.3. Rainfall over West Africa and Seasonal Forecasting

The primary rain-producing mechanism is the strong core of ascent lying between the axes of the AEJ and TEJ. This controls the large-scale tropical rainbelt in the boreal summer. It produces rainfall in the central and southern Sahel (15 – 10^0N) where rainfall is associated with easterly wave disturbances. In years when the ascent is displaced equatorward, it also produces rainfall in the coast region of West Africa (10 - 5^0N). Ascent is also associated with the band of convergence where the southwesterly winds meet the land. Presumably, the intensity of this convergence has some influence on the intensity of the ascent within the tropical rainbelt and hence on precipitation in much of West Africa. This would suggest that characteristics of the southwesterly African Monsoon flow, such as its speed, depth and compass direction, influence rainfall over West Africa in the boreal summer. Clearly, the

bulk of precipitation is linked to the AEJ and TEJ and to the wave disturbances associated with them (Lebel, Diedhiou, & Laurent, 2003; Nicholson, 2009; Ventrice, Thorncroft, & Roundy, 2011).

The characteristics of the moisture field are the following:

- A flat meridional moisture gradient over the continent between the Atlantic and the Sahara
- More moisture at low levels over the continents than over the Atlantic, and
- A moisture convergence field that is dominated by the wind field.

The implications of these characteristics are that the moisture from the Atlantic may play a lesser role during the summer 'monsoon' than evaporated over the continent itself. In the context of the role of moisture, it is interesting to note that the vapor content can higher in wet years than in dryer years, even those contrasting in the intensity of the rainbelt (Nicholson, 2009).

During the 1970s and 1980s, the Sahel, a semiarid savanna between the Sahara Desert and the Guinea moist savanna experienced severe droughts. The droughts had devastating consequences for this ecologically vulnerable transition region. Since the mid-1980s, however, rainfall and vegetation has largely recovered. The driving forces of the climate variations and the droughts are not fully understood. The views range from those blaming human caused land degradation driven by overgrazing and deforestation as the underlying forces, to those emphasizing a global system driven by annual to decadal changes in sea surface temperatures. The future of the Sahel ecosystem and the livelihoods of the farmers and herders depend on both the climate and the ecosystem services that can be sustained by the soil and vegetation (UNEP, 2012).

The Sahel is a mainly flat savanna and grassland region with a few scattered plateaus and mountain ranges. Sahel's vegetation boundaries are largely defined by annual rainfall, from approximately 100 mm in the north to 1000 mm in the south. The more rainy southern parts have a denser tree cover that continuously decreases towards the drier north. The climate of the Sahel is warm and arid, with a short summer monsoon lasting two to four months. The annual rainfall cycle is a result of the interplay between Harmattan trade winds blowing from the Sahara in the north and moist monsoon trade winds blowing from the Atlantic in the west and south of the Sahel. The monsoon winds give off their moisture as rainfall when traveling north, hence, creating the rainfall gradient typical for the Sahel. During summer in the northern hemisphere, the tropical rainbelt reaches 10˚N, attracting moist winds from the Atlantic Ocean that move north into the Sahel. Further south, the oscillating rain belt passes twice a year, when the sun migrates northwards in spring and southwards in autumn (UNEP, 2012).

According to McSweeney, New, and Lizcano (2010), in Chad, the desert regions obtain a very small quantity of rainfall. The southern and tropical regions obtain about 150 – 300 mm/month of rainfall between May and October whereas the subtropical regions in the central receive 50 – 150 mm/month from June to September. There is almost no rainfall in the country from November to March. These seasonal rainfalls are controlled by the ITCZ, which oscillated between the Tropic of Capricorn and Cancer over the course of the year). In addition, Funk, Rowland, Adoum, Eilerts, & White (2012) wrote that annual rainfall totals in Chad vary from 1000 mm in the south to 300 mm at the northern limit of the agricultural zone. Significant decreases in rainfall and increases in air temperature across Chad, especially in the eastern part of the country have been identified.

2.1.4. Factors Influencing Rainfall Variability in the Sahel

Aerosols: Aerosol in the Sahel is mainly atmospheric dust from the Sahara. The dust is one of the factors contributing to the regulation of both global climate variations and the regional climate over West Africa. The Sahara Desert exports between one third and one half of the total global atmospheric dust transport. The dust particles reflect incoming solar radiation and cool the earth during the daytime. The dust also helps form small water droplets, so clouds form faster, further increasing reflection of solar radiation from the clouds; and the dust acts as a blanket keeping the surface warm during the night. Increased dust production in the 1970s and 1980s, was a consequence of the reduction in vegetation and more exposed soils, and probably worsened droughts by decreasing rainfall. On the other hand, dust export from the Sahel is important for fertilizing not only the Sahel with minerals and nutrients, but also the Atlantic Ocean as well as other land masses around the globe, including the Amazon rainforest (UNEP, 2012).

Yang et al. (2013) had simulated the transport and vertical distribution of smoke and dust aerosols over the northern sub-Saharan Africa in the Weather Research and Forecasting Model with Chemistry (WRF-Chem) at a height of 650 m. they found that between the equator and 10^0N, Saharan dust is often mixed with smoke near the surface, and their transport patterns manifest the interplay of trade winds, subtropical highs, precipitation associated with the ITCZ, and the high mountains located near the Great Rift Valley. At the 750 hPa and above, smoke layers extend more to the north and south and are often above the dust layers over the Sahel region. They also found that 5% of the Cloud-Aerosol Lidar data with Orthogonal Polarization (CALIP) measurements in February 2007-2011 showed aerosol

layers either above or between the clouds, reinforcing the importance of the aerosol vertical distribution for quantifying aerosol impact on climate in the Sahel region.

Aerosol Optical Depth (AOD) is the degree to which aerosols, very small suspended particles in the atmosphere like dust or soot, prevent the transmission of light. The AOD or optical thickness (T) is defined as the integrated extinction coefficient over a vertical column or unit cross section, where extinction refers to the extinction of light. AOD is a dimensionless – does not express real units of measurement, percentage, ratios, or negative natural logarithms – quantity, expressing the negative logarithm of the fraction of radiation (for instance, light) that is not scattered or absorbed on a path. AOD is calculated by measuring light absorption at specific wavelengths of the visible spectrum. For the most widely used AOD data product, the absorption at 550 nanometers is preferred for measurement because, in the visible spectrum, humans perceive a light wavelength measuring 550 nanometers as a shade of green. High AOD indicates a large quantity of aerosols, and consequently a huge amount of absorption and scattering of radiation (light). Low AOD indicates clearer air with fewer aerosols and increased transmission of radiation. Increasing aerosol concentrations can thus affect global temperature and the radiation balance of the globe by reducing the amount of radiation reaching the earth's surface, which then result in lower air temperatures (GES DISC, 2013).

According to Washington et al. (2009), the Bodele Depression in Chad is distinguished as the largest single source of mineral dust on the planet. It produces about half of the Sahara's mineral aerosol loading. Mineral dust plays a key role in modifying climate through interaction with clouds physics and radiative heating. It is also involved in numerous biophysical feedbacks both on the oceans and land. With expected changes in future

atmospheric circulation in response to increasing greenhouse gas concentrations, changes to deflation in the Bodele may impose critical changes on the behavior of the Earth system in response to the role that dust plays in the biosphere and the sheer quantity emitted from this key region.

Okonkwo and Demoz (2014), studying the spatial characteristic of the anthropogenic footprint in the Lake Chad Basin, mentioned that its contribution to the changes in atmospheric dynamics – that control the rainfall – as well as through changes in land, surface, and ground water extraction related to a growing population demand can be addressed. They also cited farming practices and biomass burning among key points to be fully considered.

Atmospheric Temperature: Temperature is a fundamental variable in climate, affected by all the absorptive and reflective properties of the earth's atmosphere, oceans, and land surfaces. The surface temperature is related to the amount of solar radiation a region receives, that in turn depends on both astronomical factors (determiner of seasons and longer climate cycles) and weather (clouds, atmospheric air movements, evaporation and precipitation, etc.) The surface temperature is also related to the average global temperature that is determined by the earth's radiative balance, as set by the absorptive and reflective properties of the atmosphere. A changing average global temperature may influence local weather processes in ways that make regional temperature trends more pronounced than average global temperature trends (GES DISC, 2013).

Wu, Chen, and Wen (2013) found a positive correlation over the tropical oceans and a negative correlation over the mid-latitude lands between precipitation and surface temperature in both observations and model simulation. The evaluation of the precipitation-

temperature correlation provides important information about the performance of the climate models in simulating the co-variability of precipitation and surface temperature. It also gives helpful information for potential problems and thus, direction of future improvement of on individual models.

An increase of surface temperatures induces a decrease of precipitation causing:

- Evaporation of light rain before reaching the ground;
- Evaporation of soil moisture, a provider of a source of water vapor to produce rain;

Changes in weather patterns causing air masses with water vapor content to be carried over a given area (GES DISC, 2013).

The temperature cycle follows the sun's migration, with adjustment for rainfall that tends to cool the surface as water evaporates. The warmest months are in early summer before the arrival of the monsoon rain (May). August is the hottest month in the northern part of the Sahel, with a cooler climate south of the solar zenith where moist soils also reduce temperatures. In November, the climate in the Sahel is cooler because the wet soils cause the air to cool. In the midst of the dry season (February), the Harmattan winds blow south from the Sahara Desert and warm the Sahel (UNEP, 2012).

In Chad, annual mean temperatures, 25 – 30^0C, are almost the same throughout the country and vary in mountainous areas of the north at 15 - 25^0C. Seasonal variations are greater and vary according to the different regions. Temperature variations are obvious in the north and center of the country with summer temperatures varying from 27 to 35^0C and those of winter from 20 to 27 ^{0}C (5 - 10^0C in the mountainous localities). In the south, temperature seasonal variations are less visible even though summer months (JAS) are the coolest ones

with temperature about 22 - 25^{0}C due to the cooling effects of rain during that period (McSweeney, New, & Lizcano, 2010).

Soil moisture: According to Seneviratne et al. (2010), soil moisture generally refers to the amount of water stored in the unsaturated soil zone. It a source of water for the atmosphere through processes leading to evapotranspiration from land, which include mainly plant transpiration and bare soil evaporation. It has many effects on climate processes, especially on air temperature, boundary-layer stability, and in some cases on precipitation. Soil moisture is a key variable of the climate system. First, it constrains plant transpiration and photosynthesis with consequent impacts on the water, energy, and biochemical cycles. Second, it is a storage component for precipitation and radiation anomalies, inducing persistence in the climate system. Third, it is involved in a larger amount of feedback at the local, regional and global scales, and plays a dominant role in climate-change projections (Seneviratne et al., 2010).

Vereecken et al. (2008) stated that soil moisture plays a great role in weather and climate predictions from the regional to the global scale by controlling the exchange and partitioning of water and energy fluxes at the land surface. Agricultural and irrigation management practices, specifically in semi-arid and arid regions, principally depend on a timely and accurate characterization of temporal and spatial soil moisture dynamics in the root zone because of the impact of soil moisture on the production and health status of crops and salinization. In addition to that they also said that soil moisture plays a dominant role in the organization of natural ecosystems and biodiversity.

For UNEP (2012), when tree cover is lost, the protecting canopy disappears and the soils are more exposed to both wind and rainfall. With a loss of tree cover, evapotranspiration

also decreases, leading to a larger fraction of the rainfall forming runoff, potentiall leading to further erosion. The canopy also dampens diurnal and annual temperature variations, both by shading the soil and by cooling the surface by evapotranspiration during the summer rainy season. Higher ground temperatures and larger diurnal temperature fluctuations following the loss of a protective canopy promote the breakdown of organic matter; and with less tree cover, less new organic matter is produced. They concluded that the loss of tree cover can have devastating effects through subsequent changes in water and temperature cycles, leading to an accelerated soil and land degradation

Vegetation: Vegetation in the Sahel is a reflection of the steep south to north rainfall gradient. Climatic factors such as rainfall and relative humidity, generally, determine vegetation growth and composition. Local factors such as soil are, however, important, especially near climatic margins and where lateritic crusts, saline or water-logged soils occur. Detailed zonations include the following classes from north to south.

- Sahelo-Saharan zone
- Sahel zone
- Sahelo-Sudanian zone
- Sudanian zone (or Sahel woodland)
- Guinea Moist Savanna (or Doka)

Vegetation production mapped from a time series of the AVHRR satellite images has shown a strong south to north declining in the Sahel. The trend, determined from the Normalized Difference Vegetation Index (NDVI), closely corresponds to the steep rainfall transition from high rainfall in the south to low rainfall in the north. Vegetation growth is generally limited by water availability. The growing cycle nearly follows the seasonal

rainfall patterns. During the dry winter with almost no rain, vegetation is dormant. Vegetation growth starts immediately with the arrival of the monsoon rains in summer. The peak growing season in the Sahel is around August, when the summer monsoon reaches as far as 10˚N. That growing season lasts for about three months in the northern parts with areas towards the southern fringes having two growing seasons. Vegetation growth lags one to two months behind rainfall, and is sustained longer around ephemeral streams and larger rivers that have water flow the whole year in the Sahel (UNEP, 2012). The NDVI anomalies (i.e., differences between the NDVI at a given time from the average for a region) can indicate drought conditions or higher-than-average precipitation conditions.

Hou, Zhang, and Wang (2011) showed that climate change directly affected the variation in the NDVI of vegetation by studying the correlation coefficients between the NDVI and climate factors. The relationship between the NDVI and temperature varied with the types of vegetation, the season, and altitude. NDVI variation is highly correlated ($r = 0.7311$; $\rho = 0.01$) with variation in temperature and less considerably with precipitation. Griffith et al. (2002) found a considerable statistical relationship between NDVI, vegetation phonological metrics (VPMs), and water quality parameters or indices of streams/fish community condition. The NDVI or VPMs were more greatly correlated to water quality than land cover proportions. The NDVI and VPMs may serve as broad-scale ecological indicators and screening tools for catchment monitoring and assessment.

2.2. Climate and Socio-economic Impacts

According to Awa et al. (2003), the rural people of sub-Saharan Africa live mainly on diverse agricultural activities including raising, which plays a major role in the socio-economy of the region, as it accounts for an average of more than 11%.

According to IPCC (2001), rainfall could potentially have a wide array of economic implications anywhere in the developing world. The most direct impact of rainfall on Africa is on the agricultural activities for water is an essential to agricultural production (Masters & Wiebe, 2000).

While the African continent has several large water basins and rivers and heavy rainfall in some areas, the runoff from these water sources to the arid and semi-arid areas is particularly low. This is exacerbated by the high temperatures in sub-Saharan Africa. Moreover, within the arid and semi-arid areas, there is little water runoff as drier soil absorbs more moisture. In reality, the average runoff of about 15% is lower than on any other continent and very sensitive to changes in rainfall. A much smaller proportion of arable land is irrigated in sub-Saharan Africa comparison to other developing areas in the world. The availability of water from rainfall depends on the rate of evapotranspiration. This rate is specifically high in sub-Saharan Africa, in part because high temperatures increase the water-holding capacity of the air. Additionally, recent trends in desertification may have affected the extent of rainfall in the semi-arid areas as a reduction of vegetative cover can also translate into the absence of inter-annual soil water storage and hence, negatively impact agricultural productivity (Barrios, Bertinelli, & Strobl, 2010).

The geographical variation of water availability can be considered in terms of its implications for agricultural production in sub-Saharan Africa. In spite of the abundance of water, the tropical humid regions are usually not appropriate for crop or animal production. For crops, the combination of high temperatures and abundant rainfall fosters high rates of chemical weathering and the production of leached clay soils of low inherent fertility. Therefore, much crop production is located in the semi-arid regions, making it susceptible to

rainfall shortages. For animal production, domestic livestock in Africa other than pigs are also specifically concentrated in the arid and semi-arid regions because the relatively more humid areas provide greater exposure to animal diseases and are characterized by grasses of low digestibility. Because livestock are directly dependent on grass quantity, rainfall variations in the semi-arid and arid areas have direct consequences on livestock production (Barrios, Bertinelli, & Strobl, 2010).

Rainfall can also considerably impact the energy sector and other industrial sectors as well in sub-Saharan Africa because energy supply in that region mainly relies on water as direct and indirect input (Magadza, 1996). Over the past fifty years, African countries have importantly invested in hydroelectric power: 47% of total power generation compared to the average of 34% in other developing countries (Harrison & Whittington, 2001 in Barrios, Bertinelli, & Strobl, 2010**).** Furthermore, water serves as an important secondary input for thermal power generation as a cooling device and is needed in large quantities for this purpose. Notably, hydroelectric and other production using water as a secondary input in sub-Saharan Africa tend to be greatly reliant on rivers as their source of water. These rivers originate in tropical areas where high temperatures increase evaporation losses, and consequently, river flows are in turn sensitive to precipitation changes. Additionally, all the other sources of water for hydroelectric power like lakes and reservoirs are also highly exposed to decreases in rainfall (Barrios, Bertinelli, & Strobl, 2010; Magadza, 1996;).

The south of the Sahel, agriculture is more diversified with both cash crops, such as wheat, sugar, peanuts, cotton, cowpeas, and subsistence crops, such as sorghum, manioc, and maize. Further north, trees are harvested for a variety of products, and the main cash crop is cotton. Subsistence crops include millet, sorghum, and to some extent maize. Field sizes are

often small and crop management is adapted to utilize micro-scale variations in topography. Farmers generally also keep livestock, but they are not nomadic. They adopt a transhumance lifestyle where they move with their animals following seasonal cycles, if necessary (UNEP, 2012).

Where rainfall is above 300 mm per year, dryland agriculture (sorghum, millet) is common, but with highly variable crop yields. Crop failure also increases risk of wind erosion as the soil is laid bare after clearing of natural vegetation. The Sahel is a high-risk environment for agricultural production, and farmers traditionally plant a range of subsistence crops to secure a minimum harvest in dry years. At the onset of the rains, pastoralists migrate northwards with their cattle; then return to the south in November or December. Large herds are favored both for cultural reasons and as security for drier years. They concluded that population growth and changing political environments now limit the extents of these traditional migration patterns (UNEP, 2012).

According to the country summary from PRD (2013), the population of Chad in 2013 was estimated at 12,825,000 and the projected population for 2050 is 33,516,000 (FAO, 2013). The births per 1000 population are 51, the deaths per 1000 are 15, and the rate of natural increase is 3.6 %. The infant mortality rate is 106, and the total fertility rate is 7.0. The percent of population less than 15 years old is 49, the one that is greater than 65 years old is 2. The percent of the urban population of Chad is 22.

Funk et al. (2012) wrote that the agriculture sector in Chad engages more than 70 percent of the active population. They also stated that the main crops are millet and sorghum in the northern part of the agricultural zone, with increased crop diversification around Lake Chad and areas further south. According to their conclusion, human and animal pressures on a

degraded ecosystem, combined with limited agricultural development, have led to low levels of national food production.

Based on country summary data of FAOSTAT (2014), Chad is one of the biggest livestock producing sahelian countries. In 2012, the total number of livestock in Chad was about 32,266,692 heads. There are mainly composed of cattle and buffaloes (7800000), sheep (3150000), goats (6780000), pigs (32800), chickens (5680), horses (432000), asses (476000), camels (1450000), and beehives (123500).

Coe and Foley (2001), studying human and natural impacts on the water resources of the Lake Chad basin, illustrated the importance of taking into account human activities on water resources. They wrote that human activities acted to strongly amplify the response of the Lake Chad basin to a downward trend in precipitation. They also suggest that the drastic decline in lake level and area since the 1970s can be attributed in nearly equal part to the persistent decrease of precipitation and to the considerable increase of irrigated agriculture because the beginning of dry climate conditions led people to dramatically increase irrigation activity inducing almost the double of loss of water from the lake.

CHAPTER 3

DATA AND METHODOLOGY

The chapter methodology presents the types of data collected for this study, the sources of those data, and the methods and software used to manipulate them. The research protocol to realize this study is summarized in the following data flow diagram (figure 3).

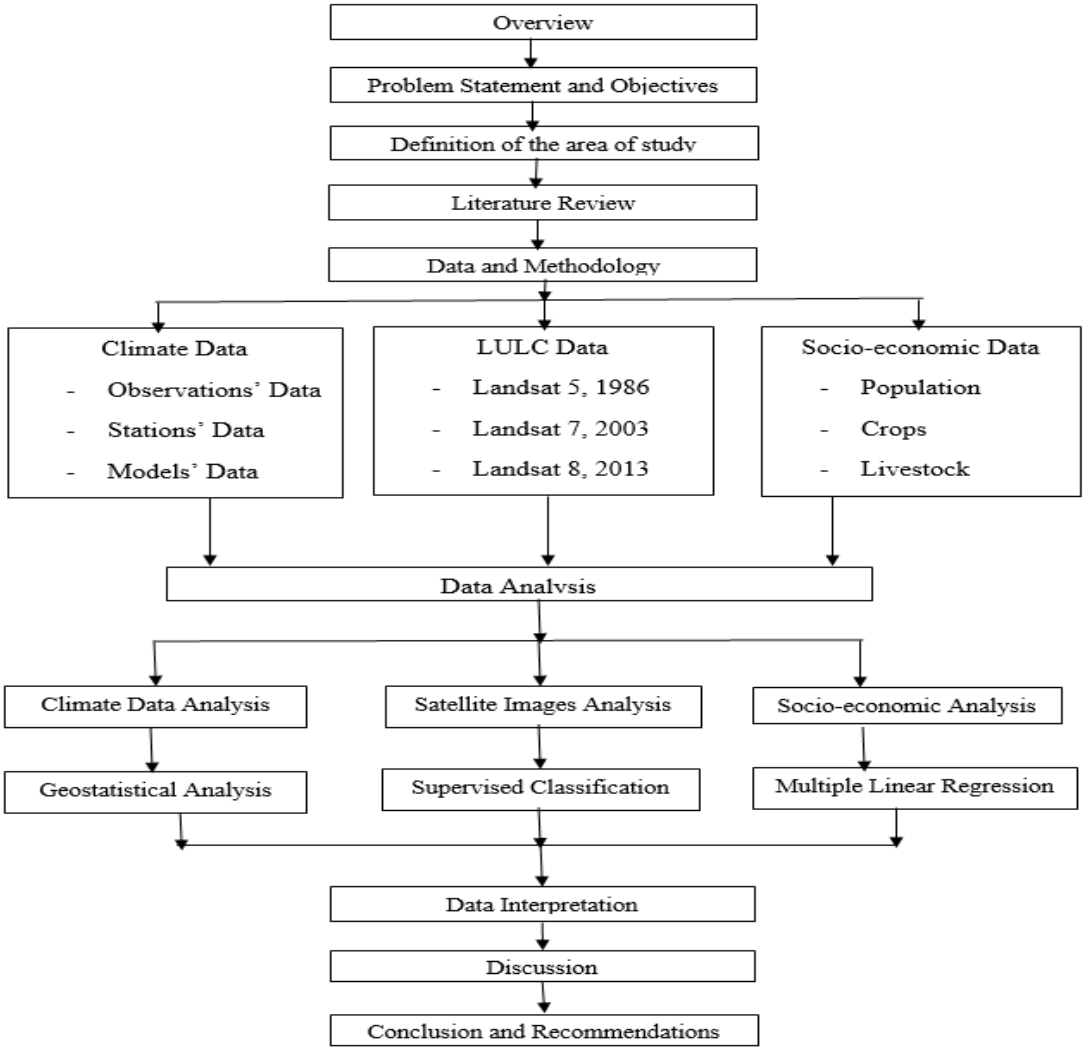

Figure 3. Flow Diagram of the Research Protocol

3.1. Data

Three main types of data were collected for this study: climate data, land use land cover data, and socio-economic data.

3.1.1. Climate Data

The climate data collected were atmospheric and land data; some are described in the chapter 2, with others described as follows:

- Atmospheric observation data: Global Precipitation, Aerosol Optical Depth, Surface Air Temperature, and cloud fraction
- Atmospheric Models data: Eastward and Northward Winds, and Specific Humidity at 250, 500, and 850 hPa
- Land observation data: Evapotranspiration, soil moisture, and the NDVI.

The Global Precipitation Climatology Project (GPCP): GPCP was established by the World Climate Research Program to quantify the distribution of precipitation around the globe over many years (GES DISC, 2013). Gruber and Levizzani (2008) said that one of the major goals of the GCPC is to develop a more complete understanding of the spatial and temporal patterns of global precipitation. The GPCP provides an opportunity to study global-scale precipitation in ways that were previously difficult to impossible. The strength of the GPCP data is as:

- Consistent data analysis, quality control, and data processing
- An analysis of precipitation over both land and ocean, and
- The use of a consistent set of global precipitation estimates

Atmospheric Temperature: Atmospheric Temperature is literally a measure of average kinetic energy (energy of motion) of air molecules in the atmosphere, either over land or over

water. Its units of measure are in Kelvin or Celsius degrees. Atmospheric temperatures are expressed by several types of data products: a. Near surface air temperature data express the temperature of the air over land; they are measured by thermometers placed roughly 1 meter above the ground. b. The average surface temperature presents the actual temperature on the surface of both land and ocean. For land surfaces only, there are surface "skin" temperatures calculated from measurements of microwave radiation at the land's surface taken by satellite. c. Surface air temperatures and surface skin temperatures can be slightly different because of their definitions and measurement methods; however, they are sufficiently related so that either can be used to examine temperature trends (GES DISC, 2014).

Cloud Fraction: Cloud fraction is the fraction of the sky that is covered by clouds; also referred to as cloud amount or cloud cover. In a satelite image, cloud fraction is the number of cloudy pixels divided by the total numer of pixels. It is calculated from microwave wavelength measurements (called "brightness temperatures"). Cloud fraction is unitless. It is indicative of weather patterns and the movement of the air in the atmosphere. Cloud fraction is one of the basic average weather conditions that determines climate. Trends over time in cloud fraction can indicate changes in weather patterns related to precipitation and storms, and they may also indicate changes in atmospheric temperature and humidity (GES-DISC, 2014).

Evapotranspiration: Evapotranspiration is the sum of evaporation and plant transpiration. Evaporation accounts for the movement of water to the air from various sources on the earth's surface such as soil, ocean, etc. Transpiration accounts for the movement of water within a plant and the subsequent loss of water vapors through the stomata in its leaves. The evapotranspiration rate expresses the amount of water lost from a

unit of surface per unit of time. The unit of time can be an hour, day, month, year, and even a decade. The applications of evapotranspiration are mainly water cycle, energy cycle, weather forecast, and the climate prediction model (GES DISC, 2014).

Normalized Difference Vegetation Index (NDVI): According to the broad definition, the Normalized Difference Vegetation Index shows the "greenness" of a surface without any specification of the origin of said greenness even though the green color is always associated with green plants. From the technical and practical point of view, the NDVI is calculated from measurements of spectral reflectance in the near infrared (NIR) and visible (VIS) portions of the electromagnetic spectrum. These spectral reflectances are calculated from the wavelengths of the observing instruments. NDVI is calculated as: (NIR-VIS) / (NIR+VIS)

These spectral reflectances are ratios of the reflected to the incoming radiation in each spectral band individually; so, their values are between 0.0 and 1.0. By design, the NDVI values vary between -1.0 and +1.0. Consequently, land cover values range from 0.0 to +1.0; with clouds and water values from -1.0 to 0.0. For areas with seasonal differences in greenness (changes in growing vegetation cover), the NDVI shows large changes between the seasons. The NDVI is also helpful in showing the impact of precipitation; high or low precipitation affects the NDVI by either increased or decreased greenness due to enhanced or diminished growth of vegetation (GES DISC, 2014).

3.1.2. Land Use Land Cover Data

To perform the land use land cover of this study, three free Landsat scenes from three types of Landsat sensors were used:

- Landsat 5, Thematic Mapper (TM) of November 14th, 1986
- Landsat 7, Enhanced Thematic Mapper Plus (ETM+) of January 5th, 2003 and

- Landsat 8, OLI (Operational Land Imager) and TIRS (Thermal Infrared Sensor) of October 23rd, 2013.

All of those images are from the path 183 and the row 51 with the following characteristics: Projection: UTM, Zone 33, Spheroid: WGS 84, Datum: WGS 84. The images from the end of the rainy season were chosen in order to better assess the impact of rainfall on vegetation and other human activities.

3.1.3. Socio-economic Data

Socio-economic data were mainly collected from the website of the Food and Agriculture Organization Statistics (FAOSTAT). Those data are related to:

- Population
- Land: agricultural area
- Crops production: cereals such as sorghum, maize, and rice paddy and commercial crops such as cotton, sugar cane, and tobacco
- Live animals production: sheep, goat, and cattle.

3.2. Data Sources and Platforms

To collect and analyze necessary data for the study, the following sources were used:

- GES-DISC Interactive Online Visualization and Analysis Infrastructure (Giovanni)
- Global Visualization (GloVis) Viewer
- **FAOSTAT** of Food and Agriculture Organization of the United Nations.

3.2.1. Giovanni (GES-DISC Interactive Online Visualization and Analysis Infrastructure**)**

Giovanni is a Web-based application developed to provide a simple, intuitive way to visualize, analyze, and access vast amounts of earth science remote sensing data, specifically from satellites, without having to download the data. Giovanni is an acronym for the

Geospatial **I**nteractiv**e** **O**nline **V**isualization **AN**d a**N**alysis **I**nfrastructure. From the researcher's point of view, it is comprised of a number of interfaces, each tailored to meet the needs of specific fields of earth science research. Each interface, known as a portal, provides functions and parameters applicable to that particular area of earth science. Giovanni helps get information easily about the world's atmosphere without the need to retrieve and process data. Data can be varied and from different instruments with all the statistical analysis already done via a regular browser (GES-DISC, 2013).

Giovanni was used to obtain the following: atmospheric observation data (Global Precipitation, Aerosol Optical Depth, Surface Air Temperature, and cloud fraction), atmospheric models data (Eastward and Northward winds, and Specific Humidity at 250, 500, and 850 hPa), and land observation data (Evapotranspiration, soil moisture, and NDVI). NDVI provided by the National Oceanic & Atmospheric Administration/Advanced Very High Resolution Radiometer (NOAA/AVHRR).

3.2.2. Global Visualization (GloVis) Viewer

GloVis is a browser based image search and order tool that can be used to quickly review the land remote sensing data inventories held at the U.S. Geological Survey (USGS) Center of Earth Resources Observation and Science (EROS). It was funded by the American View project to reduce the difficulty of identifying and acquiring data for user-defined study areas.

Updated daily with the most recent satellite acquisitions, GloVis displays data in a mosaic, allowing users to select any area of interest worldwide and immediately view all available images for the following Landsat datasets: Multispectral Scanner (MSS), Multi-Resolution Land Characteristics (MRLC), Ortho-rectified, Thematic Mapper ™, Enhanced Thematic Mapper Plus (ETM+), and ETM+ Scan Line Corrector-off (SLC-off). Other data

sets include Terra Advanced Space-borne Thermal Emission and Reflection Radiometer (ASTER) and Moderate Resolution Imaging Spectroradiometer (MODIS), Aqua (MODIS), and the Earth Observing-1 (EO-1) Advanced Land Imager (ALI) and Hyperion data.

Special features: Some special features include the ability to navigate and review data simultaneously, user-specific map layer options and search capabilities, interaction with other users via the GloVis Forum, cloud cover, date limits, and access to metadata, as well as both USGS and National Aeronautic and Space Administration Land Processes Distributed Active Archive Center ordering capabilities. Among the wide variety of users are emergency response and natural resources managers, crop forecasters, urban planners, earth scientists, university researchers, government agencies, elementary and secondary schools, and the general public (USGS, 2005). GloVis websites were used to place free orders and/or download the satellite data of Landsat 5, TM, 1986, Landsat 7, ETM+, 2003, and Landsat 8, OLI_TIRS, 2013.

3.2.3. FAOSTAT of Food and Agriculture Organization of the United Nations.

The Statistics Division of the FAO has launched a new version of FAOSTAT, which is part of the organization's mission to improve data collection and dissemination for the development and fight against global hunger and malnutrition.

Significant time-series and cross sectional data relating to hunger, food, and agriculture for 245 countries and territories and 35 regional areas, from 1961 to the most recent year, served as the source of socio-economic related data. FAOSTAT was used to acquire data on population, production (crops and live animals), and land (agricultural area).

3.2.4. Global Historical Climatology Network (GHCN)

The Global Historical Climatology Network is an integrated database of climate summaries from land surface stations across the globe that have been subjected to a common suite of quality assurance reviews. The data were obtained from more than 20 sources. Some data are more than 175 years old while others are less than an hour old. For this study, the GHCN was used to obtain station rainfall data on Chad.

3.3. Software Platforms

The following software was used for data analysis: Giovanni web-portal, for data visualization and analysis and downloading ASCII data; Erdas Imagine 2013, for processing and classifying satellite images; ArcGIS 10 and 10.1, for making maps and geostatistical studies; and IBM SPSS 21 Statistics, for statistic studies.

3.3.1. Erdas Imagine 2013

ERDAS IMAGINE performs advanced remote sensing analysis and spatial modeling to create new information. In addition, with ERDAS IMAGINE, one can visualize results in 2D, 3D, movies, and on cartographic-quality map compositions. The core of the ERDAS IMAGINE product suite is engineered to scale with geospatial data production needs. Optimal modules providing specialized function are also available to enhance productivity and capability.

- IMAGINE Essentials is the entry-level image processing product for map creation and simple feature collection tools. It enables serial batch processing.
- IMAGINE Advantage enables advanced spectral processing, image registration, mosaicking and image analysis, and changes in detection capabilities. It also enables parallel batching processing for accelerated output.

- IMAGINE Professional includes a production toolset for advanced spectral, hyper-spectral, radar processing, and spatial modeling. It includes ERDAS ER Mapper.

New Tools and Technology for Handling Point Clouds: ERDAS IMAGINE 2013 enables one to more thoroughly visualize, analyze, and manage point clouds. New viewing technology allows one to simultaneously view point clouds in 2D, 3D, and through a user-specified profile, reveal cross sections of the point cloud. There are also tools that classify, define subsets, and filter, as well as encode the data.

Next-Generation Spatial Modeler: The next-generation spatial modeler features an all-new, modern interface and provides real-time preview of results. In addition to the ERDAS IMAGINE raster operators, the new spatial modeler incorporates GeoMedia vector and grid operators to greatly expand the problem solving capability.

New Tools in the IMAGINE Radar Mapping Suite: IMAGINE Radar Mapping Suite provides new tools that enable an easier and more thorough use of radar data sources. Many of the radar tools are now presented using a ribbon interface for faster and easier access. Other features include real-time ship tracking with Automatic Identification System (AIS) feeds, on-the-fly georeferencing, and quick and easy detection of flood or spills.

Better Results for Object-based Feature Extraction: ERDAS IMAGINE Objective uses a new segmentation algorithm, Fast Least Squares (FLS), which provides us with the ability to fine-tune the creation of segments based on shape, size, texture, and spectral value.

Additional Indices and a Streamlined Interface for Working with Indices: ERDAS IMAGINE 2013 includes more than 35 of the most commonly used indices (band algebra formulas that enable easier information extraction from imagery), and the interface used to

work with indices is now streamlined, with the indices tool connected to the spatial modeler for easy editing (ERDAS IMAGINE, 2013).

3.3.2. ArcGIS 10.1 (for geostatistical and statistical analyses and map-making)

ArcGIS 10.1 signals a major development in the way geographic information will be accessed and managed by GIS professionals and their organization in the years to come. ArcGIS 10.1 gives GIS professionals a complete GIS that further integrates desktops and servers, as well as mobile and web applications. The ESRI ArcGIS Geostatistical Analyst extends ArcMap by adding an advanced toolbar containing tools for exploratory spatial data analysis and a geostatistical wizard to guide the process of creating a statistically valid surface. New surfaces generated with Geostatistical Analyst can subsequently be used in geographic information system (GIS) models and in visualization using ArcGIS extensions such as ArcGIS Spatial Analyst and ArcGIS 3D Analyst.

This geostatistical analyst is revolutionary because it bridges the gap between geostatistics and GIS. Surface fitting using the geostatistical analyst involves three key steps: exploratory spatial data analysis, structural analysis (calculation and modeling of the surface properties of a nearby location), and surface prediction and assessment of results.

Exploratory spatial data analysis: using measured sample points from a study area, geostatistical analyst can create accurate predictions for other unmeasured locations within the same area.

Semivariogram modeling: geostatistical analysis of data occurs in two phase: 1. modeling of semivariogram or covariance to analyze surface properties, and 2. kriging; ordinary, simple, universal, indicator, probability, and disjunctive kriging.

Surface prediction and error modeling: various types of map layers can be produced using a geostatistical analyst, including prediction, quantile, probability, and prediction standard error maps.

Threshold mapping: probability maps can be generated to predict where values exceed a critical threshold.

Model validation and diagnostics: cokriging, and the advanced surface modeling method included in the geostatistical analyst can be used to improve surface prediction of a primary variable by taking into account secondary variables, provided that the primary and secondary variables are spatially correlated (ESRI, 2003).

3.3.3. IBM SPSS 21 **(**International Business Machine – Statistical Package for the Social Sciences). SPSS is an integrated family of products that addresses the entire analytical process, from planning to data collection, as well as analysis, reporting and deployment for some elementary and descriptive statistical analyses.

IBM SPSS Statistics is a comprehensive system for analyzing data. It offers rich statistical capabilities paired with features that make it easier to access and manage data.

SPSS Statistics supports the entire analytical process. It helps people validate assumptions faster, guides them to use the right statistical capability at the right time, gives analysts flexible access to powerful analytical techniques, and helps organizations make the most of their analytical resources by scaling from the simplest to the most widespread initiative (IBM Corporation, 2012).

Some of the available options are as follows:

- Statistics Base gives a wide range of statistical procedures for basic analyses and reports (crosstabs, descriptive statistics etc.)

- Advanced statistics focus on techniques often used in sophisticated experimental and biomedical research (including procedures for general linear models (GLM), linear mixed models, variance components analysis, loglinear analysis, ordinal regression, etc.)
- Bootstrapping is a method for deriving robust estimates of standard errors and confidence intervals for estimates such as the mean, median, proportion, odds ratio, and correlation and regression coefficients.
- Categories perform optimal scaling procedures, including correspondence analysis.
- Missing Values describes patterns of missing data, estimates means and other statistics, and impute values for missing observations.
- Regression provides techniques for analyzing data that do not fit traditional linear statistical models.

Version 21 of SPSS allows some of the following operations:

- Simulation, predictive models such as linear regression
- Descriptive statistics that provide summary descriptive statistics: mean, median, and frequency counts
- Correlation between data
- Comparison of datasets, with the comparison of data values and metadata attributes (dictionary information) of two data sets

SPSS 21 was used to analyze bivariate correlation and multiple linear regression between the atmospheric and land parameters, and agricultural observations respectively (IBM Corporation, 2012).

3.4. Analytical Methods

Figure 4 below is a graphical summary of how climate, LULC, and socio-economic data were integrated through the means of software and geostatistical analysis tools, generating the data output and thematic maps necessary for interpretation during this study. There were mainly three analytical methods which this study used: climate, LULC, and agricultural data analytical methods.

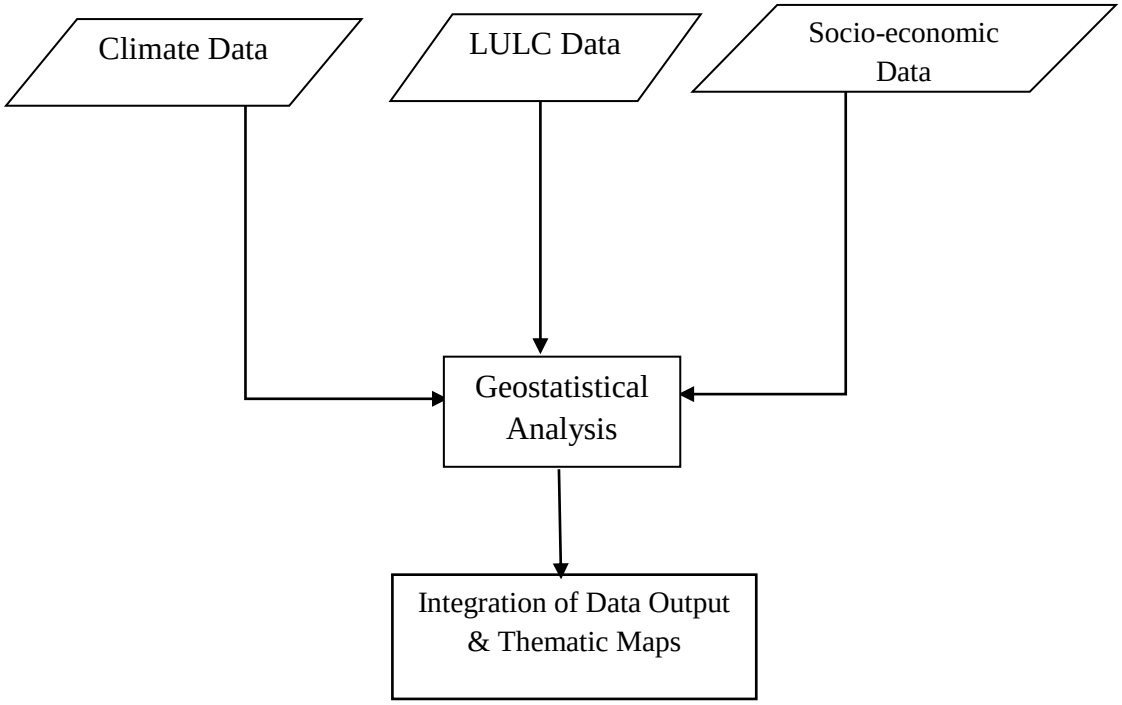

Figure 4. Research Design Data Flow Diagram

3.4.1. Climate Data Analytical Method

All the climate data (observation and model) except for stations were obtained from Giovanni web-based portal. The steps of processing were as follows (figure 5):

- Step 1. After specifying the spatial resolution of the area of study through the geographic coordinates in the area of interest, five desired parameters were selected at

a time (based on the limitation of the web-application) through the radio button check boxes. Then the temporal resolution was specified (from 1980 to 2012 for some, and from 2003 to 2012 for others) and the mode of visualization selected. Only two types of visualization were used based on the needs of this study: the Lat-Lon map, Time-averaged visualization which provides Lat-Lon data and the Time series visualization which provides monthly data. The visualizations were generated and the data downloaded and saved as ASCII compressed Tape ARchaive. GNU Zip (.tar.gz) files.

- Step 2. The 7-Zip File Manager Tool was used to extract those files into .txt files. The text files were brought into Excel files, processed, and tranformed from text to columnar data and saved as .xls files.
- Step 3. The Excel files had two destinations according to the ways they were generated and their contents. The files generated through Lat-Lon map, Time averaged visualization and containing lat-lon data were used for geostatistcal analysis in ArcGIS 10.1 and SPSS 21 (kriging interpolation and correlation). Those generated through Time series visualization, containing monthly data, were used for statistical analysis in SPSS and for processing graphs in Excel 2013.

The results of these processings were data output and maps which were integrated and interpreted.

The stations' data especially rainfall data obtained from two stations in Chad, were used in Excel to draw the rainfall annual cycles graphs for the rainy season at those stations.

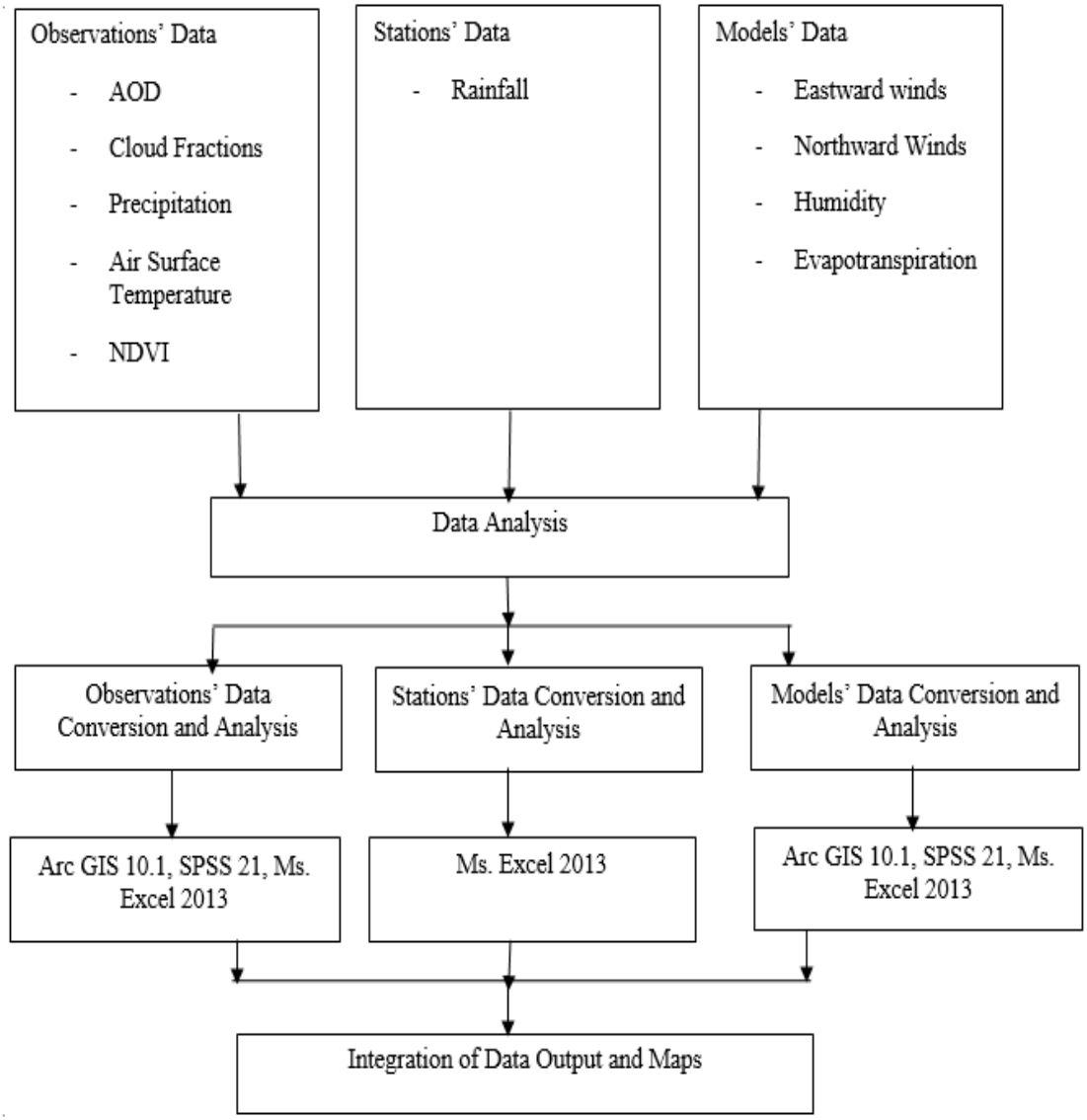

Figure 5. Climate Data Processing Flow Chart Diagram

3.4.2. Land Use Land Cover Data Analytical Method

The main descriptive steps of performing the land use land cover data analysis is shown in figure 6 below.

Data preparation: the scenes obtained from GloVis were compressed files .tar.gz of bands of Tagged Image File Format (tiff) format. The 7-Zip File Manager was used to decompress those files. Then, in Erdas Imagine 2013, all the tiff bands were stacked together and transformed into an image format (.img) using the tool Raster/Spectral/Layer Stack. Since all the satellite images have the same source with the same projection, no geometric correction (image rectification) was performed. No radiometric resolution, correction and image enhancement was performed because the five classes are clear enough to be distinguished. The areas of interest were delineated using the subset tool in Erdas Raster/Subset & Chip/Create Subset Image.

Guide tools for classification: Since there was no ground truth control data, Google Earth, land use land cover maps of 2000 and 2013, and a vegetation map related to the soil, were used as guides for a better classification.

Classification: A supervised classification was conducted using the "Supervised Maximum Likelihood" method; five (5) classes were identified: Water bodies, Wetland, Bare soils, Forest-Savanna-Steppe, and Grassland-Farmland. These classes are described as follows:

- Water bodies include the lake itself, rivers and wadi.
- Wetland: inundated or saturated areas at a frequency and duration sufficient to support a prevalence of vegetation. It generally encompasses swamps, marshes, bogs, and similar areas (33 CFR 328 Definitions (b) in Darden, 2011).
- Grassland-farmland includes open land in which grasses are dominant and there is cultivated land.

- Forest-Savanna-Steppe includes all the vegetative forms other than grasses, from trees to shrubs.
- Bare soils includes soil and sand not covered by vegetation.

After the supervised classification was accomplished, the post-classification processes were as follows:

Post classification: after performing the supervise classification**,** the images were filtered; the unclassified were eliminated.

Accuracy assessment: the Accuracy Assessment (Error matrix, Accuracy Totals, and Kappa Statistics) was reported with 256 random points.

Area table: an area table was added for the classes in Erdas using the tool table/Add Area. The changes were computed image by image.

Recode: each class was extracted from the others by using the Recode tool in Erdas Raster/Thematic/Recode.

Rate of Change: the rates of changes in land use land cover classes from 1986 to 2003 and 2003 to 2013 were computed using the formula:

$R = [(A2/A1)^{1/(t2-t1)} -1]*100$ where:

r = rate of change, t1 = the starting time data, t2 = ending time data

Source : FAO, 1990.

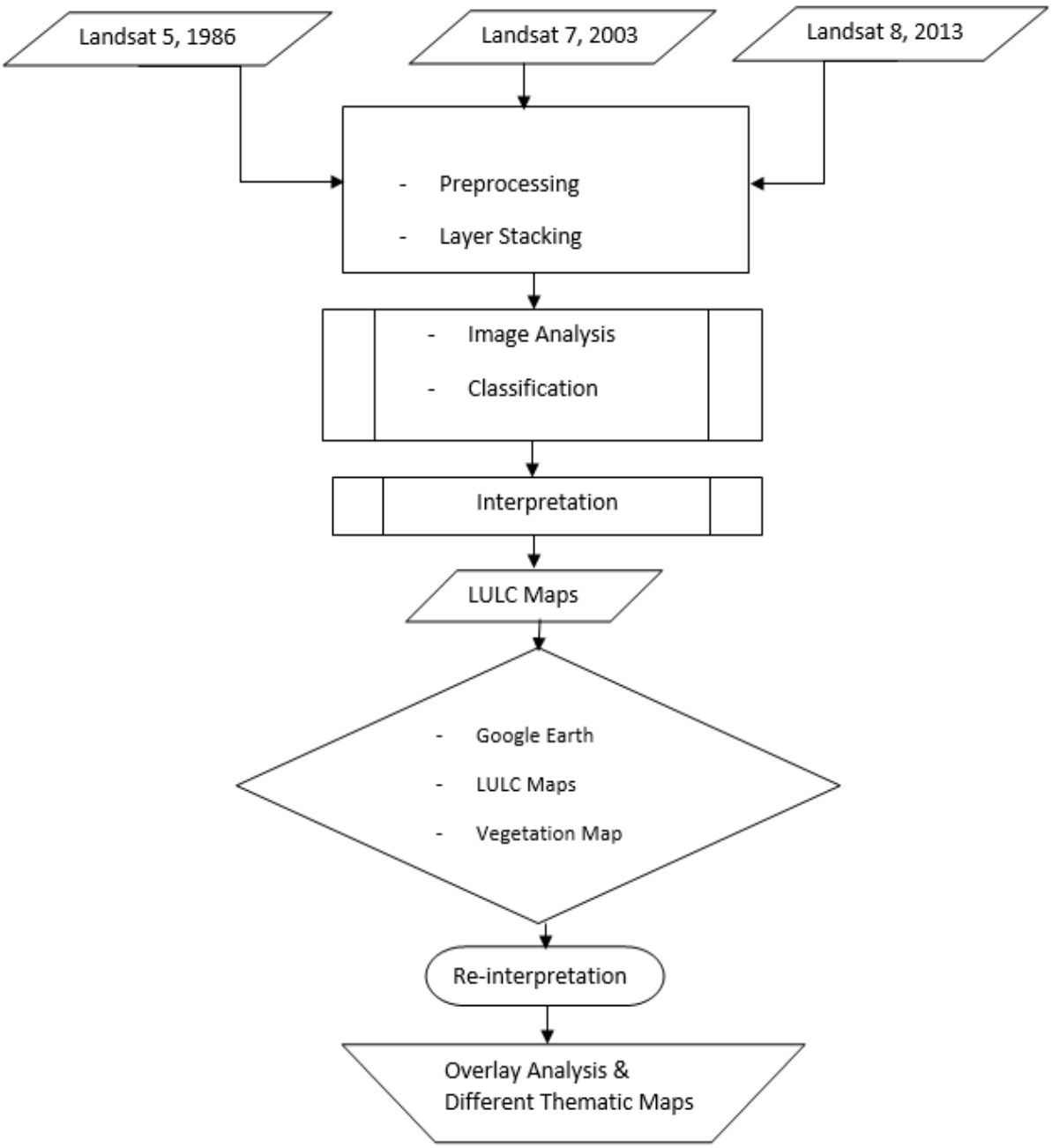

Figure 6. LULC Data Processing Flow Chart Diagram

3.4.3. Socio-economic Data Analytical Method

All the socio-economic data were obtained from the FAO Statistics website in Excel format (.xls). Once downloaded, all of them were exported to Ms. Excel 2013 for processing

and graphs creation. Then production (cereals, commercial and industrial) and livestock (sheep, goat, and cattle) data were brought into SPSS 21 for Multiple Linear Regression analysis. The general steps for implementing the socio-economic data analysis is shown in figure 7.

Some of the hypotheses of the standard multiple linear regression (MLR) analysis to verify in order to accept the model are:

- Sample size**:** The larger sample size the better for an analysis because to have predictions about outcomes we need to have enough variance or variability in predictors as well as in outcomes (dependent variables) to be able to make a most accurate prediction. One of the rules is to have 15 participants per predictor variable if the dependent variable is normally distributed; the number of participants would be increased is the distribution is skewed. For two predictor variables, the absolute minimum number of participants will be 30.
- Multicollinearity**:** Refers to the relationship among the independent variables. There is multicollinearity when the independent variables are highly correlated to each other. An R value typically of 0.9 or higher between predictor variables indicates multicollinearity. Multicollinearity means there are some redundant predictive variables that would tend to make the model less accurate because more than one variables are used to measure the same thing. The correlation between predictive variables must not exceed 0.7 to not have multicollinearity.
- Tolerance indicates how much of the variability of the specified predictive variable is not explained by the other predictive variable in the model. Its value indicates that

there might be high multiple correlations suggesting multicollinearity. A value of less than one (1) means there is no multicollinearity.

- VIF (Variance Inflexion Factor) is the inverse of tolerance and indicates multicollinearity if its value is greater than 10.
- R Square is used to evaluate the effectiveness, statistical significance, and the accuracy of the prediction. It tells us how much of the variance of the dependent variable is explained by the model. The Adjusted R Square corrects the R Square value and provides a better estimate.
- The significant value in the ANOVA Table (Sig) must be less than 0.5 for the model to have statistical significance and accurately predict the outcome.
- Outliers: Check for outliers for both the independent and dependent variables and delete them because multiple regression is very sensitive to outliers (very high or very low scores).
- Relationship between predictive and dependent variables: The relationship between the independent and dependent variables need to be linear. The correlation between independent and dependent variables must be greater than 0.3 to not have multicollinearity.
- The normality or linearity distribution**:** The dependent variables need to be normally distributed. The dots of the Normal Probability Plot should form reasonably close to the line of best fit or line of normality. There must not be major deviation from the line of normality. In the Scatterplot, there should be a rectangular distribution of points.

- The standardized coefficient (Sig) tells us which of the independent variables have made strong impact on the dependent variables in a MLR.
- Coefficients Significant value (Sig) tells us whether a variable makes a statistically unique significant contribution to the prediction of the model. This depends on which variables are included in the model, how much overlap there might be among them, and also how much collinearity there might be.

- If Sig < 0.5, the variable has made a significant unique contribution to the prediction of the outcome.
- If Sig > 0. 5, the variable has not made a significant unique contribution to the prediction of the outcome; this might be due to some overlap of the predictive variables or some multicollinearity (TheRMUoHP Biostatistics Resource Channel, 2013).

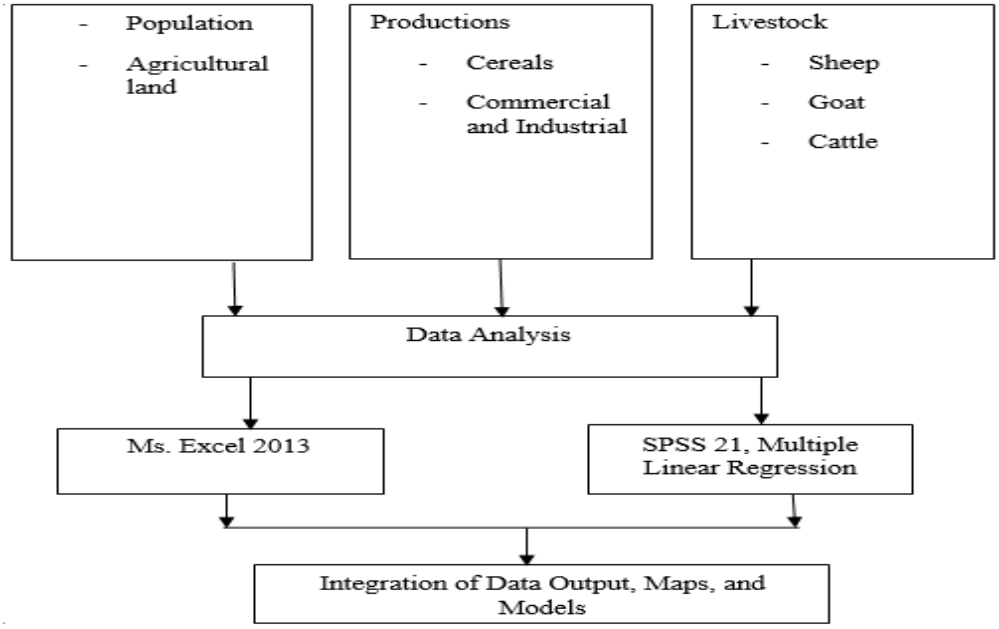

Figure 7. Socio-economic Data Processing Flow Chart Diagram

CHAPTER 4

DATA ANALYSIS AND RESULTS

Knowledge about the impacts of atmospheric and land parameters and their interactions on land use and livelihoods is important in understanding natural ecosystems evolution and durability. Our study was focused in Chad with extension to Cameroon, Central African Republic, Niger, Nigeria, and Sudan, especially in the shaded area as shown in figure 1. Atmospheric parameters studied are mainly the Global precipitation, Aerosol Optical depth, and Surface Air Temperature; however, some other parameters such as the Humidity, Winds, and Clouds associated with precipitation are also considered. Land parameters are Evapotranspiration, Soil Moisture, and the Normalized Difference Vegetation Index (NDVI).

4.1. Atmospheric Parameters

The atmospheric parameters considered in this study are global precipitation, Aerosol Optical Depth (AOD), and Surface Air temperature. Figure 8 shows the trend of those parameters from 2002 to 2012. It is shown that the precipitation has two significant peaks, one in 2006 and the other in 2012 (the highest); its lowest value was in 2009. Temperature had its peak in 2009 and the lowest value was in 2012. AOD's values decreased from 2003 to 2012 with 2003 and 2007 as the peak years. Statistical analyses done through SPSS IBM provided the following means for precipitation (2.21), OAD (0.30) and Surface Air Temperature (33.96) with respective standard deviation of 1.01, 0.09, and 2.03. The correlations are negative for precipitation – AOD (-0.343) and highly negative for precipitation – air temperature (-0.862). AOD and air temperature are lowly positively correlated with (0.138).

We can conclude that precipitation and surface air temperature evolve inversely; the higher the precipitation, the lower the surface air temperature and vice versa. Likewise for the relationship between precipitation and AOD.

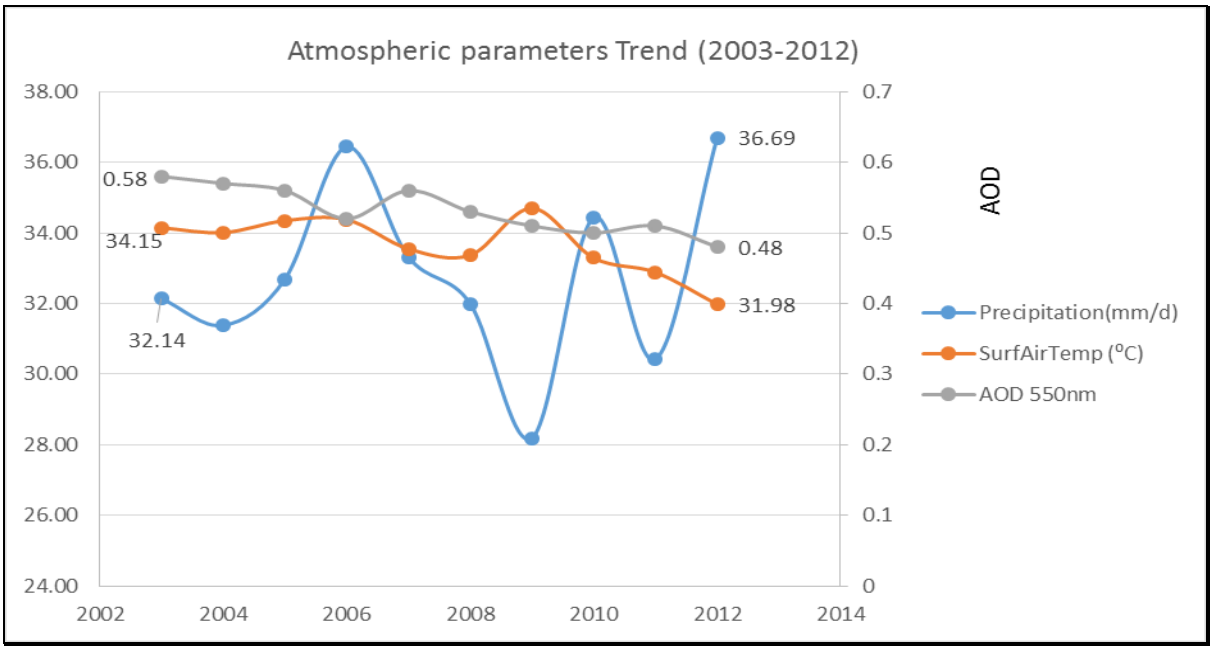

Figure 8. Atmospheric Parameters Graph from 2003 to 2012

4.1.1. GPCP

Figure 9 shows the evolution of the global precipitation in our area of study from 1980 to 2012. There are annual and decadal variations.

The decade 1980 – 1990 was the dryest. The year 1980 was wetter, then the precipitation continuously decreased until 1984 (dryest). The recovery was weak until 1988. The early and the late 1980s were relatively wetter with peaks in 1980 and 1988, but the mid-1980s was dryer; that period corresponds to the 1980s drought. The oscillation high – low precipitation with negative anomalies continued until 1995.

The decade 1990 – 2000 had an almost constant situation with a peak in 1999 except for the years 1990, 1993, and 2000 showing negative anomalies. In the last decade, from to 2000 to 2012, precipitation has increased with positive anomalies, exception for 2009 and 2011.

The years of peak precipitation from 1980 to 2012 were: 1988, 1999, 2006, and 2012. The years of lowest precipitation were: 1983, 1984, 1987, and 2009. The other years are intermediate.

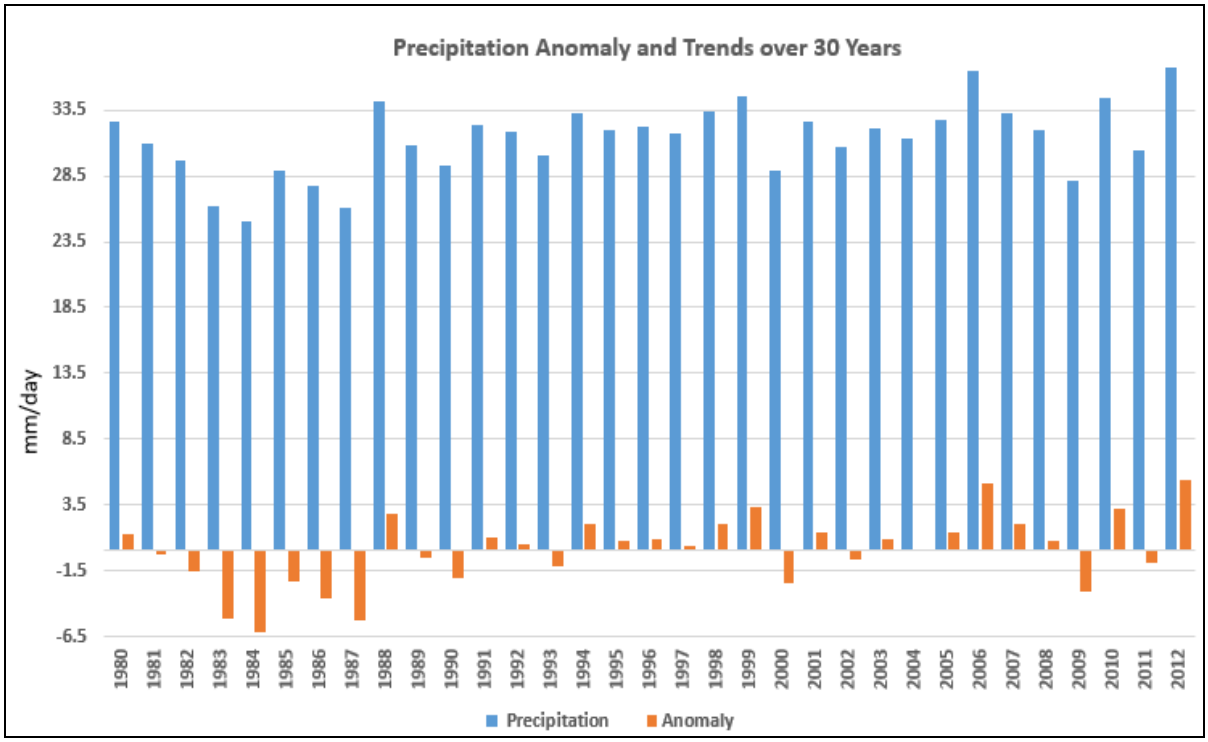

Figure 9. Precipitation and Anomaly Trends from 1980 to 2012

Ultimately, the years of highest precipitation (above 30 mm/year) were 1980, 1988, 1999, 2006, and 2012. Those of lowest precipitation (below 25 mm /year) were 1983, 1984, and 1987. The driest years are in the 1980s; the wettest years are in the late 1990s and 2000s.The precipitation trend increased from 1980 (28.5 mm) to 2012 (33.5 mm).

Figure 10 is the one of global precipitation annual cycle in millimeter per day, from 1980 to 2012. Precipitation was insignificant in January, with about 0.08 mm/day, gradually increased to reach its highest amount in August with about 7mm/day, then decreased to 0.07 mm/day in December.

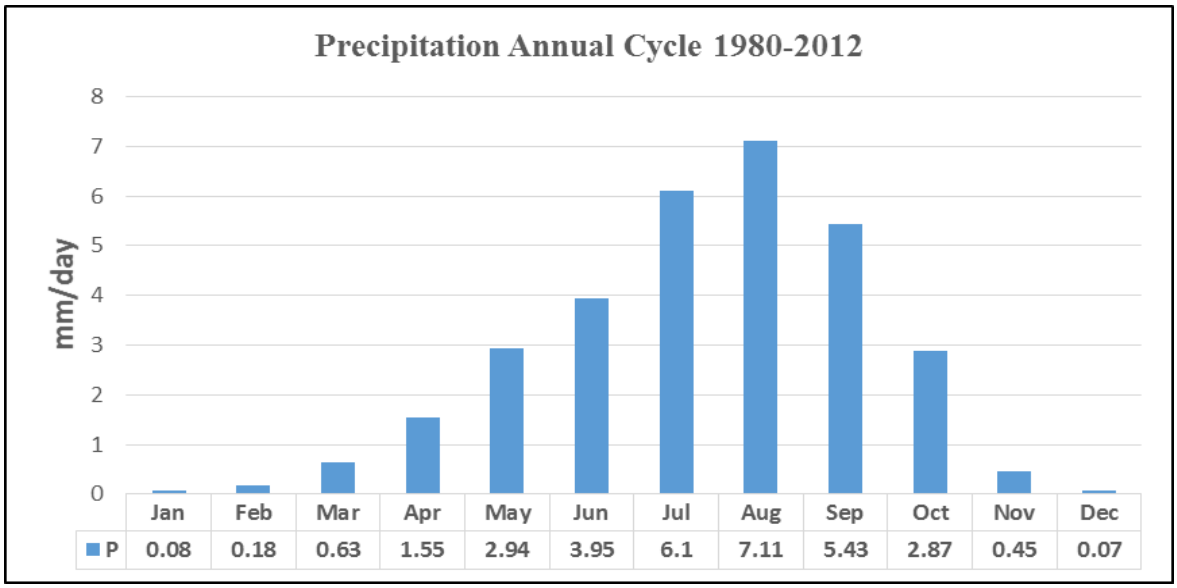

Figure 10. Precipitation Annual Cycle from 1980 to 2012

The global precipitation krigging interpolation is shown in figure 11. The mean center and the median center of distribution are not superposed to each other. That means that global precipitation distribution is not normal. The histogram of the global distribution with a skewness of 0.23; the skewness value is positive and between -1/2 and +1/2. That means that the global precipitation distribution is positively skewed and approximately symmetric (Bulmer, 1979). The Normal QQPlot distribution of the global precipitation confirms that the precipitation does not follow the line of normal distribution.

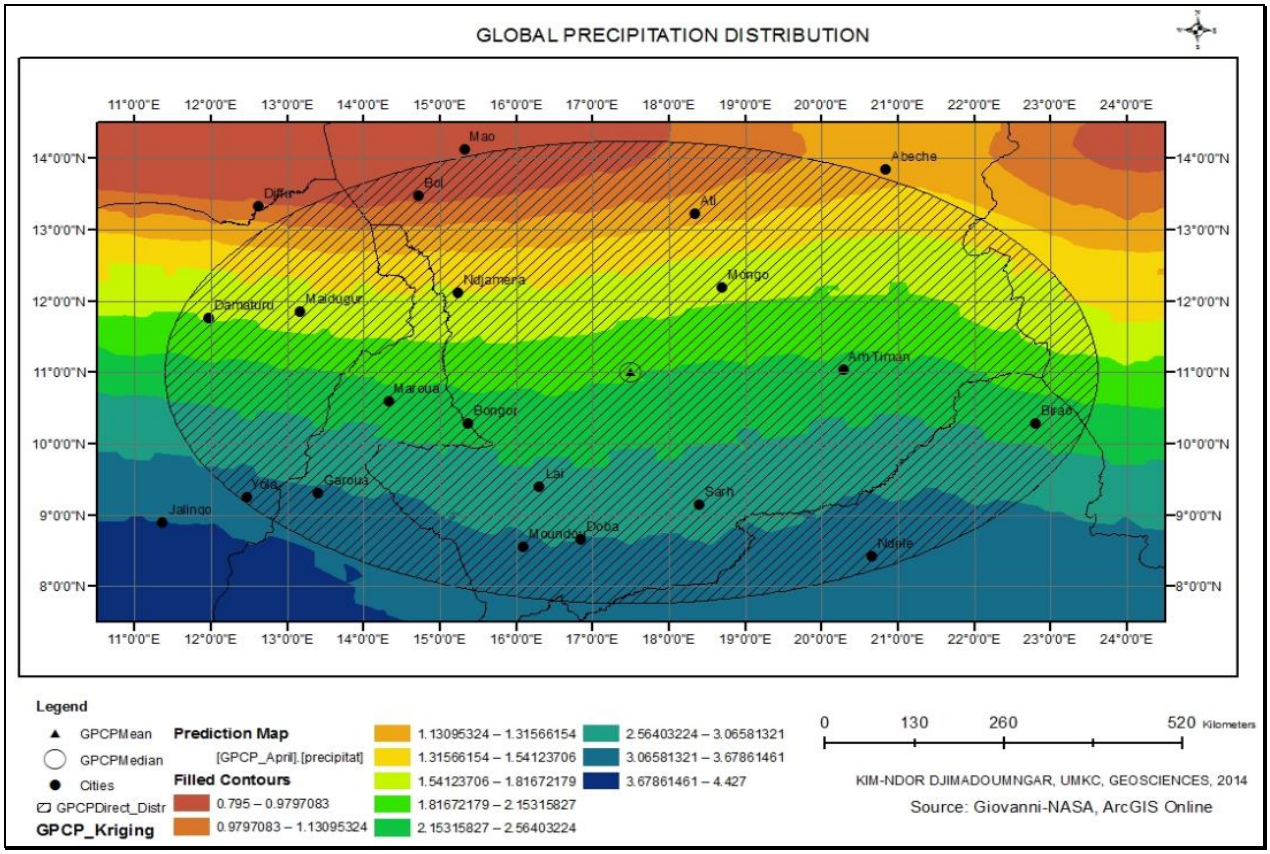

Figure 11. Precipitation Distribution Map

4.1.1.1. Station Data Analysis

The figure 12 shows the location of weather stations in Chad for which we have found data, especially rainfall. The names and geographic coordinates of those locations are:

- Am-Timan: Latitude 11.03, Longitude 20.28, Elevation: 412
- Moundou: Latitude 8.56, Longitude 16.08, Elevation 415

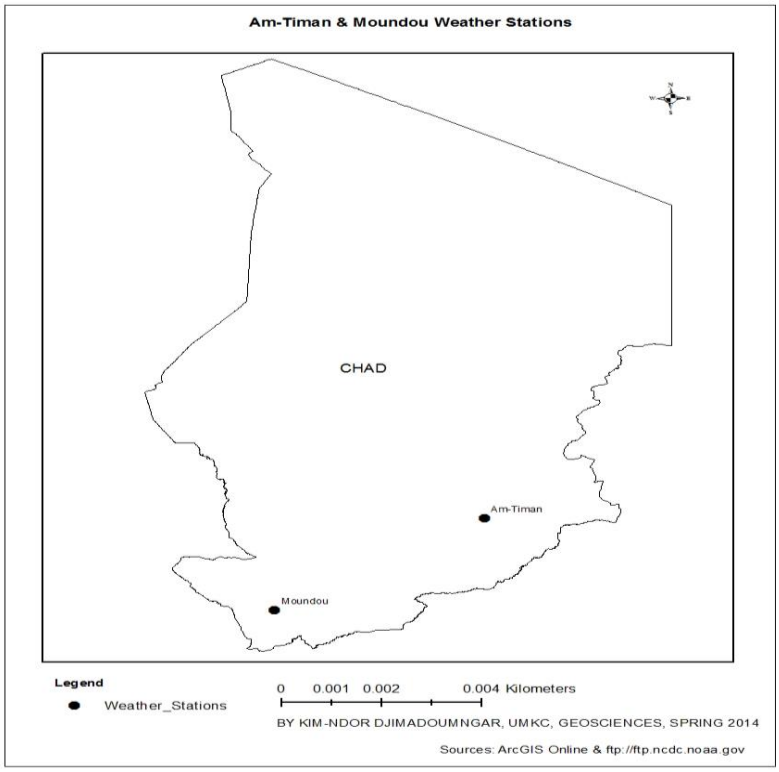

Figure 12. Weather Stations Locations maps

Figure 13 below shows the monthly rainfall in the two weather station mentioned above. As we see in the graph, rainfall distribution was unequal throughout the year. The rainy months extended from April to October with the maximum of the rainfall received between June and September. For instance, the computation of the total rainfall at the station of Moundou from May to October was about more than 500 mm, the one of Am-Timan was about 350 mm. The station of Moundou located furthermore in the south received more rainfall than the one of Am-Timan showing a gradient of precipitation. This result needs to be confirmed by another study because our study's data had a lot of gaps.

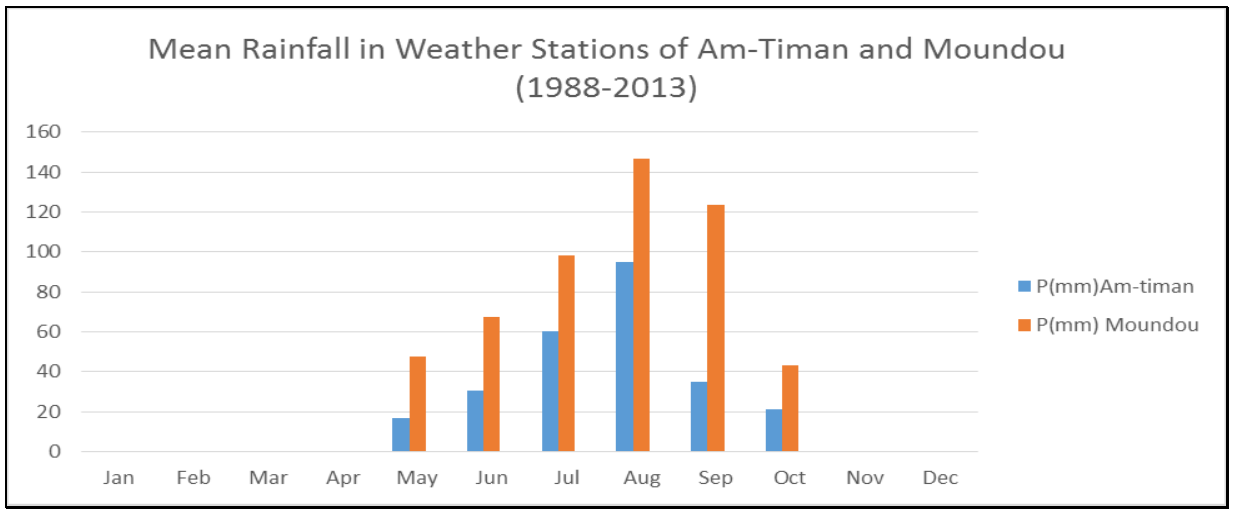

Figure 13. Monthly Rainfall in Weather Stations

4.1.1.2. Composite Analysis Wetter / Dryer Years

The observation of the global precipitation trend graph let us figure out that the wetter years were 1988, 1999, 2006, and 2012, and the dryer years were 1983, 1984, 1987, and 2009. Figure 14 shows those years indicated by stars. The composite analysis is based on those years for all the parameters studied in this document.

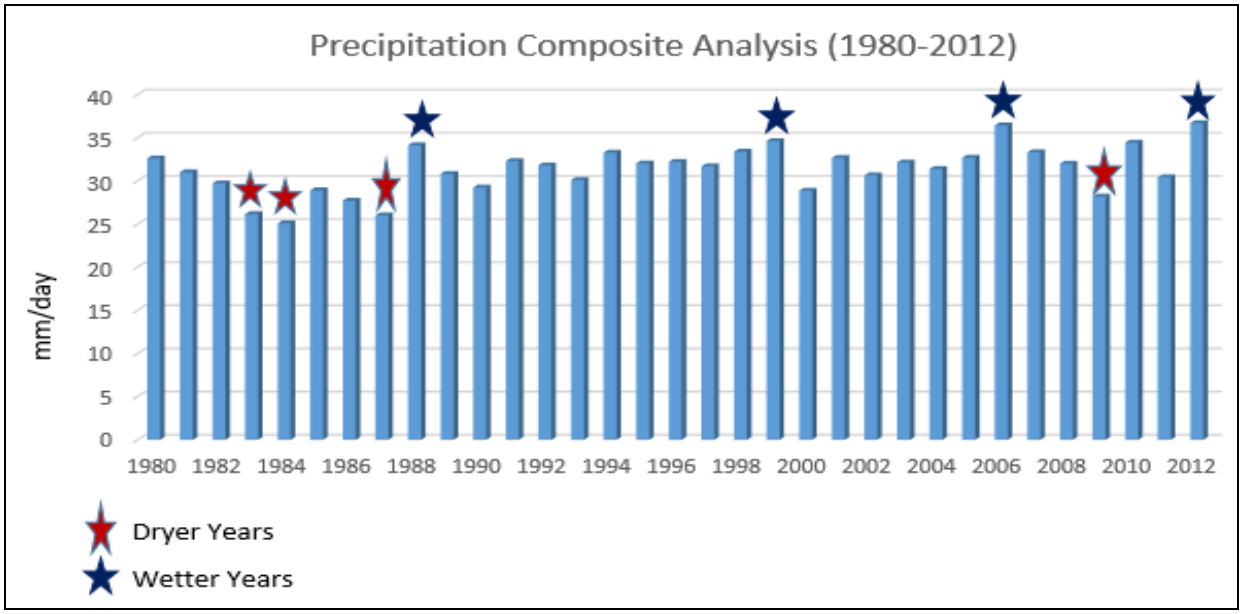

Figure 14. Precipitation Wetter and Dryer Years Graph

4.1.1.2.1. Cloud Composite Analysis

Figure 15 shows the cloud fraction and precipitation trend from 2000 to 2012. The observation clearly lets us see that the precipitation pattern follows the cloud fraction patterns. All the cloud fractions (Day, Day &Night, and Night) have lower values in January (~0.2 - ~0.3). Those values continuously increase to reach their peaks in August (~0.6 – ~ 0.85) and decrease to ~0.9 to ~0.2 in December. In the meantime, precpitation has its lower values in January and December (~0.07) and reaches its optimum in August with about 7 mm/day, then decreases to 0.07 in December.

In addition to the patterns, the statistical analysis gave the following information on the relationship between cloud fractions and precipitation. Precipitation is highly and positively correlated with all the cloud fractions. But the correlation is higher with cloud fraction Day & Night (0.928) than with cloud fraction Night (0.918) and cloud fraction Day (0.886).

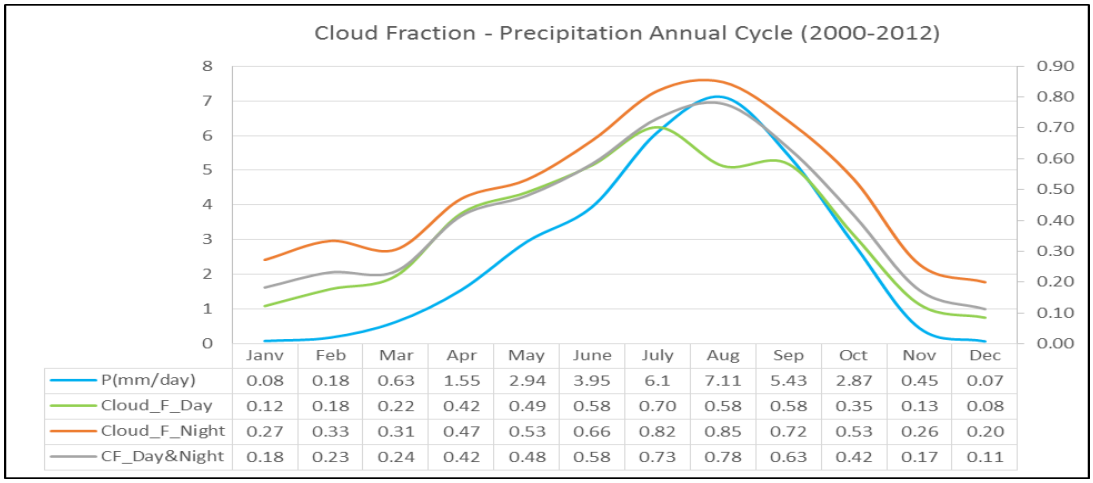

	Janv	Feb	Mar	Apr	May	June	July	Aug	Sep	Oct	Nov	Dec
P(mm/day)	0.08	0.18	0.63	1.55	2.94	3.95	6.1	7.11	5.43	2.87	0.45	0.07
Cloud_F_Day	0.12	0.18	0.22	0.42	0.49	0.58	0.70	0.58	0.58	0.35	0.13	0.08
Cloud_F_Night	0.27	0.33	0.31	0.47	0.53	0.66	0.82	0.85	0.72	0.53	0.26	0.20
CF_Day&Night	0.18	0.23	0.24	0.42	0.48	0.58	0.73	0.78	0.63	0.42	0.17	0.11

Figure 15. Cloud Fraction - Precipitation Annual Cycle

Figure 16 shows the average cloud amount during the wetter (16.a) and dryer (16.b) years of the area of study.

In the wetter years, all the cloud amounts were between ~0.67 to ~0.7 in June. The cloud fraction Night amount reached ~0.89 in July, decreased to ~0.86 in August and ~0.82 in September. Then, the cloud fraction Day & Night amount increased to ~0.8 in July and is almost constant until August and then decreased to ~0.7 in September. Finally, for the cloud fraction Day, the amount increases to ~0.77 in July, reached ~0.8 in August and decreased to ~0.62 in September.

In the dryer years, cloud fraction amounts were ~0.57 (Day and Day & Night) and 0.65 (Night) in June. The cloud fraction Night amount increased to 0.8 in July, reached 0.85 in August and decreased to ~0.66. The cloud fraction Day & Night reached 0.7 in July, 0.75 in August and decreased to ~0.55 in September. For the cloud fraction day, the values were 0.67 in July, 0.75 in August and 0.53 in September.

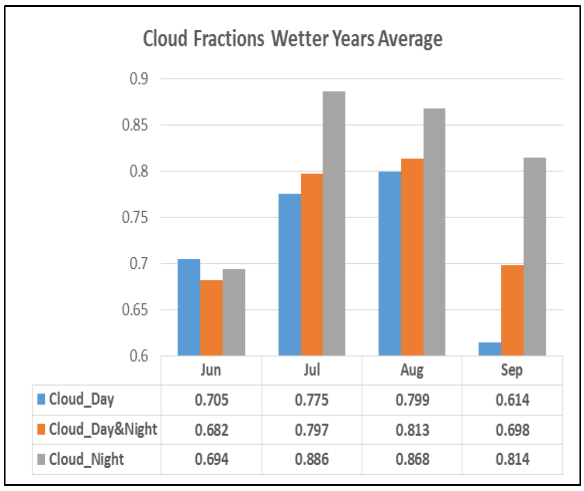

16.a

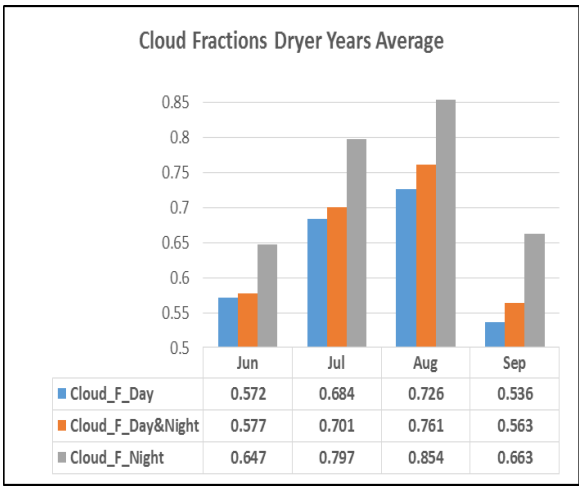

16. b

Figure 16. Cloud Fraction Composite Analysis Graph

The calculations give approximately the following values as the difference between a wetter and dryer July and August: The percent changes of cloud fractions amount from dryer to wetter are shown in the table 1 below.

The difference in an average cloud Night amount between June in dryer years and June and in wetter years is 7 %, the one of July is 11%. A August in dryer and wetter years had relative insignificant difference (1%) whereas the difference between September in dryer and wetter years was almost 23%.

For the cloud fraction Day & Night, the amount in June in wetter years was 18 % greater than the one of June in dryer years. The month of July had 13% more clouds in wetter years than in dryer ones. August and September in wetter years were respectively almost 7 and 24% more cloudy. Finally, for the cloud fraction Day, June in wetter years was 23% cloudy than June dryer years. July, August, and September in wetter years were respectively, approximately 13, 10, and 14 % more cloudy.

Table 1. Cloud Fractions Percent Change from Dryer to Wetter Years

	Cloud_Night (%)	Cloud_Day&Night (%)	Cloud_Day (%)
Jun	7.26	18.20	23.25
Jul	11.17	13.69	13.30
Aug	1.64	6.83	10.06
Sep	22.78	23.98	14.55

Ultimately, it is clear through figure 16 (a & b) that the amount of clouds in wetter years was greater than the one of dryer years. It is also shown that the cloud fraction Night was greater than the cloud fractions Day & Night, which were also greater than the cloud fraction Day.

The comparison of monthly values per type of cloud gives the following obervations: In June, the cloud Day amount difference (23%) was greater than cloud Day & Night difference

(18%), which was greater than cloud Night difference (7%). In July, there was no significant difference between the cloud fraction amounts. In August, the cloud Day amount difference (10%) was greater than the Day & Night amount difference (7%) and Night amount difference (1.6%). Cloud Night and Day & Night differences were almost equal in September (~23%) and greater than the cloud day amount difference (14%).

4.1.1.2.2. Winds Speed Composite Analysis

The Northward winds at 250 hPa (V250) and Eastward winds at 250 hPa (U250) both had negative signs but at different magnitudes according to the figures 17 a and b; so, the Northward wind at 250 hPa blew from north to south and the Eastward wind at 250 hPa blew from east to west.

For the V250 wind, speed values were almost greater in the wetter years than in the dryer years with 0.26 Vs. -0.2 in June, 0.93 Vs. -0.89 in July, and 1.23 Vs. 1.16 in August; however, we see a change with the wind speed in September of the wetter year (0.34) smaller than the one of the September in dryer years (0.67). The wind speed trend is almost the same for the U250 wind. Wetter months had higher wind speeds than the dryer months of June (5.48 Vs. 4.23), July (12.42 Vs. 11.64), August (12.83 Vs. 11.33), and September (7.83 Vs. 6.52).

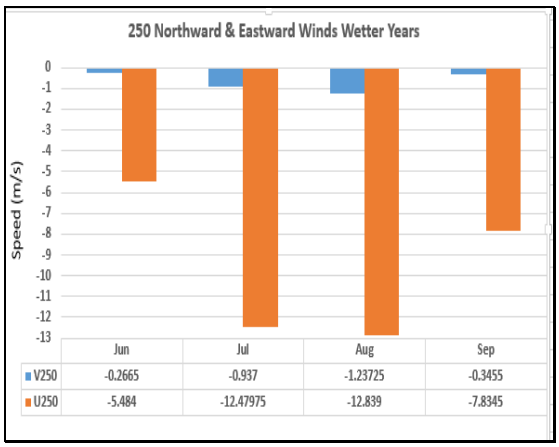

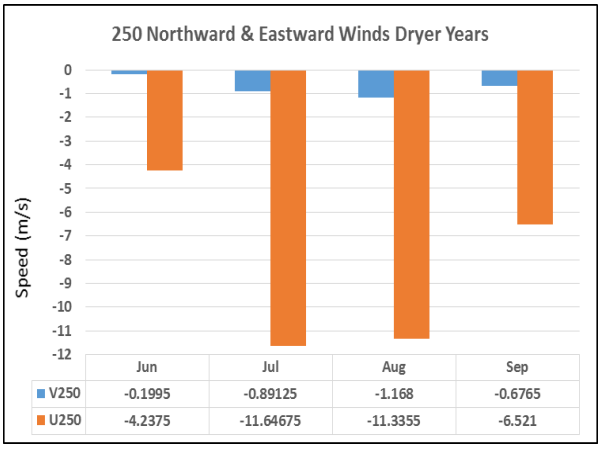

17.a 17.b

Figure 17. V250 & U250 Winds Composite Analysis Graphs

Generally, figure 17 above show that 250 Northward wind speed increased from June, reached its highest value in August and then decreased in September for both wetter and dryer years. The 250 Eastward wind speed increased from June, reached its highest point in August (wetter years) / July (dryer years) then decreased in September for both wetter and dryer years.

Close examination of graphs 18 a and b lets us see that the V850 wind speed was positive in both wetter and dryer years, meaning a south – north direction. Speed values were greater in dryer years than in wetter for Jun (-0.8 Vs. -0.4), July (-1 Vs. 0.8), and August (0.8 Vs. -0.7). The situation changed with September's wind speed in wetter years (0.4) higher than the one of September in dryer (-0.28).

The U850 presented two situations:

- wind speeds in June and September were negative in both wetter and dryer years, indicating an east – west direction with wind speed in June of wetter years (0.68)

smaller than the one in June of dryer years (1), and the wind speed in September of wetter years (1.3) smaller than the one in September of dryer years (2);

- wind speeds in July and August were positive in wetter years - west to east direction - , with respectively about 1.4 and 1.2 m/s; negative – east to west direction - in dryer years with about -0.11 and -0.13 m/s, respectively.

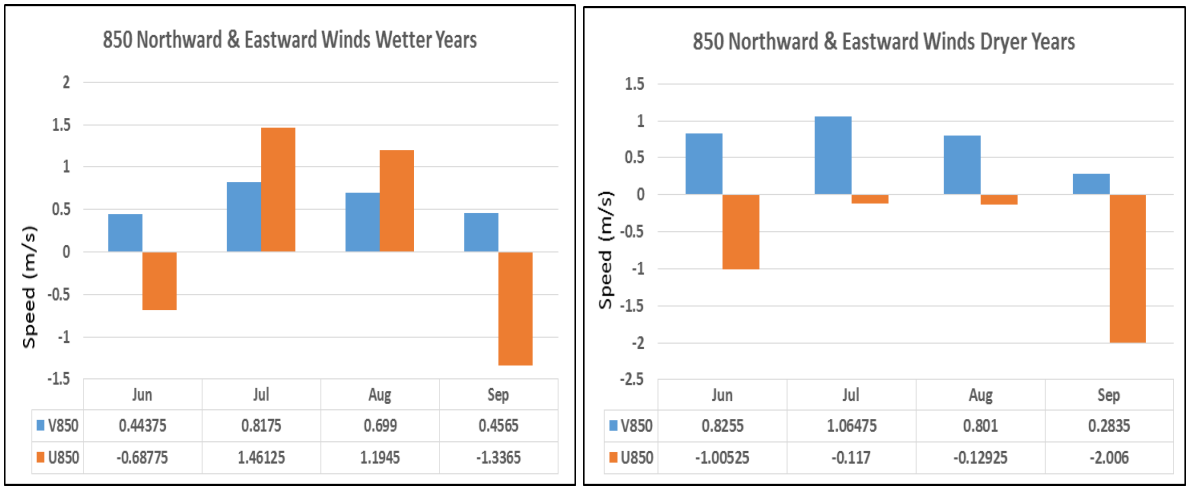

18.a 18.b

Figure 18. V850 & U850 Winds Composite Analysis Graphs

Generally, we see through figure 18 that the V850 wind blew from south to north and that its speed increased from June, reached its peak in July and then decreased until September for both wetter and dryer years.

The U850 wind speed increased from the direction east - west in June, reached its highest value in July in the direction west - east, while maintaining the same direction in August, and then decreased in the east – west direction in September for the wetter years. For dryer years, the wind blew from east to west during all the months with the peak value in September.

It is expected higher wind speeds at 250 and 850 hPa during the wetter years to bring moisture from the ocean to the continent, but this study shows that wind speeds were lower

in wetter years than in dryer years. This confirms the suggestion of Nicholson (2009) for which much of the moisture in the monsoon layer is recycled water deriving from local evaporation over the continent, rather than transport from Atlantic. Consequently, the precipitation regime over West Africa is controlled by atmospheric dynamics rather than low-level moisture.

4.1.1.2.3. Specific Humidity Composite Analysis

Specific humidity and precipitation have almost the same patterns. Precipitation, specific humidity at 850 hPa (Q850, monsoon), and specific humidity at 500 hPa (Q500, AEJ) decreased from their higher values in 1980 to lower values in 1984. Then, there was an increase in 1985 and a decrease in 1986 and 1987. The year 1988 had peak values followed by fluctuations between higher and lower values until 1999 when it had other peaks. The values fell again and fluctuated until 2006 where there was another peak. Then, another fluctuation of relatively lower magnitude started after 2006 and finished in 2012 with another peak.

The close observation of figure 19 below lets us clearly see the precipitation, Q850, and Q500 have all 1983, 1984, 1987, 2000, and 2009 as years of lowest values, and 1980, 1988, 1999, 2006, and 2012 as years of highest values.

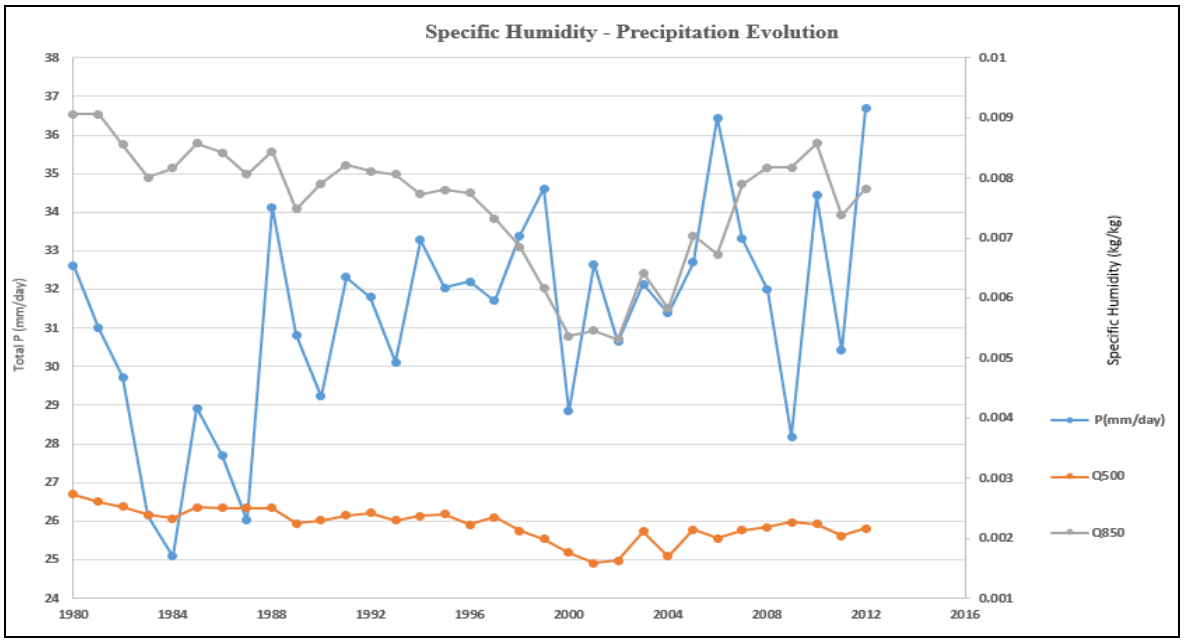

Figure 19. 500 & 850 Specific Humidity – Precipitation Trends 1980 to 2012

In addition to the general trend from 1980 to 2012, the composite analysis specific wetter /dryer years was one on the specific humidity at 850 hPa (Q850) and 500 hPa (Q500) for the rainy season. It provided the following information in figures 20 a and b:

Q850 had greater values in June (0.0115), July (0.0112), and September (0.011) of wetter years than in June (0.011), July (0.011), and September (0.010) of dryer years . The situation inversed for August (0.0113) of dryer years that had greater value than the August (0.012) wetter ones. Then, Q500 in wetter years had greater amounts in June, July, and almost the same value in August, and a greater amount in September. Finally for Q500, all the wetter months had greater amount than the dryer ones.

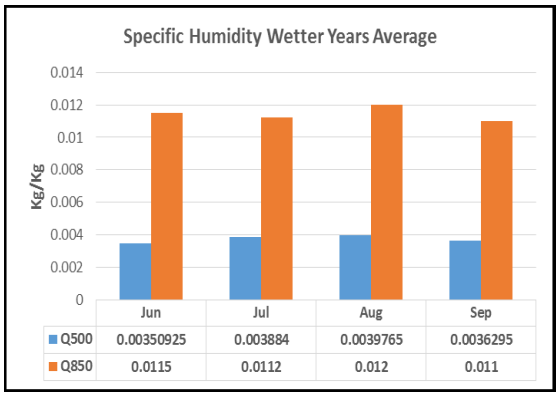

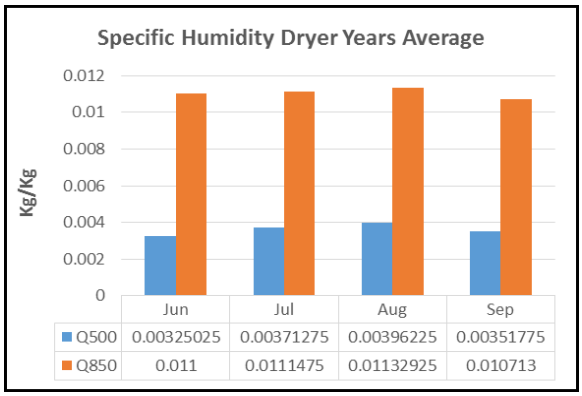

20.a 20.b

Figure 20. Specific Humidity Composite Analysis Graph

The table 2 shows the specific humidity at 500 and 850 (Q500 & Q850) percent change from dryer to wetter years. Both of the types of humidity have higher amount in wetter years than in dryer. Specifically, the specific humidity at 500 hPa was higher in wetter years than in dryer ones at about 8% in Jun, 4.6 in July, 0.36% in August, and 3.18 % in September. Q850 in wetter years was higher than Q850 in dryer years at about 4.5% in Jun, 0.5 in July, 6% in August, and 2.7 % in September.

Table 2. Q500 & Q850 Composite Analysis Percent Change

	Q500 (%)	Q850 (%)
Jun	7.97	4.55
Jul	4.61	0.47
Aug	0.36	5.92
Sep	3.18	2.68

It is observed in this study that the specific humidity was higher in wetter years than in dryer years despite the fact that the wind speeds presented an inverse situation (wind speeds

were lower in wetter years than in dryer years). This situation confirms once more the conclusion made by Nicholson in 2009 stating that much of the moisture in the monsoon layer is recycled water deriving from local evaporation over the continent, rather than transport from Atlantic.

4.1.2. Aerosol Optical Depth

The aerosol optical depth directional distribution and krigging interpolation revealed an asymmetric distribution for mean and median center were not superposed (figure 21). The distribution was highly skewed with a skewness of 1.5; a skewness less than -1 or greater than +1: means distribution is highly skewed (Bulmer, 1979). The Normal QQPlot showed a non-linear distribution of aerosol optical depth along the line of normal distribution. The krigging interpolation shows an almost southwest – northeast distribution of the aerosols.

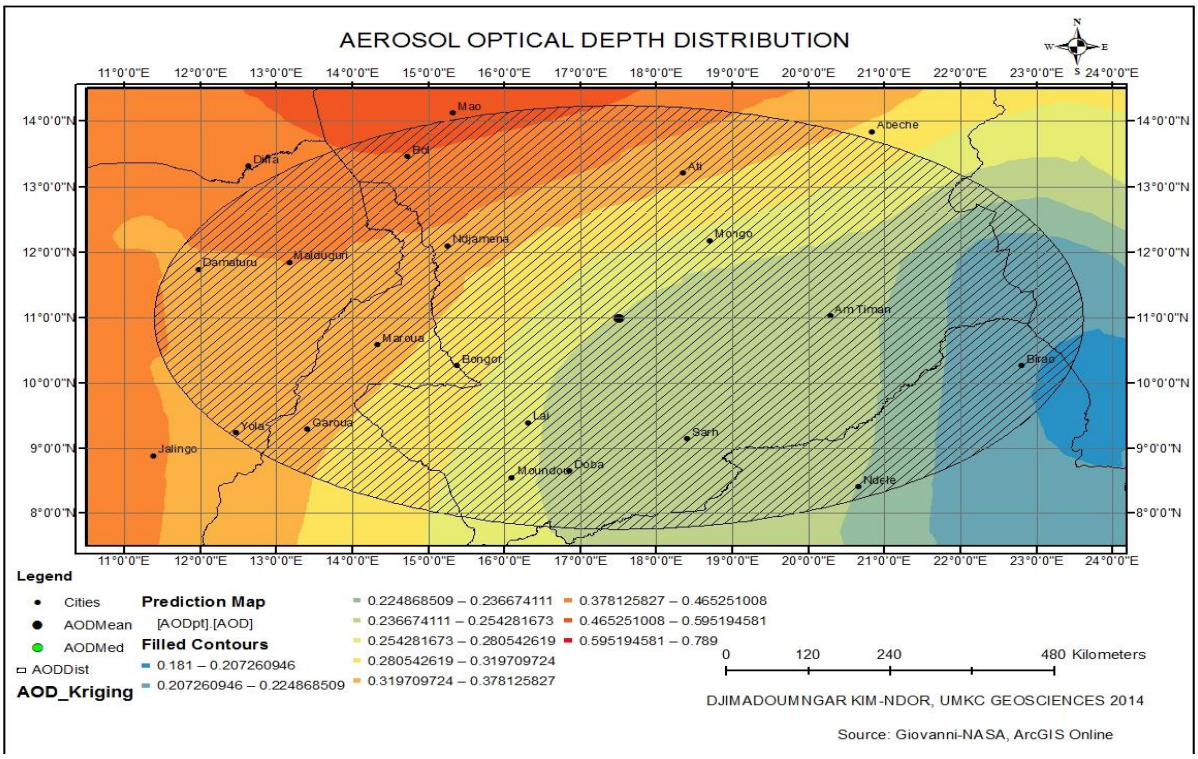

Figure 21. Aerosol Optical Depth Distribution Map

Figure 22 shows the average monthly AOD and cloud fraction values from 2000 to 2012. The peak value of AOD in March was 0.45. That value progressively decreased to reach the lowest in December (0.17).

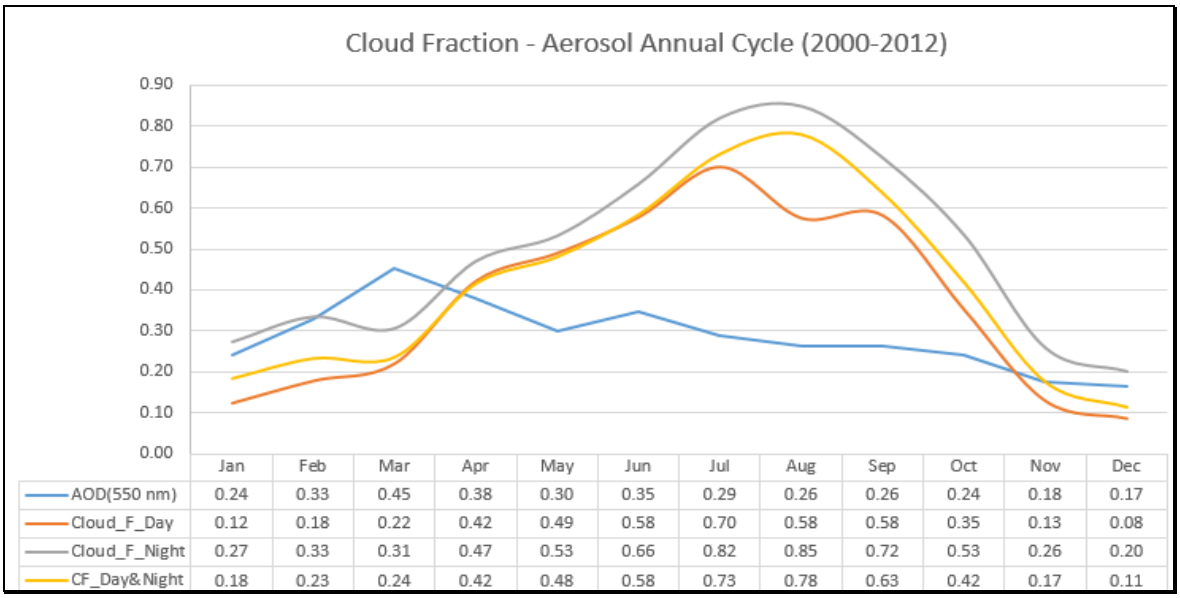

	Jan	Feb	Mar	Apr	May	Jun	Jul	Aug	Sep	Oct	Nov	Dec
AOD(550 nm)	0.24	0.33	0.45	0.38	0.30	0.35	0.29	0.26	0.26	0.24	0.18	0.17
Cloud_F_Day	0.12	0.18	0.22	0.42	0.49	0.58	0.70	0.58	0.58	0.35	0.13	0.08
Cloud_F_Night	0.27	0.33	0.31	0.47	0.53	0.66	0.82	0.85	0.72	0.53	0.26	0.20
CF_Day&Night	0.18	0.23	0.24	0.42	0.48	0.58	0.73	0.78	0.63	0.42	0.17	0.11

Figure 22. Cloud Fraction - Aerosol Optical Depth Trend

The composite analysis of AOD shown in figure 23 let us see that AOD was higher in June in the wetter (about 0.37) than in June in the dryer (about 0.27). July of the wetter years had about 0.27 compared to July in the dryer years (0.24). August in the wetter years had a greater amount of AOD (~0.25) than August in the dryer years (0.18). The situation changed in September where dryer years had a greater amount (0.25) than the wetter years (~0.22).

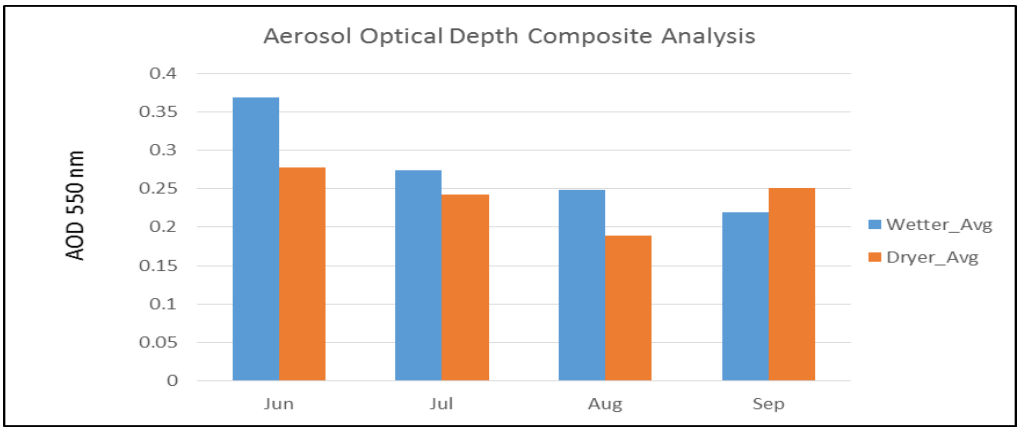

Figure 23. Aerosol Optical Depth Composite Analysis

The AOD percent changes from June to September are shown in table 3. As we can see, AOD was higher in wetter years than in dryer years at about 32% in June, 12% in July, and 32% in August. The situated changed in September where the dryer AOD years was higher than the wetter one at about 13%.

Table 3. AOD Composite Analysis Values and Percent Change

	AOD_Dryer	AOD_Wetter	% Change
Jun	0.278	0.3685	32.55
Jul	0.243	0.2735	12.55
Aug	0.189	0.249	31.75
Sep	0.251	0.219	-12.75

4.1.3. Surface Air Temperature

Figure 24 shows surface air temperature trend from 2003 to 2012. Temperature was about 34.2°C in 2003, it decreased in 2004 to 34°C, increased 2005 and 2006 to reach about 35.3 and 34.4, respectively. Then we observe a decrease in 2007 (33.5°C) and 2008 (33.4°C). The

maximum temperature was reached in 2009 with about 35.7°C. From there temperature continuously decreased to reach its lowest level in 2012 with less than 32°C. The figure lets us clearly see that the beginning of 2000s is hotter that its end except for 2009, and since 2010 temperature is decreasing.

Compare with the precipitation composite analysis (figure 10) we find out that 2009 with the highest temperature was one of the dryer years, and 2012 with the lowest temperature was one of the wetter years. That shows the inverse relationship between precipitation and temperature.

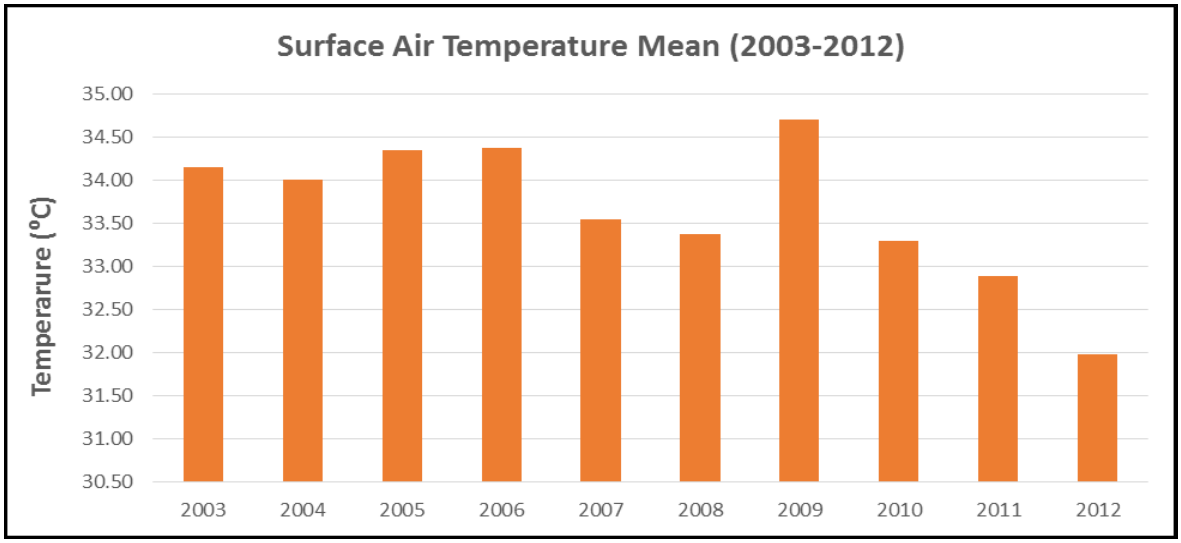

Figure 24. Surface Air Temperature Mean (2003-2012)

The annual cycle of the surface air temperature is shown in figure 25. Temperature progressively increased from January with about 30^0C to reach its highest values in April and May (~35.1^0C). Then it gradually decreased to reach its lowest value in August with about 28 ^{0}C. From there, another gradual increase was observed to get to another peak in November with about 34^0C followed by a decrease in December (~32^0C).

Compare with precipitation annual cycle we notice that August with the highest precipitation corresponds to the lowest temperature. That once more confirm the inverse relationship between precipitation and temperature.

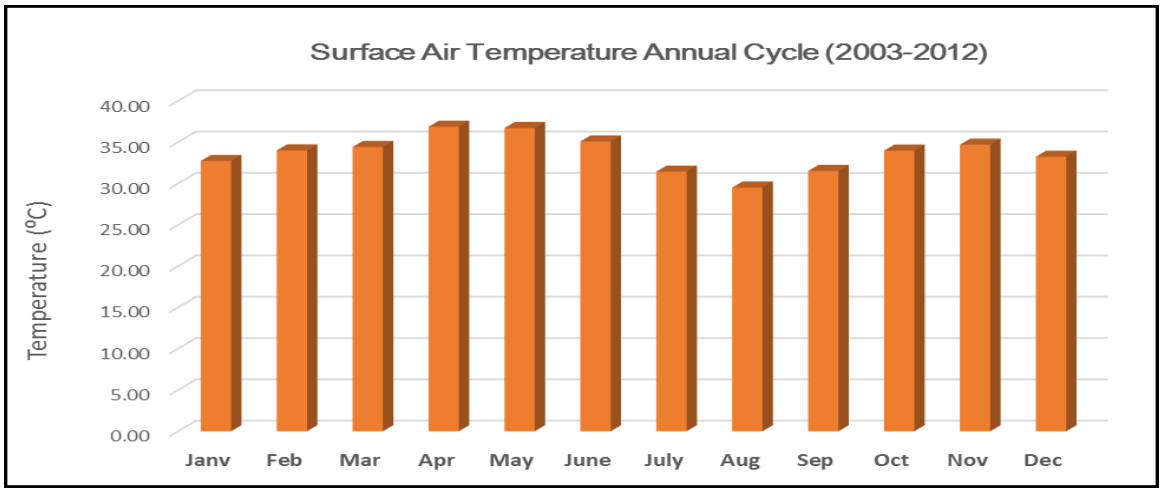

Figure 25. Surface Air Temperature Annual Cycle (2003-2012)

The krigging interpolation realized using surface air temperature data (figure 26) revealed the following information:

- There is a gradient of surface air temperature from the south to the north of the Sahel. The temperature ranges from 28 to 32˚C are from 7˚N to 10˚N. From 10˚N to 12˚N, the temperatures range is 33 to 34˚C. The temperature of 34˚C continues towards the north between 13.5˚E to 15.5˚E. From 12 to 14.5˚N, the temperature ranges from 34.75 to 36.76 ˚C. The latter temperature (the hottest) is distributed around from 13 to 14.5 ˚N and from 19 to 21.5˚E;
- The positions of the Mean and Median centers show an asymmetric distribution (figure 22). The histogram shows a skewness of -0.47, negative value and between -1 and -1/2, indicating a negatively and moderately skewed distribution (Bulmer, 1979).

The Normal QQPlot diagram shows the distribution of temperatures along the normal line of distribution; this confirms the skewed distribution compare to the normal. The values are below the normal distribution in the beginning, become greater, and decrease again to be lower than the normal distribution.

- Figures 11 and 26, put beside each other, show that the highest the precipitation is, the lowest the temperature is and vice versa.

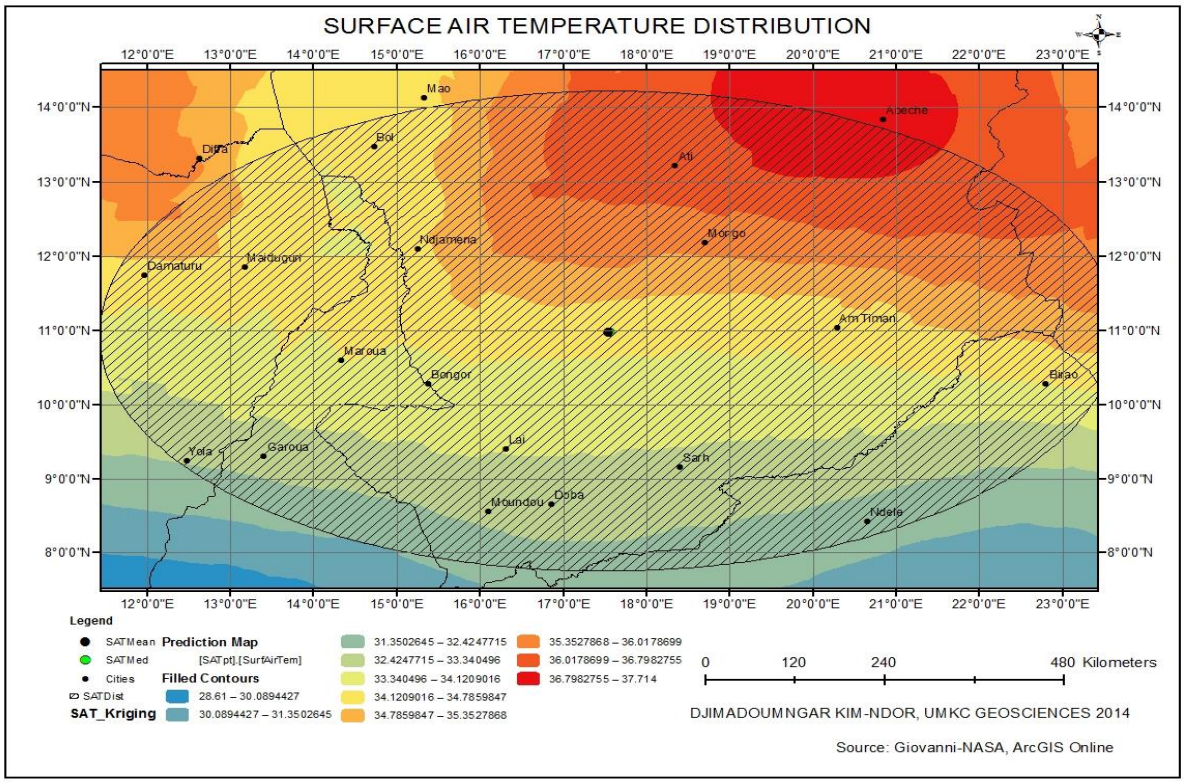

Figure 26. Surface Air Temperature Distribution Map

The composite analysis (figure 27) clearly shows that the temperature is higher in dryer years than in wetter years during the rainy season. The increase in temperature is expressed in percentage and recorded in table 4. Temperatures were about 7.5, 3.4, 7, and 6.4% higher in June, July, August and September in dryer years than in the same months in wetter years.

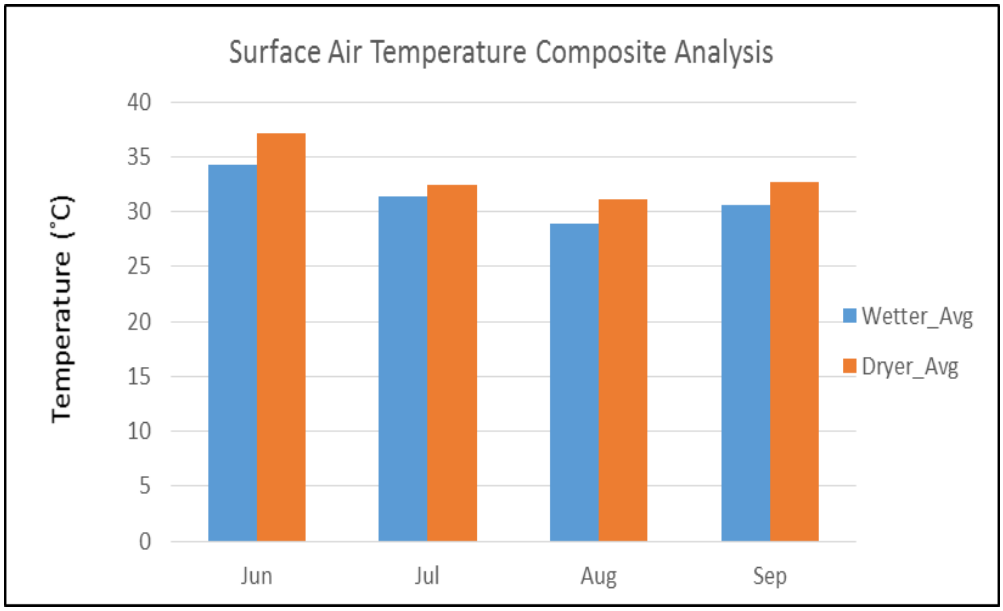

Figure 27. Surface Air Temperature Composite Analysis

Table 4. Surface Air Temperature Composite Analysis Values and Percent Change

	Dryer_Avg (˚C)	Wetter_Avg (˚C)	% Change
Jun	37.09	34.31	-7.49
Jul	32.44	31.35	-3.37
Aug	31.08	28.95	-6.84
Sep	32.70	30.61	-6.39

Annex I summarizes the relationships of some atmospheric parameters.

V250 and V500 had negative and low to moderate correlation with all the types of cloud fractions while V850 had positive and low correlation with them (Cloud Fraction Day, 0.276; Cloud Day & Night ; 0.0.256; Cloud Night ,0.233). In fact, V250 values were -0.223 with Cloud Fraction Day, -0.248 with Cloud Fraction & Night, and -0.264 with Cloud Fraction Night. V500 correlation values were -0.046 with Cloud Fraction Day, -0.043 with Cloud Fraction Day & Night and -0.031 with Cloud Fraction Night. In addition, V250 was negatively and lowly correlated with precipitation (-0.231), Q250 (-0.108), considerably with Q500 (-0.641), Q850 (-0.555) and positively and lowly correlated with SAT (0.140).V500 was negatively lowly correlated with AOD (-0.077) and precipitation (-0.32), moderately with Q250 (-0.330) and positively lowly correlated with SAT (0.127), Q500 (0.181) and Q850 (0.05). V850 was positively lowly correlated with AOD (0.036), precipitation (0.279), considerably with Q250 (0.628), Q500 (0.679) and Q850 (0.636) and negatively lowly correlated with SAT (-0.219).

So, for Northward winds, V250 and V500 had negative and low correlation with all the cloud fractions whereas V850 had positive and low correlation. All the cloud fractions are negatively lowly correlated with AOD. The specific correlation values were -0.117 for cloud Day, -0.263 for cloud Day & Night, and -0.322 for cloud Night. They were all negatively considerably correlated with U250, specifically at -0.525, -0.557, -0.568 for cloud fraction day, day & night, and night, respectively. With U500, cloud fractions were negatively lowly correlated with -0.144, -0.150, -0.083 for day, day & night and night, respectively whereas the correlation coefficients with U850 for the same types of cloud were -0.037, -0.064, and -

0.083. So, all the cloud fractions types had negative and low to moderate correlation with Eastward winds.

We can also see that all the cloud fractions had positive and significant correlation with specific humidity at 850 hPa (Q850) with 0.748, 0.773, and 0.762 and specific humidity at 500 hPa (Q500) with 0.585, 0.607, and 0.596 for cloud fractions day, day & night, and night, respectively. On the contrary, there correlations were negative and low with specific humidity at 250 hPa (Q250) for cloud fractions day & night (-0.017) and night (-0.031), and positive and low cloud fraction day (0.017). So, the correlation was positive and considerable between cloud fractions and Q850 and Q500 and negative (day & night, and night) to positive (day) and low with Q250.

All the cloud fractions had negative and considerable correlation with SAT. The correlations values were -0.828, -0.874, and -0.879 for cloud fractions day, day & night, and night, respectively. On the contrary, they had positive and considerable correlation with precipitation; 0.881, 0.932, and 0.929 for cloud fractions day, day & night, and night, respectively.

Precipitation had negative and significant correlation with AOD (-0.344). It had negative low (U500, -0.149; U850, -0.089) to moderate (U250, -0.555) correlation with the Eastward winds; negative and considerable correlation with SAT (-0.862). We also observed a negative and low correlation with and Q250 (-0.009) and a positive and considerable correlation with Q500 (0.605) and Q850 (0.737). It naturally had positive and considerable correlation with all the cloud fractions with 0.881, 0.932 and 0.929 for cloud fractions day, day & night, and night, respectively. SAT was positively lowly correlated with AOD (0.139). It had a positive low (V250, 0.14; V500, 0.127) and negative low (V850, -0.219) correlation with Northward

winds. The correlations with the Eastward winds were positive low (U500, 0.024; U850, 0.079) to moderate (U250.433). Its correlations with specific humidity were negatively low (Q250, -0.025) to considerable (-Q500, 0.599; Q850, -0.738).

4.2. Land Parameters

The land parameters included in this study are evapotranspiration, soil moisture, and Normalized Difference Vegetation Index (NDVI). Figure 28 shows the trend of the first two parameters and total precipitation from 1980 to 2012.

The evapotranspiration curve shows a succession of the same value presenting a plateau from 1980 to about 1994 where the value dropped from 0.00003 to 0.0000009. Then the value increased again around 1996 and 1997 and decreased again to reach 0.000021 and was constant until around 2007/ 2008. In 2009, there was an increase to the plateau until 2012. Based on the curve seen in the graph, we can say that the evapotranspiration did not really follow the global precipitation pattern although the part after 2000 seemed to be the consequences of lower and fluctuated precipitation.

On the contrary, soil moisture followed the precipitation pattern where their higher and lower amounts correspond. A close examination of figure 28 shows that 1983, 1984, 1987, 2000, and 2009 are the years of lower values for both precipitation and soil moisture, and 1980, 1988, 1999, 2006, and 2012 are the years of higher values.

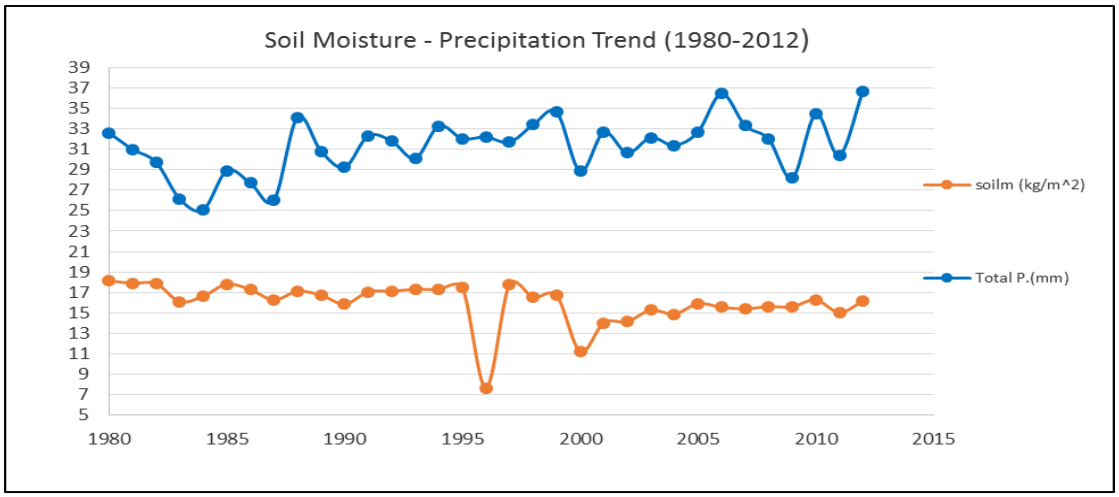

Figure 28. Soil Moisture – Precipitation Trend

Figure 29 shows the evolution of mean evapotranspiration, soil moisture, and precipitation from January to December from 1980 to 2012. All three parameters progressively increased in value from January, reached their peaks in August and then gradually decreased to December. This is a sign of significant correlation between those three parameters that we will discuss further.

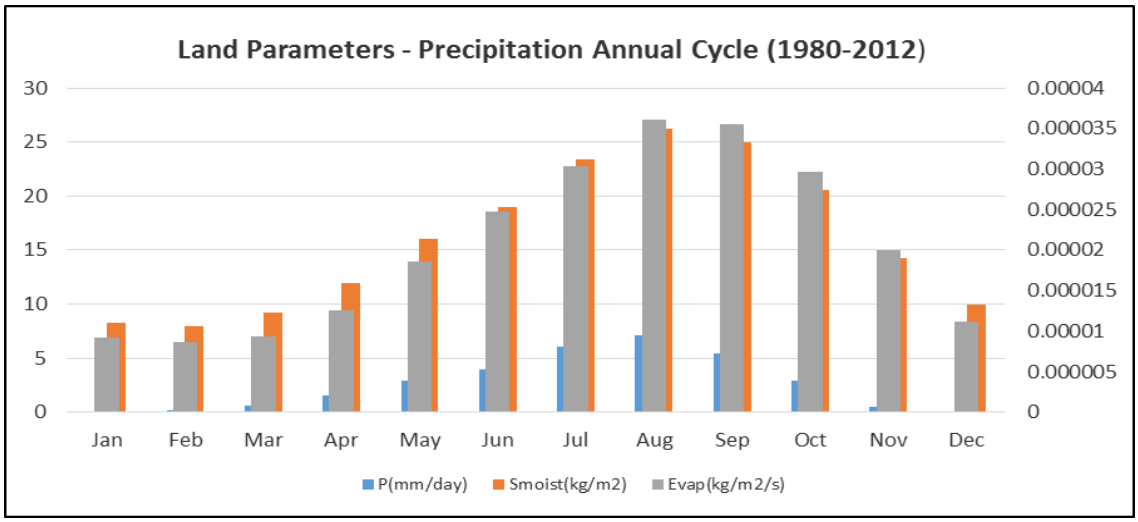

Figure 29. Land Parameters Annual Cycle

4.2.1. Evapotranspiration

This study revealed a gradient of evapotranspirations from south from north, with the highest from about 7 to 9.5˚N, and the lowest ones from 13˚N to above. The mean and median centers of the directional distribution and krigging interpolation (figure 30) show an asymmetric distribution because those two parameters do not have the same value (they are not superposed to each other). The skewness of -0.15, a negative value between -1/5 and +1/2 indicating an approximately symmetric distribution was observed. We found out through figures 11 and 30 that the evapotranspiration follows the patterns of rainfall; the higher the rainfall, the higher the evapotranspiration.

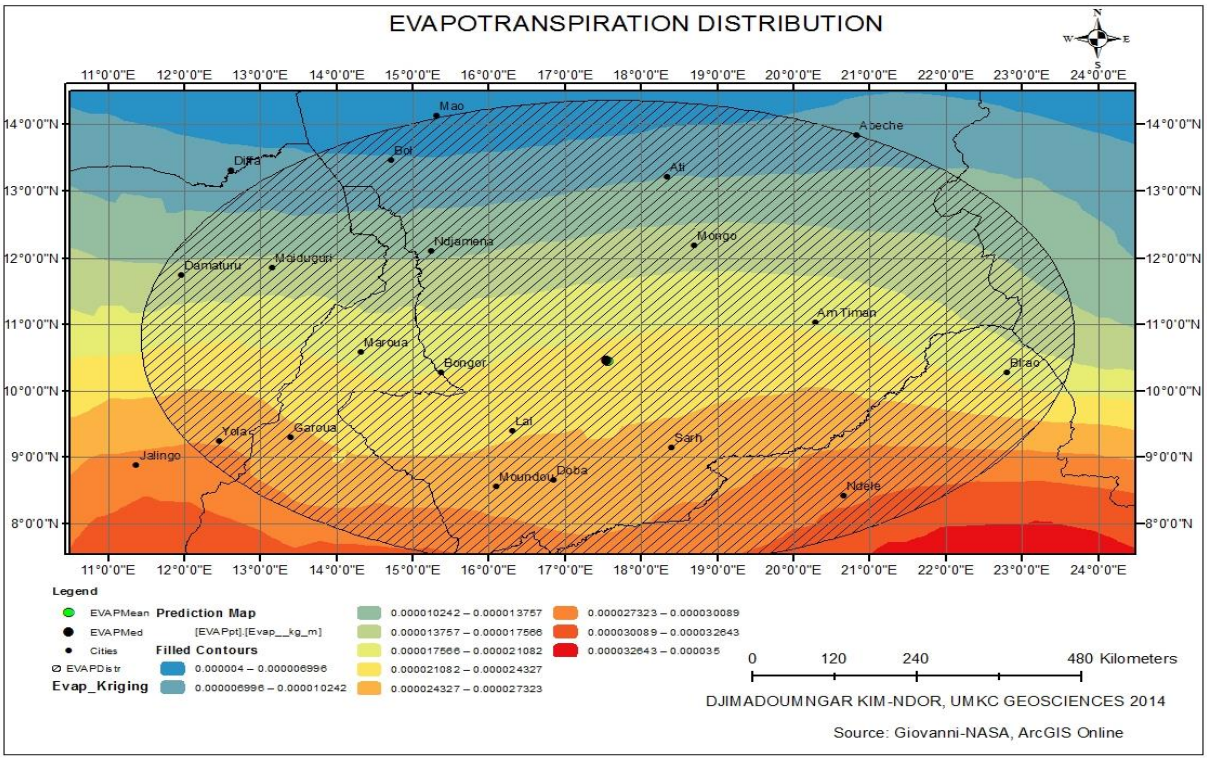

Figure 30. Total Evapotranspiration Distribution Map

4.2.1.1. Evapotranspiration Composite Analysis

Figure 31 below shows the situation of evapotranspiration in wetter and dryer years. June in wetter years and June in dryer years seemed to have the same of amount evapotranspiration, about 0.000026. The value of evapotranspiration became greater in July and August in wetter years with respectively about 0.000032 and 0.000039 than in the correspondent months in dryer years with 0.00003 and 0.000038, respectively. Then the situation changed again in September with higher evapotranspiration in dryer year, with about 0.000039, than in wetter year with about 0.000038.

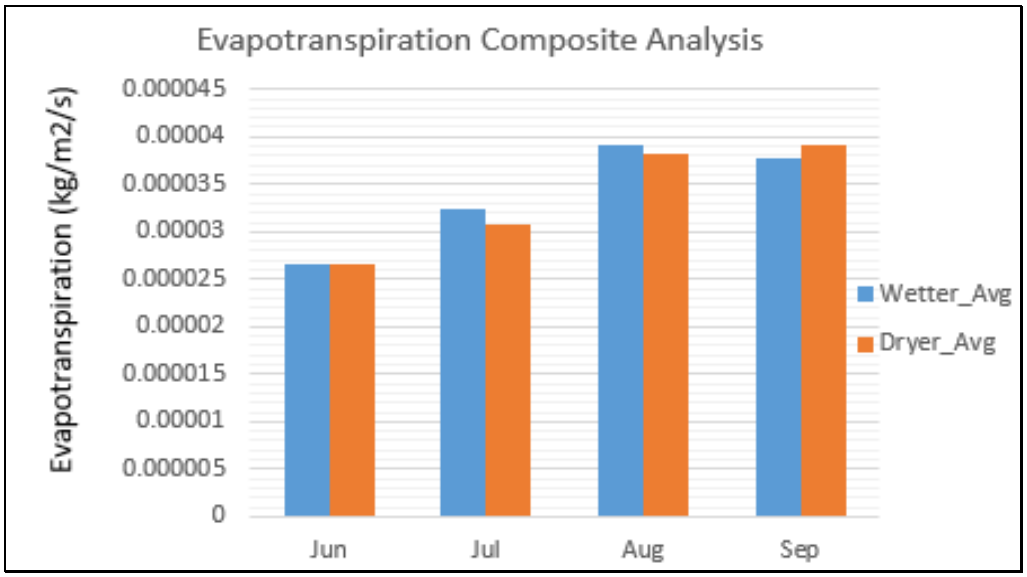

Figure 31. Total Evapotranspiration Composite Analysis Graph

Table 5 shows the percent change of total evapotranspiration from dryer to wetter years. The change is null in June, increased about 5% in July, then decreased to about 2%. In September, evapotranspiration was higher in dryer than in wetter year.

Table 5. Total Evapotranspiration Percent change

	Dryer_Avg	Wetter_Avg	% Change
Jun	0.0000265	0.0000265	0.00
Jul	0.00003075	0.0000325	5.69
Aug	0.00003825	0.00003925	2.61
Sep	0.00003925	0.00003775	-3.82

4.2.2. Soil Moisture

The krigging interpolation and the directional distribution of soil moisture of our area of study (figure 32) lets us know that:

- There is a gradient of moisture from south to north. The soils that are the most moist are around 7 to 8.5˚N, and the less moist are from around 12.5 to 14.5˚N; between the two ranges are the intermediate;
- The mean and median center are almost superposed giving an idea of a quasi-normal distribution. The value of the skewness of 0.07, indicates an approximately symmetric distribution. The Normal QQPlot showed that almost all points are aligned along the line of normal distribution.

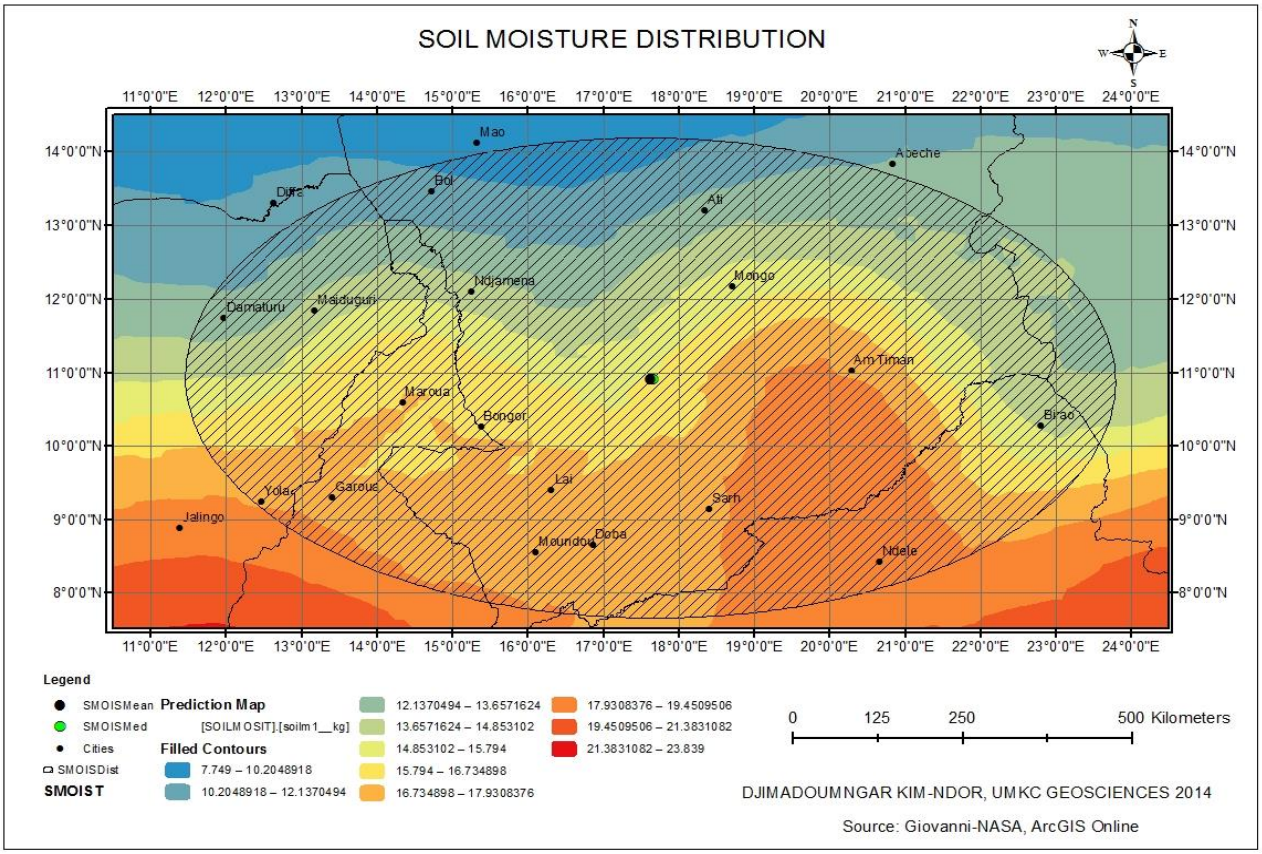

Figure 32. Soil Moisture Distribution Graph

4.2.2.1. Soil Moisture Composite Analysis

The composite analysis of average soil moisture in wetter and dryer years is shown in figure 33. It also shows that except for June, all the wetter months have greater amounts of soil moisture than in the dryer months. The table 6 shows the differences between dryer and wetter months. June in the wetter years had 8.86 less soil moisture amount than June in the dyer years. This might be explained by unfavorable meteorological conditions and/or a difficult precipitation recovery after a precedent dyer year.

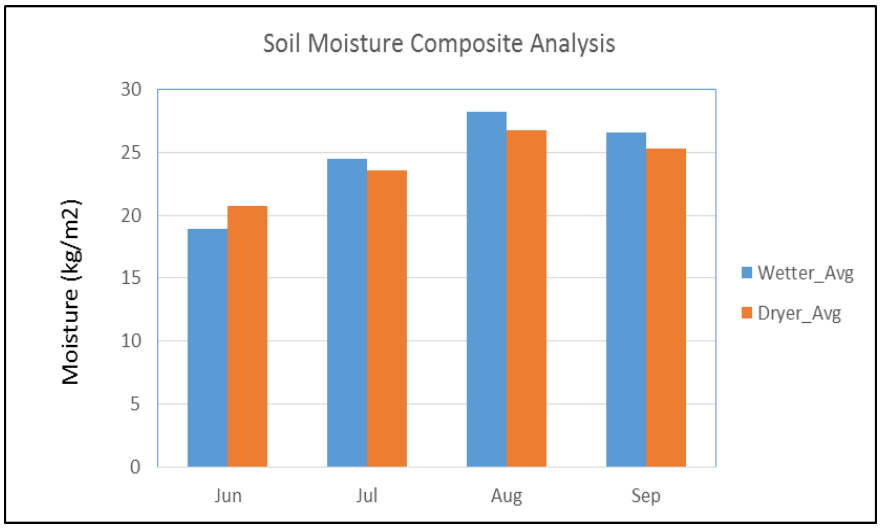

Figure 33. Soil Moisture Composite Analysis graph

The difference between July in the wetter years and July in the dry years is about 3.81 %. Those for August and September is more than 5%. We noticed that the percent change of soil moisture between dryer and wetter years increased from June to August and tended to stagnated. This may be explained by the types of soil itself, saturation, etc.

Table 6. Soil Moisture Composite Analysis Values and Percent Change

	Dryer_Avg	Wetter_Avg	% Change
Jun	20.71	18.87	-8.86
Jul	23.57	24.47	3.81
Aug	26.69	28.21	5.70
Sep	25.29	26.60	5.18

4.2.3. Normalized Difference Vegetation Index, NDVI.

We have mainly used the Monsoon Asia Integrated Regional Study (MAIRS) to generate NDVIs maps of our study. The temporal resolution is 10 years, from 2000 to 2010.

Figure 34.a shows a gradient of the NDVI from south to north drawn in GES GISC. The highest (0.6 to 0.7) NDVI is about from 7.5 to 8.5˚N and from 18 to 24.5˚E, with a peak at 8.5˚N and 22˚E; that means that the highest NDVI is concentrated towards the southeast portion of our area of study. The NDVIs of 0.5 and 0.6 are distributed between 7.5 and 8˚N (approximately) from the west to the center with a peak at 9 ^{0}N at about 18 ^{0}E, and continues steadily towards the east.

The range of the NDVI from 0.4 to 0.5 was the widest and extended from about 8^{0}N in the southwest to about 8.5^{0}N in the southeast with a peak in the center at 11^{0}N from about 16 to 22 ^{0}E. The NDVI of the range from 0.3 to 0.4 extended from 10 to 11.5 ^{0}N in the southwest with a peak at 13.5 ^{0}N from 13 to 16 ^{0}E. The area of that range became smaller from about 11 to 12 ^{0}N and 16 to 22 ^{0}E. The range of 0.2 to 0.3 in the west from about 11.5 and 14 ^{0}N and about 11 to 13 ^{0}E , and in the east from 14 to 14.5 ^{0}N and 17 to 23 ^{0}E with a peak between 20 to 22 ^{0}E. The lowest NDVIs (0.1 to 0.2) are between 14 and 14.5 ^{0}N and mainly from 11 to 19 ^{0}E.

Once again, looking at figures 11 and 34 lets us understand that the NDVI distribution follows the precipitation patterns. The NDVI is higher where precipitation is higher, and lower where precipitation is lower.

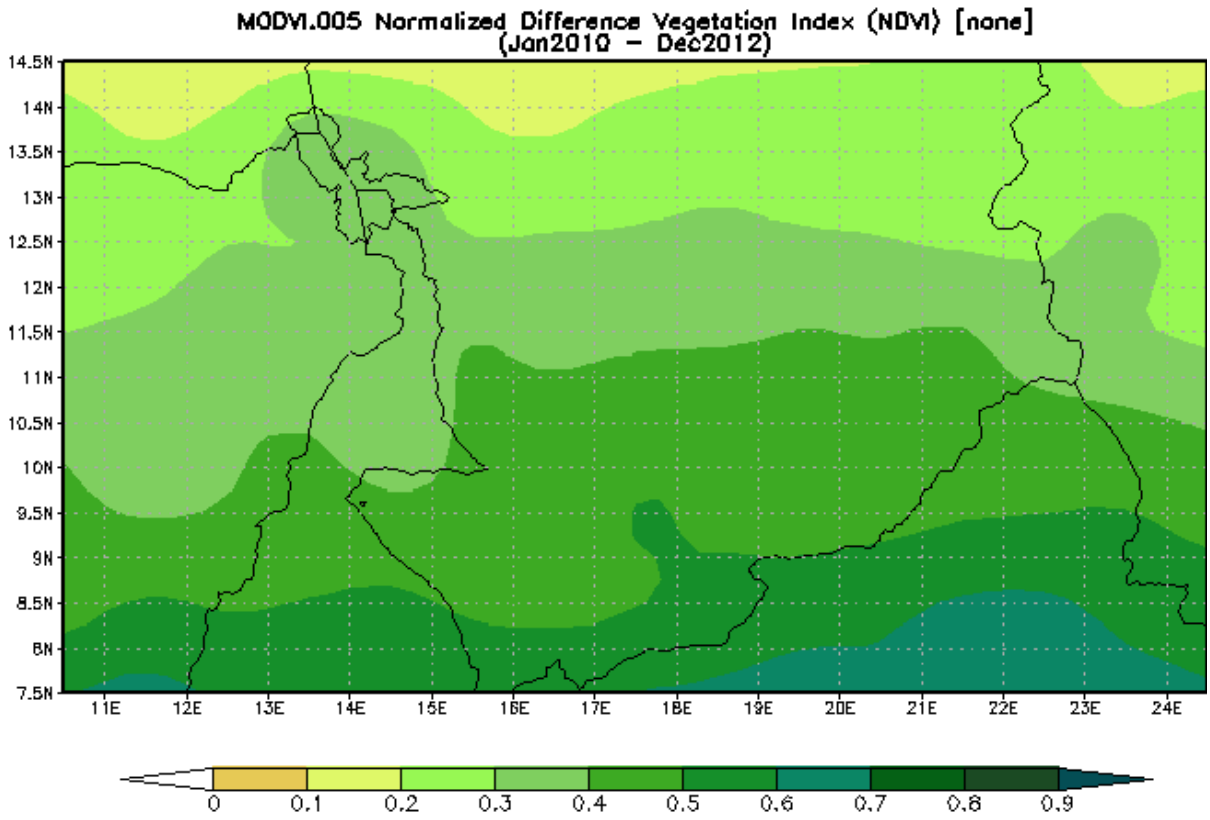

34.a

The analysis of figures 34.b and c lets us see that, although the general pattern of distribution is the same from south to north in 2000 and 2012, there were shifts of width of the NDVI areas in 2012. For instance, the maps show:

- The highest NDVI range, 0.7 - 0.8, mostly spread in the southeast and had its peak about 9.5 ^{0}N and 23 and 24˚E in 2002, then increased in width from 18 to 24˚E in 2012;
- The lowest NDVI range, 0.1 - 0.2, was from about 14 to 14.5˚N in 2002, then did not exist in 2012. This is an indication that the northern part of the Sahel was greener in 2012 than it was in 2002.

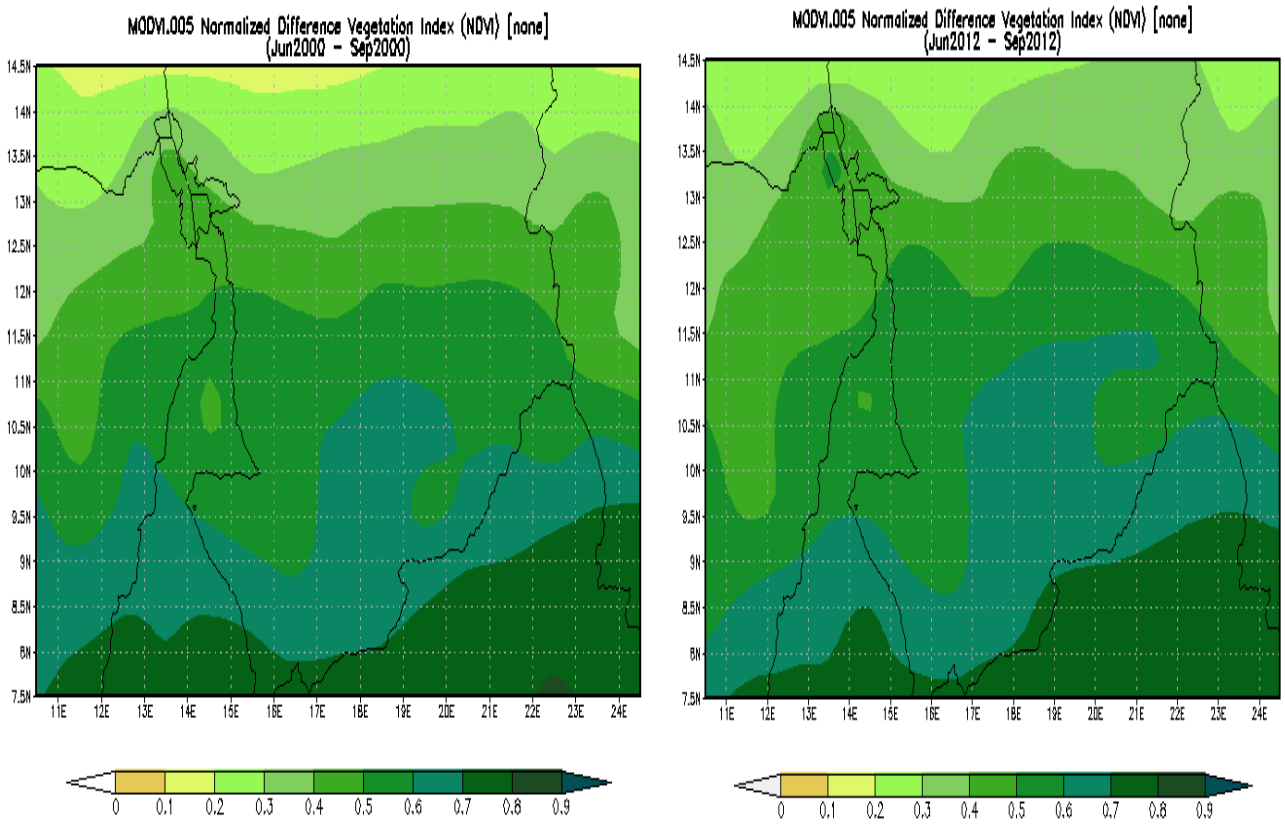

34.b 34.c

Figure 34. NDVI Distribution Maps

4.2.3.1. Normalized Difference Vegetation Index Composite Analysis

The NDVI composite analysis was done on two different locations, one in the center and another in the south of Chad as indicated in figure 35 below. The years taken into consideration are 2006, 2012 (wetter), and years (dryer).

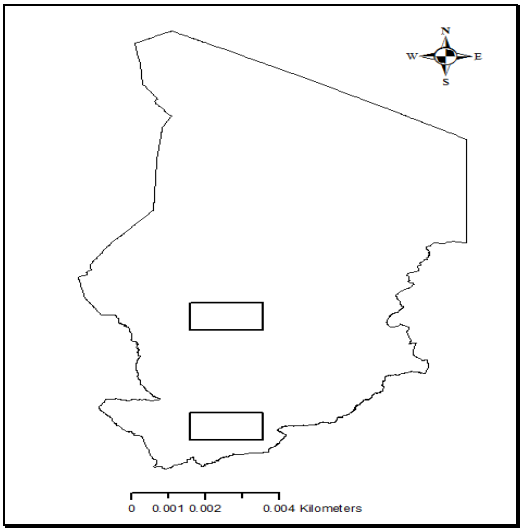

Figure 35. NDVI Composite Analysis Location Map

In the center, both in the dryer and wetter years, the NDVI amounts increased from June to September with greatest amounts in August with 0.44 and 0.49. Then, the NDVIs amounts stagnated (dryer) and decreased (wetter) in September as shown in figure 36. The NDVI values in wetter years were higher than in the dryer ones for all the months considered in that study.

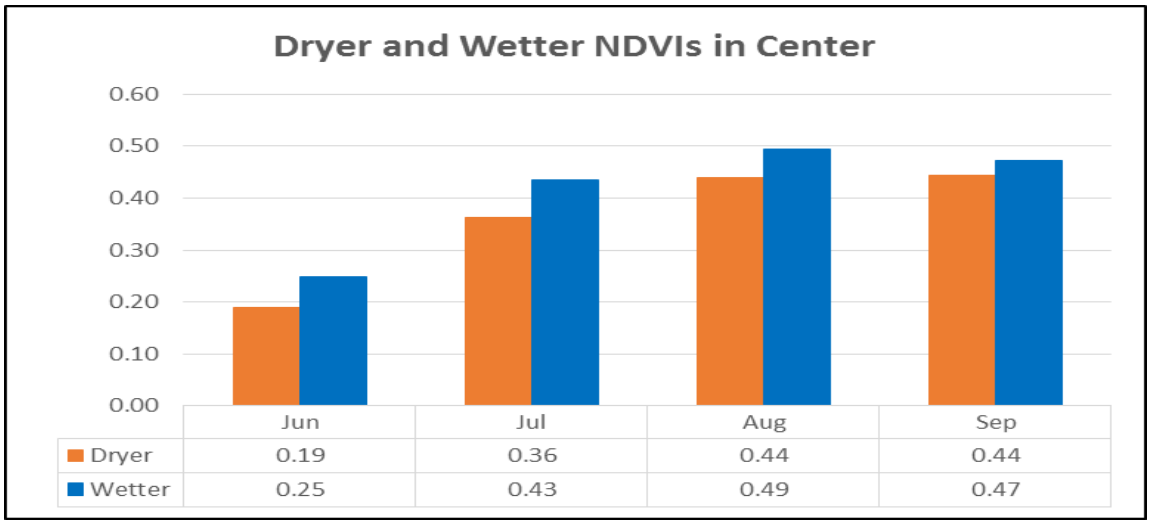

Figure 36. Dryer and Wetter NDVIs in the Center

Table 7 lets us see that NDVI in the center in wetter years was greater than in dryer years at about 30% in June, 19% in July, 12% in August, and 6% in August. The difference in NDVI amount was greater in the beginning of rainy season, became progressively smaller in the end.

Figure 37 below shows the NDVIs in dryer and wetter in South. It is clearly seen that the NDVI amount increased from June to September with highest values in September for both dryer and wetter years. There also, we can notice that the difference dryer – wetter NDVI was higher in June and July (0.49 Vs 0.57 and 0.60 Vs 0.65) than in August and September where the values were almost identical (0.66 Vs 0.67 and 0.67 Vs 0.68).

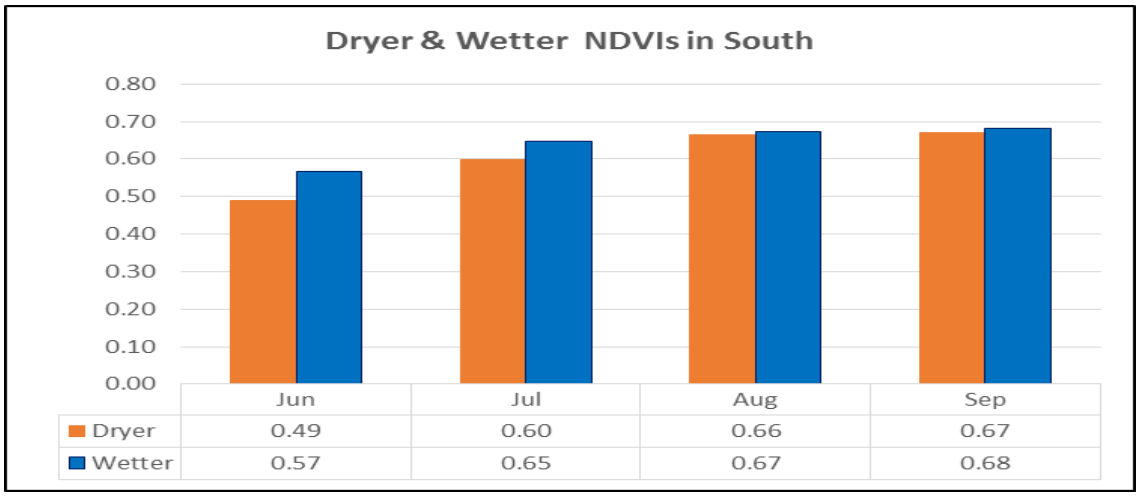

Figure 37. Dryer and Wetter NDVIs in the South

Table 7 gives us also the NDVI percent change from dryer to wetter years in the south. The NDVI amount was higher at about 16% in June, 8% in July, 11.3 % in August, and 1.5% in September during wetter years than during dryer years. The percent change was higher in June, then progressively decreased to reach about 1 in the end of rainy season.

Table 7. NDVI Percent Change in Center and South

	Center (%)	South (%)
Jun	30.53	15.98
Jul	19.56	7.93
Aug	12.53	1.28
Sep	6.53	1.49

Table 8 shows percent changes in NDVIs values in dryer and wetter years in the center Vs south. As we can see, dryer NDVI was about 157% in June, 65% in July, 51% in August and September higher in south compare to center. Wetter NDVI also followed the same pattern even though the percentages were lower. It was higher at about 132, 49, 32, and 43 % in June, July, August, and September in South than in Center, respectively. In both dryer and NDVIs, we notice that the percent change was higher in June and decreased the more we go toward September.

Table 8. NDVI Composite Analysis Center Vs South

	Dryer NDVI			Wetter NDVI		
	Center	South	% Change	Center	South	% Change
Jun	0.19	0.49	156.84	0.25	0.58	131.85
Jul	0.36	0.60	65.01	0.43	0.65	49.08
Aug	0.44	0.66	51.25	0.49	0.66	33.81
Sep	0.44	0.67	50.90	0.47	0.68	42.71

The examination of the NDVIs in dryer and wetter years in the center and south lets us conclude that the NDVI is a function of precipitation. The lower NDVI values were observed in June (beginning of the rainy season) whereas the higher ones were observed in September. In both center and south, the percent change between the NDVIs in dryer and wetter years is higher in June and smaller in September; this might be explained by the fact the NDVI is close to its optimum due to the growing vegetation. A spatial comparison of the NDVI distribution in the center and south of Chad lets us clearly figure out the following points:

- The NDVI values are a function of precipitation in both the center and south, increase from June to September, and are higher in the south in both wetter and dryer years.
- The range of the NDVI is 0.49 – 0.67 in the south and 0.19– 0.44 in the center in dryer year, while it is 0.57 - 0.68 in the south and 0.25 -0.47 in wetter years.

The land parameters we have studied have the following statistic characteristics: Evapotranspiration is positively highly correlated with precipitation (0.943), soil moisture (0.885), and the NDVI (0.941). Soil moisture has a mean of 15.98, a standard deviation of 4.2 and is positively highly correlated with the NDVI (0.809). the NDVI has a mean of about 0.4 with a standard devaiation of 0.14. All the land parameters studied are positively correlated with each other.

4.3. Atmospheric - Land Parameters Correlation

Using SPSS IBM, the correlations between atmospheric and land parameters are computed (table 9).

Precipitation is positively correlated with evapotranspiration, soil moisture, and the NDVI with respective values of 0.943, 0.820 and 0.897. Precipitation is negatively highly correlated with a surface air temperature (-0.862) and negatively correlated with AOD (-

0.343). Surface air temperature is negatively highly correlated with evapotranspiration (-0.825), correlated with soil moisture (-0.739) and the NDVI (-0.783). AOD is positively lowly correlated with air surface temperature (0.138) and negatively correlated with evapotranspiration (-0.445), soil moisture (-0.348) and the NDVI (-0.4). Evapotranspiration is positively highly correlated with soil moisture (0.885) and the NDVI (0.941). Soil moisture and the NDVI are also positively highly correlated (0.809).

Table 9. Atmospheric and Land parameters Correlations

Correlations

		precipitation	AOD	SurfAirTemp	Evapotranspiration	SoilMoisture	NDVI
precipitation	Pearson Correlation	1	-.343**	-.862**	.943**	.820**	.897**
	Sig. (2-tailed)		.000	.000	.000	.000	.000
	N	120	120	119	120	120	107
AOD	Pearson Correlation	-.343**	1	.138	-.454**	-.348**	-.399**
	Sig. (2-tailed)	.000		.134	.000	.000	.000
	N	120	120	119	120	120	107
SurfAirTemp	Pearson Correlation	-.862**	.138	1	-.825**	-.739**	-.783**
	Sig. (2-tailed)	.000	.134		.000	.000	.000
	N	119	119	119	119	119	106
Evapotranspiration	Pearson Correlation	.943**	-.454**	-.825**	1	.885**	.941**
	Sig. (2-tailed)	.000	.000	.000		.000	.000
	N	120	120	119	133	133	120
SoilMoisture	Pearson Correlation	.820**	-.348**	-.739**	.885**	1	.809**
	Sig. (2-tailed)	.000	.000	.000	.000		.000
	N	120	120	119	133	133	120
NDVI	Pearson Correlation	.897**	-.399**	-.783**	.941**	.809**	1
	Sig. (2-tailed)	.000	.000	.000	.000	.000	
	N	107	107	106	120	120	120

**. Correlation is significant at the 0.01 level (2-tailed).

4.4. Land Use Land Cover Analysis: Case Study of Lake Fitri

The land use land cover analysis was performed on Landsat satellite images of 1986, 2003, and 2013.

4.4.1. Land Use Land Cover Analysis 1986 – 2003

In 1986, the major land cover was bare soils (62%), followed by forest-savanna-steppe (23%), wetland (14%), grassland-farmland (~0.4%) and water bodies (~0.2%), respectively. In 2003, while bare soil, still the major land cover (~78%), grassland-farmland (~9%), and water bodies (0.6%) increased, forest-savanna-steppe (~12%) and wetland (~1%) decreased. The class percentages in 1986 and 2003 are given in table 10 below and the land use land cover maps of 1986 and 2003 are shown in figures 38 and 39.

Table 10. Land Use Land Cover Change from 1986 to 2003

Land Use Land Cover Change 1986-2003					
Class	Area (km2) 1986	%_1986	Area (km2) 2003	%_2003	%Change
Bare soils	19437.99	62.25	24937.54	77.84	15.59
Wetland	4410.52	14.12	280.5	0.875	-13.245
Forest-Savanna-Steppe	7202.5	23.06	3766.1	11.75	-11.31
Water Bodies	57.45	0.18	198.8	0.62	0.44
Grassland-Farmland	118.14	0.38	2852.32	8.9	8.52
Total	31226.6	100	32035.26	100	

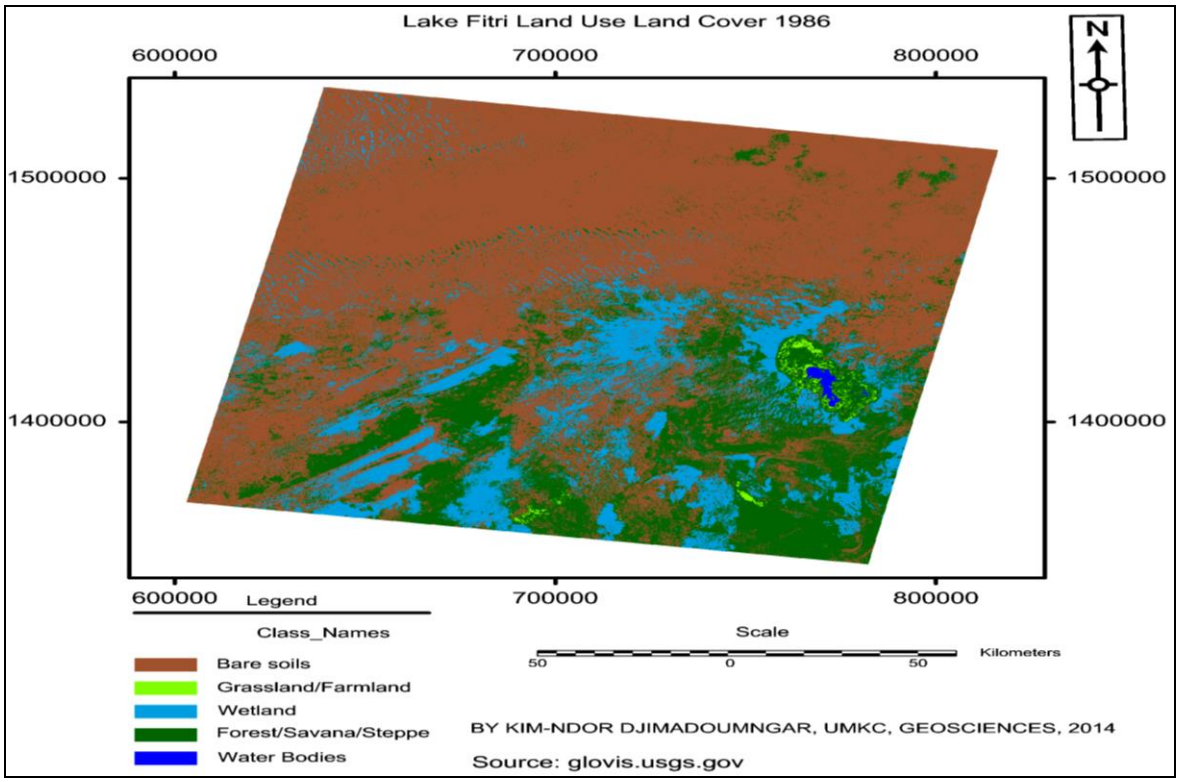

Figure 38. Land Use Land Cover in 1986

The comparison of the classified maps of 1986 and 2003 (associated with the percentage in the table 10) shows that bare soils continued to increase from the north to the south and the west to the east with a percent change of 15.6%, whereas forest-savanna-steppe continued to uniformly decrease with a percent change of -11.3 %. Meanwhile, wetland decreased (-13.2%), whereas grassland-farmland increased (8.5%). Some wetland and wooded areas in 1986 are shown as grassland-farmland in 2003. Water bodies increased (0.62%); that may be explained by the higher precipitation of the 17 years between 1986 and 2003, except for year 2000.

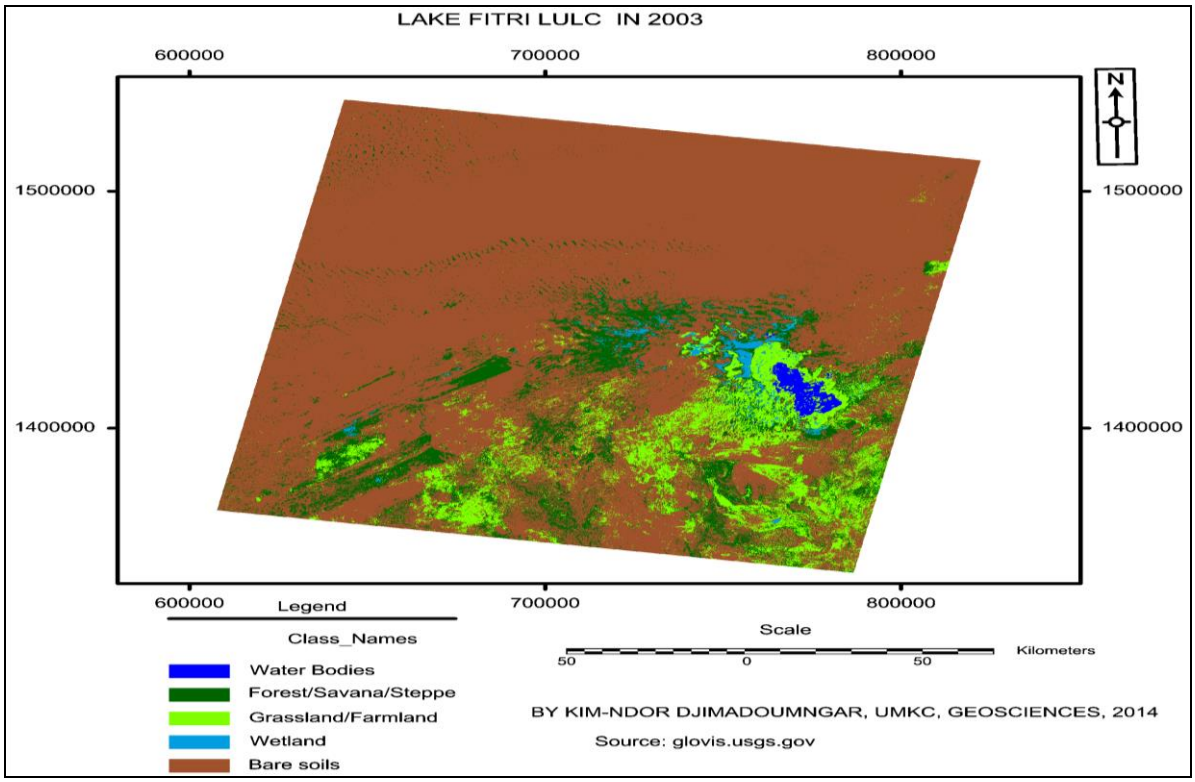

Figure 39. Land Use Land Cover in 2003

4.4.2. Land Use Land Cover Analysis 2003 – 2013

In 2013, bar soils decreased but were still the major land used land cover (48%); grassland-farmland (41%), and wetland (~ 3%), increased while the forest-savanna-steppe continued to decrease (7%). Water bodies remained almost constant (~0.5%) as shown in the table 11 below. The land use land cover map of 2013 is shown in figure 40.

The charts representing the percent changes of each class from image to image are shown in the figures 41, 42, 43, 44 & 45.

Table 11. Land Use Land Cover Change from 2003 to 2013

Land Use Land Cover Change 2003-2013					
Class	Area (km2) 2003	%_2003	Area (km2) 2013	%_2013	% Change
Bare soils	24937.54	77.84	18053.38	48.3	-29.54
Wetland	280.5	0.875	1039.05	2.78	1.905
Forest-Savanna-Steppe	3766.1	11.75	2764	7.39	-4.36
Water Bodies	198.8	0.62	182.7	0.49	-0.13
Grassland-Farmland	2852.32	8.9	15349.54	41.05	32.15
Total	32035.26	100	37388.67	100	

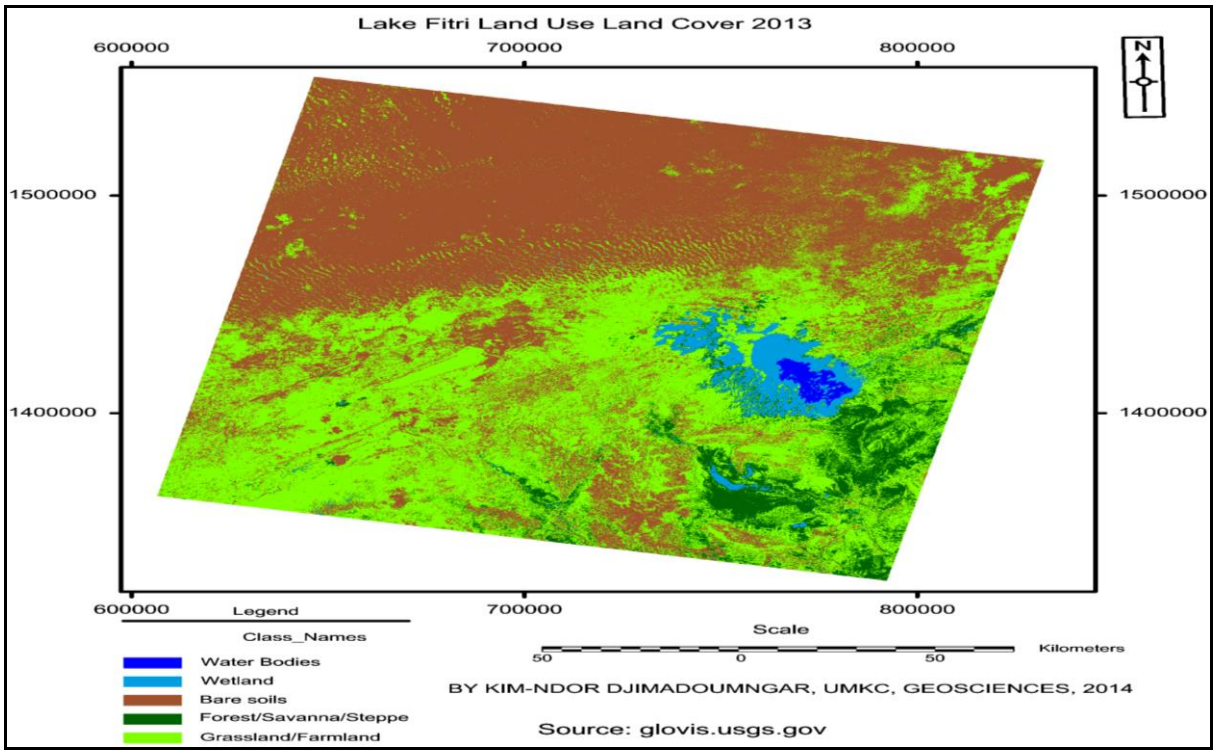

Figure 40. Land Use Land Cover in 2013

Looking at the classified map of 2013 (figure 40) and comparing it to the one of 2003 and the land use land cover table (table 11) let us see that grassland-farmland and wetland increased with a percent change of respectively 32 and 2 %; meanwhile, forest-savanna-steppe and bare soils decreased with a percent change of -4.36 and -29.5%, whereas water bodies remained almost constant with ~0.1 .

The total accuracy assessments are 89.84, 88.28 and 92.18 % for 1986, 2003, and 2013, respectively (Annexes A, B, & C).

Water Bodies Changes

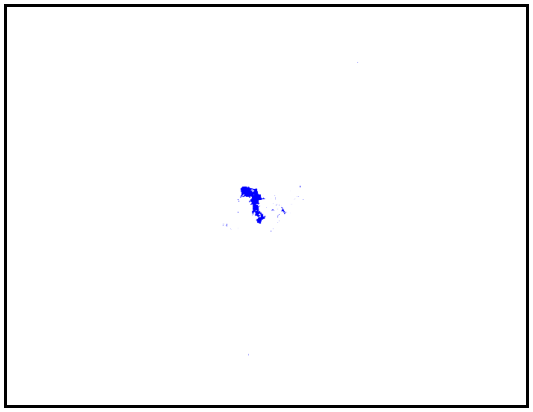

1986 0.18%

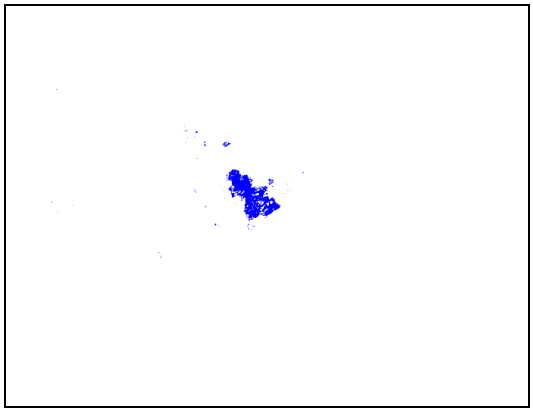

2003 0.62%

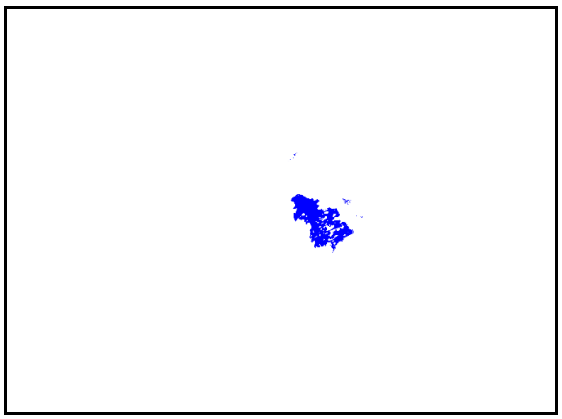

2013 0.49%

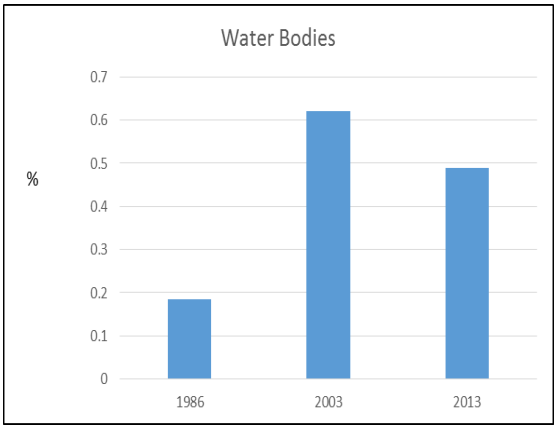

Figure 41. Water Bodies Changes

Wetland Changes

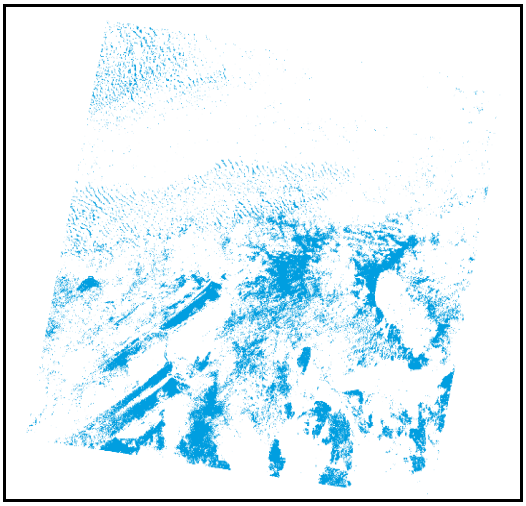

1986 14.12%

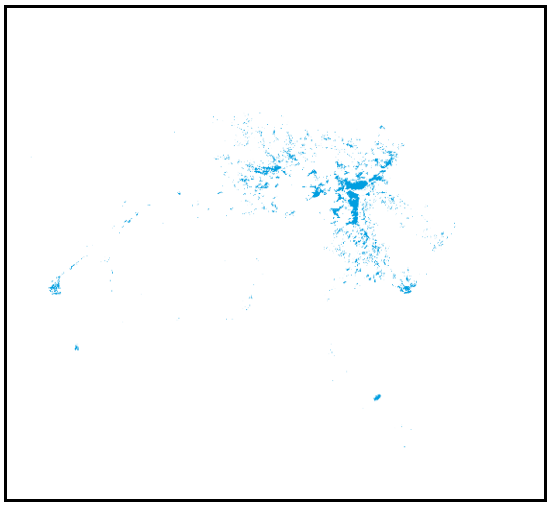

2003 0.875%

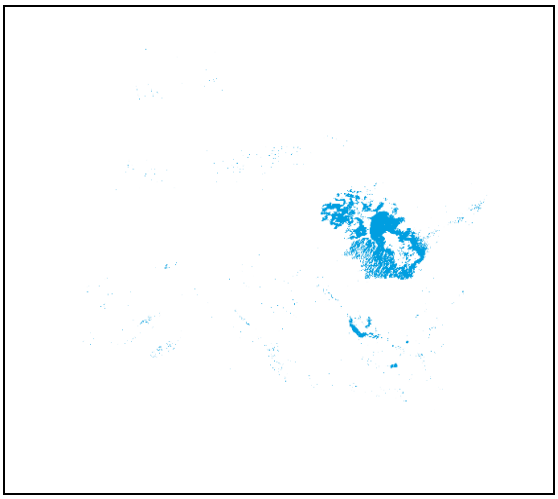

2013 2.78%

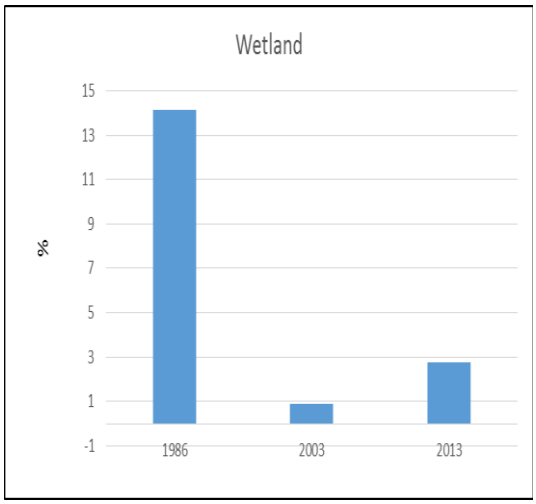

Figure 42. Wetland Changes

Forest-Savanna-Steppe Changes

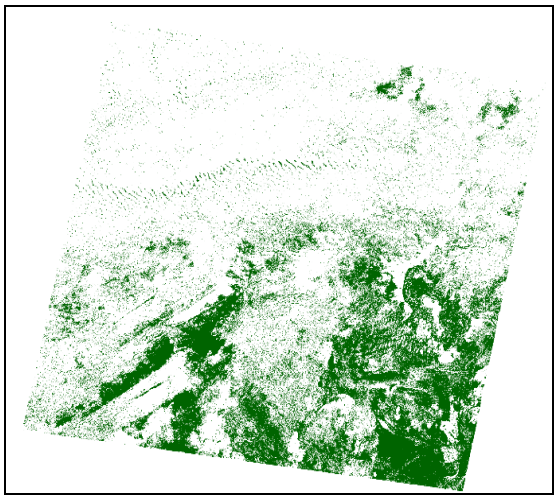

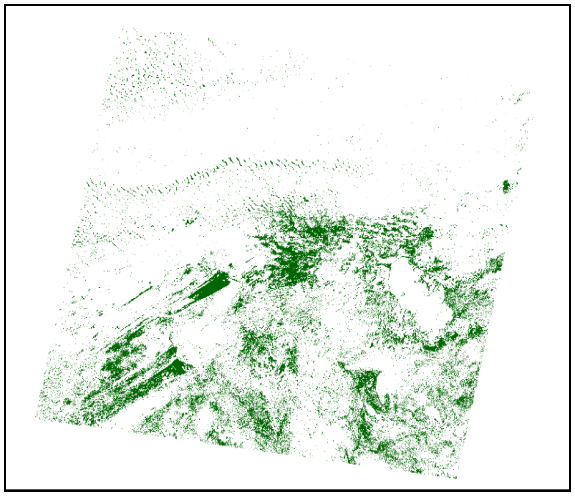

1986 23.06 % 2003 11.75%

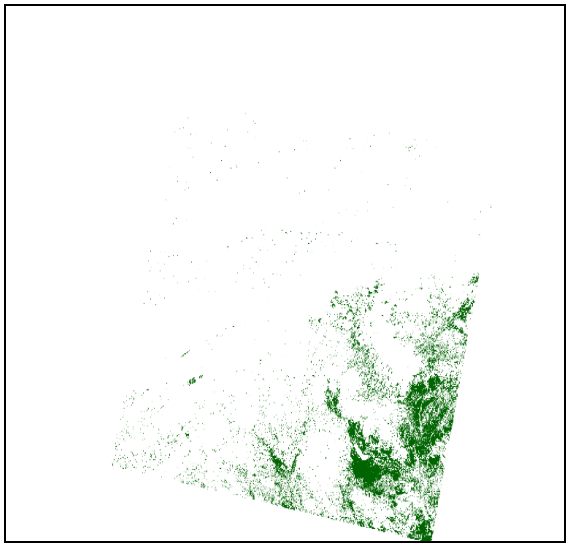

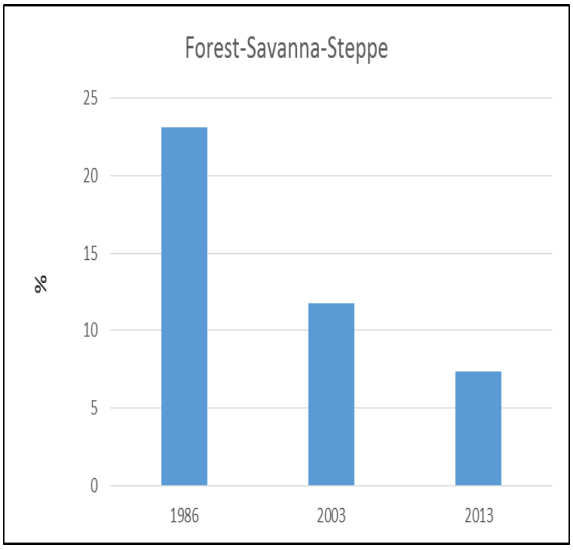

2013 7.39

Figure 43. Forest-Savanna-Steppe Changes

Grassland-Farmland Changes

1986 0.38%

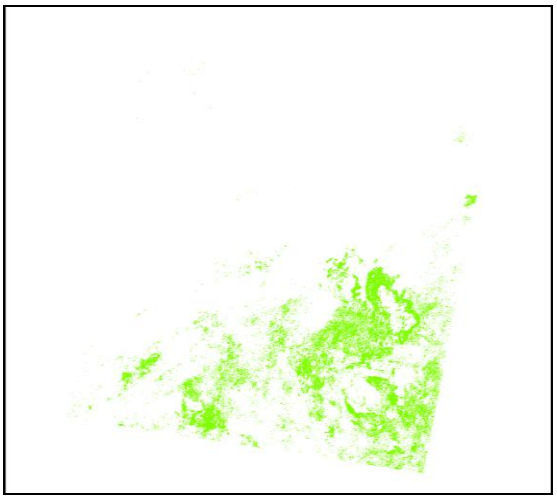

2003 8.9%

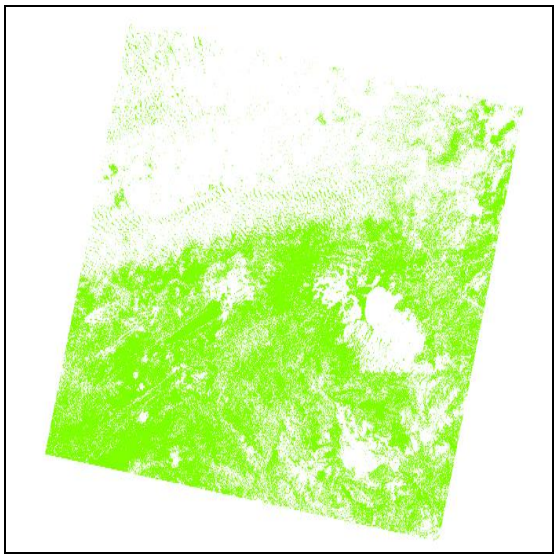

2013 41.05%

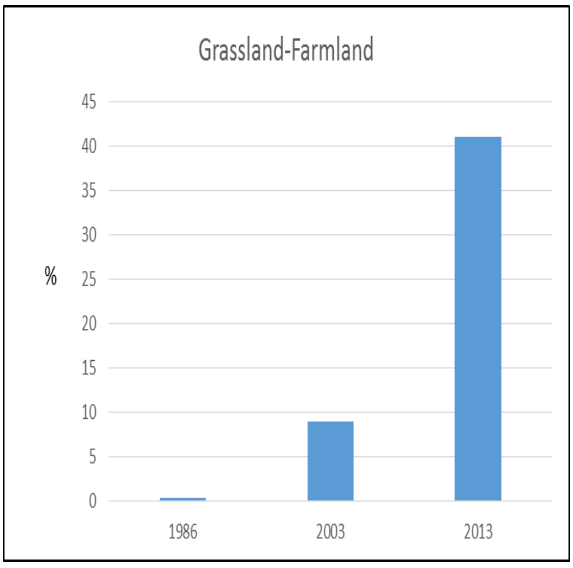

Figure 44. Grassland-Farmland Changes

Bare Soils Changes

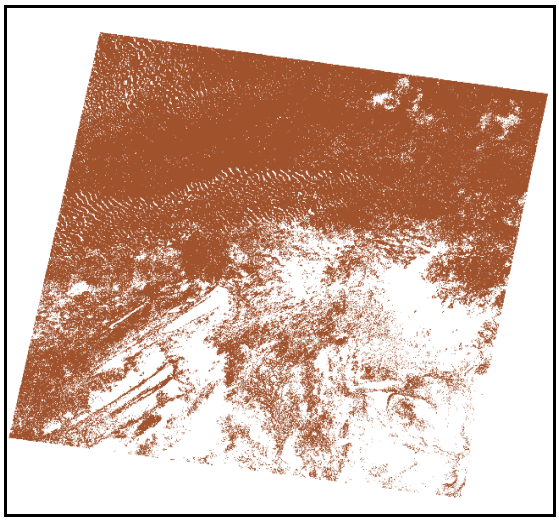

1986 62.25%

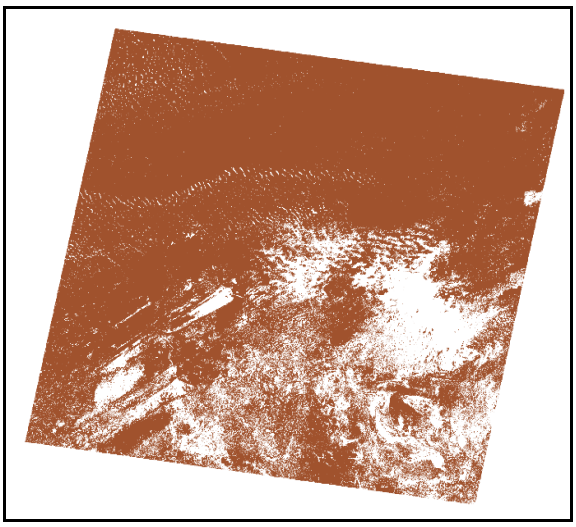

2003 77.84%

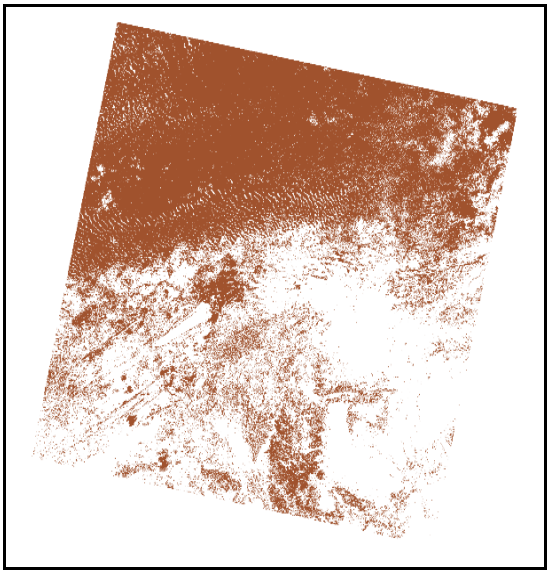

2013 48.3%

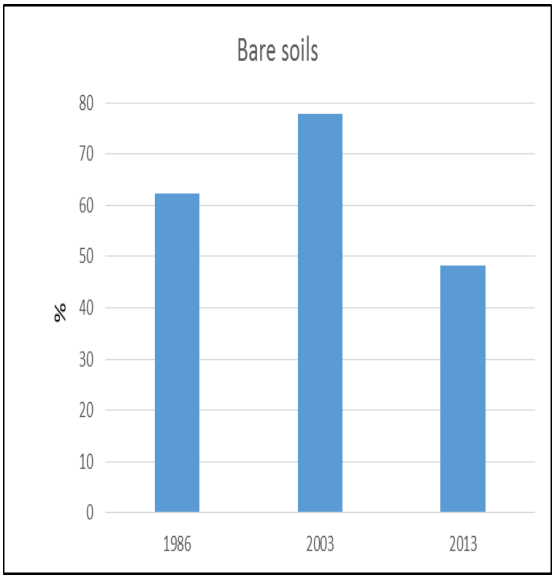

Figure 45. Bare Soils Changes

4.4.3. Land Use Land Cover Rate of Change

The rate of change of the land use land cover pattern of Lake Fitri in table 12 below indicates that bares soils increased at the rate of 1.5 km^2 / year from 1986 to 2003, then decreased at the rate of 3.18 km^2 /year from 2003 to 2013. Wetland decreased at the 15.23 km^2 / year from 1986 to 2003, then increased at 14 km^2 /year to 2013. Forest-savanna-steppe decreased at a rate of 3.81 km^2 / from 1986 to 2003 then 3 km^2 / year to 2013. Water bodies increased at a rate of 7.7 km^2 /year from 1986 to 2003 and 0.84 km^2 / year from 2003 to 2013. Finally, grassland-farmland increased at 21 km^2 each year from 1986 to 2003 then 18.32 km^2 to present.

Table 12. Land Use Land Cover Rate of Change

Land Use Land Cover Rate of Change		
Class	1986 - 2003	2003 - 2013
Bare soils	1.5	-3.18
Wetland	-15.23	14
Forest-Savanna-Steppe	-3.81	-3
Water Bodies	7.7	0.84
Grassland-Farmland	21	18.32

4.5. Socio-Economic Data Evolution Associated With Global Precipitation from 1980s to 2010s

4.5.1. Population and Agricultural Land Trends

The statistical analysis gave us a positive and moderate correlation between population and agricultural area (0.412). Figure 46 shows the trend of population and agricultural area from 1980 to 2011.

The population trend is almost exponential from 1980 to 2011. The curve shows a rapidly increasing population. The agricultural area was almost steady from 1980 to 1985, then increased to about 48200 (* 1000). After that year, the agricultural area trend exponentially increased until 1995. At about 1996, there was a jump to 48600 and that remained steady until 2000. From 2000 to 2005, the number of hectares fluctuated and rapidly increased to about 49500. Then the number of hectares decreased and remained constant from about 2007 to 2009, and increased again to its highest value in 2011.

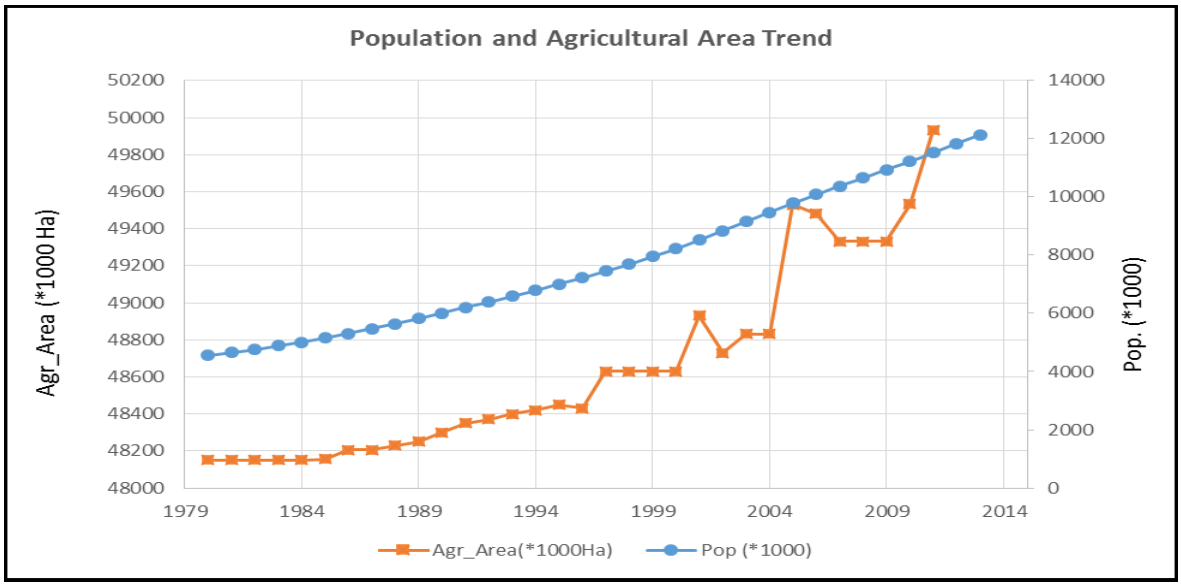

Figure 46. Population and Agricultural Area Trend Graph

4.5.2. Agricultural Production

In figure 47 below are the evolution of precipitation, rice paddy, sorghum, and maize production from 1980 to 2011. It is clear that all the types of cereal production rapidly increased. All of the four curves show almost the same pattern. Almost all the lower values of the three cereals' curve correspond to the lower values of precipitation, and almost all the higher values of those cereals' curve correspond to the higher values of precipitation.

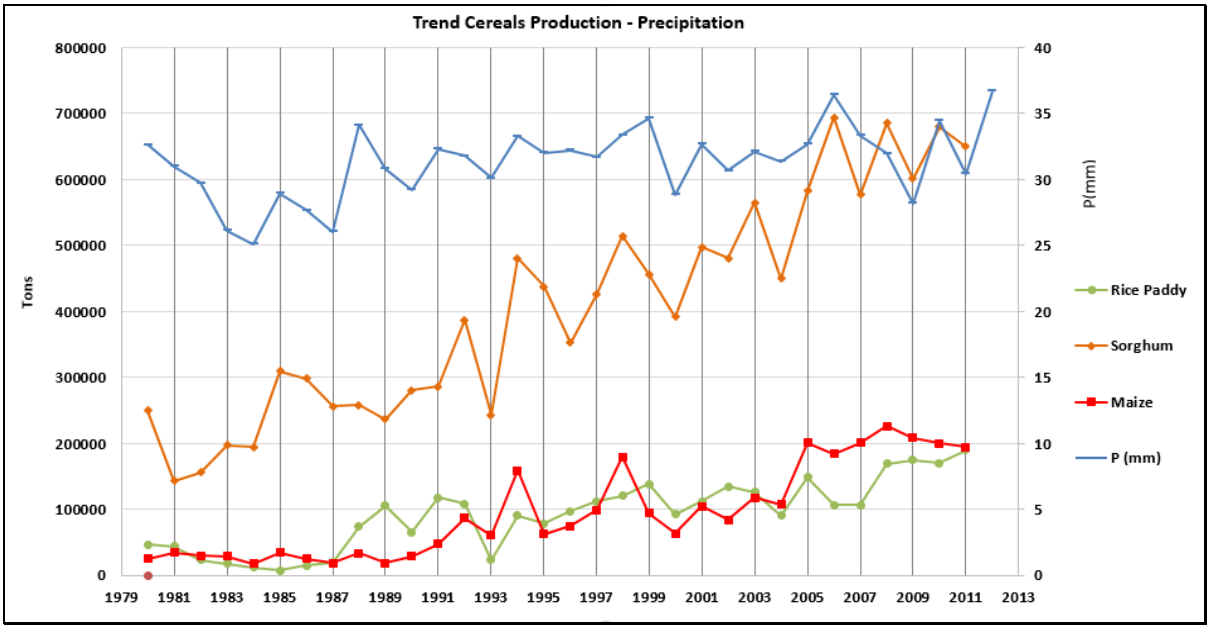

Figure 47. Cereals – Precipitation Trend Graph

4.5.3. Commercial and Industrial Production

Cotton, sugar cane, and tobacco are some of the main commercial and industrial productions in Chad. Figure 48 shows those crops production from 1980 to 2011.

Cotton, with higher productions in about 1997 and 2005 is a function of precipitation (although its production did not follow the precipitation rainfall). This might be explained by the fact that the crop itself is less grown in the later years. Its years of higher production were about 1988, 1997, and 2005; all of those years correspond to the years of higher precipitation.

Tobacco follows precipitation patterns. Its production decreased as precipitation decreased from 1980 to about 1987, then remained constant but then slightly decreased in about 1990. From 1990 to 1999, the production increased following the fluctuated and relatively higher and lower precipitation. The production remained constant again until about 2004, then increased in 2005, 2006, and 2007, but then decreased again until 2009. We observe another growth spurt from about 2001/2012.

The sugar cane production decreased as the precipitation decreased in the beginning of the 1980s. From the mid-1980s to 1990, the production increasingly fluctuated to reach a first peak value in 1995. Then it progressively decreased until about 1999/2000. The production then increased and decreased again in 2005. Another increase cycle happened until 2008, then a decrease in 2009, and finally an increase from 2010. The sugar cane did not really follow the precipitation pattern for it is also an irrigation crop.

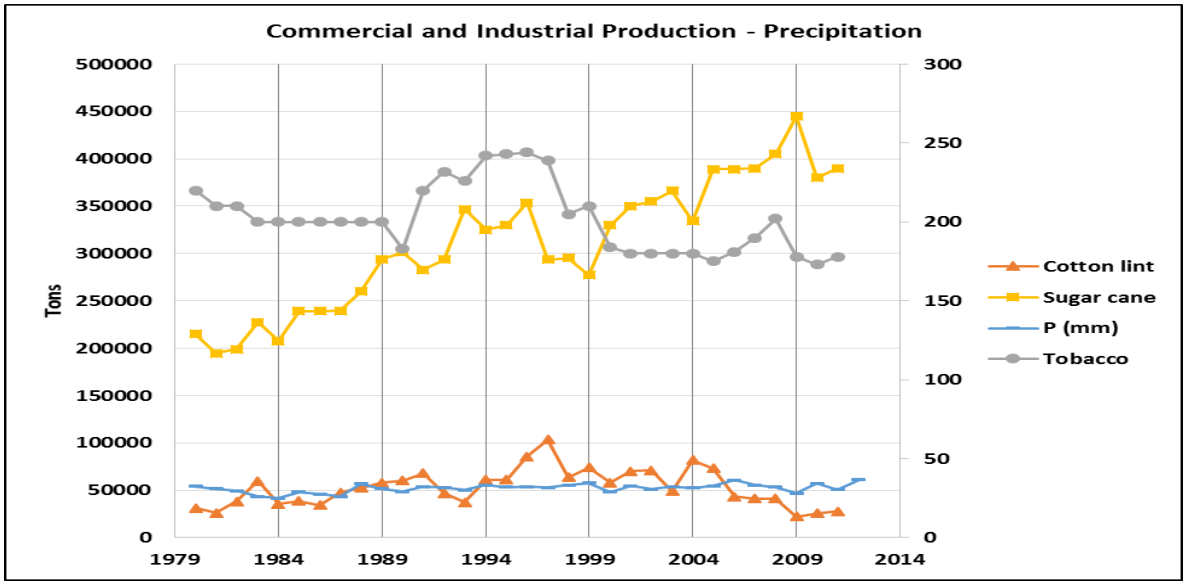

Figure 48. Commercial and Industrial Crops – Precipitation Trend Graph

4.5.4. Livestock

Figure 49 shows the trend of cattle and chicken from 1980 to 2011 in Chad.

Cattle, sheep, and goats increased from 1980 to about 1983 then began to decrease and reached their lowest number in 1984 and 1985, corresponding to the 1980s drought. There was a relative rapid recovery after 1985 with an exponential increase until 1995, then another rapid increase after 1995 for cattle and goats. However, for sheep, the recovery slope was slow until 1996 when another decrease happened in 1997; its increase was almost exponential but with a lower slope from 1998 to 2012. The growth in the number of cattle and goats was almost exponential from 1997 to 2011, although the goats' curve changed slope from 2010. Except during the drought of the mid-1980s, the livestock trend seemed not to be disturbed by precipitation fluctuations.

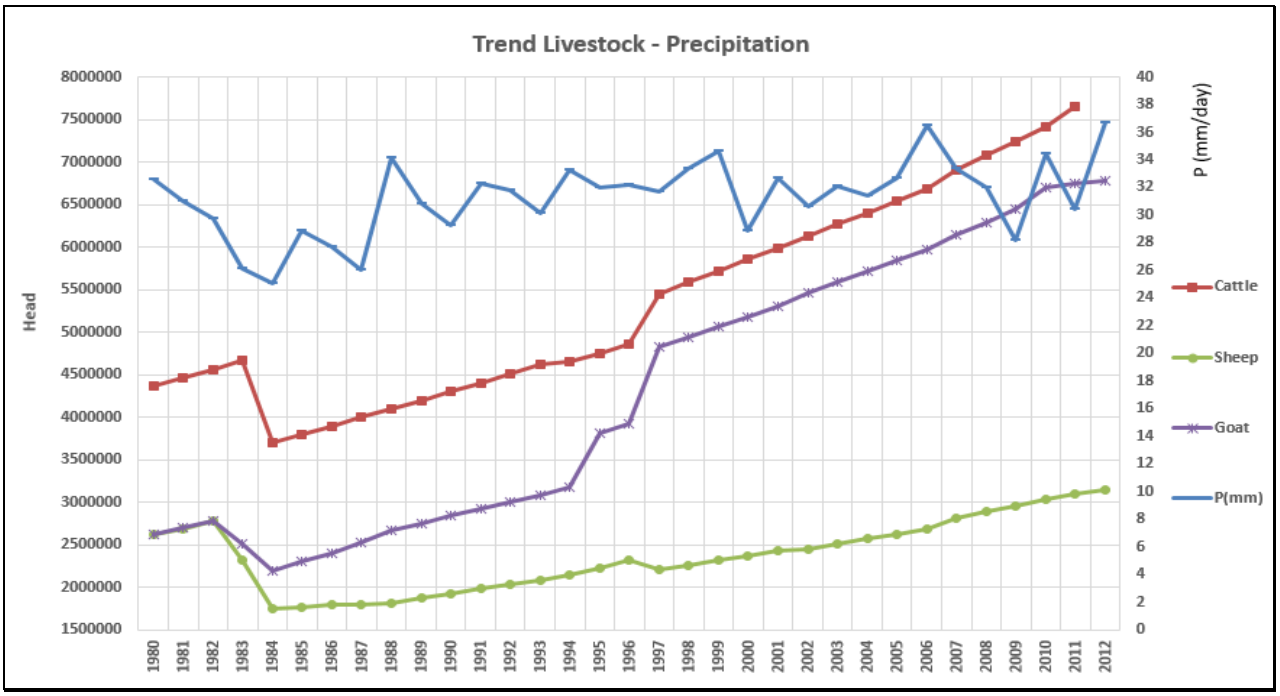

Figure 49. Livestock – Precipitation Trend Graph

4. 6. Socio-economic Data Multiple Linear Regression Analysis

A multiple linear regression analysis had been conducted. The predictive or independent variables are population and precipitation. The dependent variables are categorized as:

- Cereals: sorghum, maize, and rice paddy;
- Commercial and industrial crops: cotton, sugar cane, and tobacco;
- Livestock: cattle, sheep, and goats.

The relationship between the predictive variables, population and precipitation, is indicated by a correlation coefficient of 0.419, less than 0.7. Table 13 shows the values of tolerance and the Variance Inflexion factor in our model. The value of tolerance for both population and precipitation is 0.824, less than 1, while both population and precipitation have a VIF of 1.213, very much less than the critical value 10.

Table 13. Predictive variables Tolerance and VIF Table

	Tolerance	VIF
Population	0.824	1.213
Precipitation	0.824	1.213

Thus, both of these statistical analyses demonstrate that there is no multicollinearity.

4.6.1. Cereals Multiple Linear Regression Analysis

Table 14 summarizes all the statistical characteristics of the three cereals. Both population and precipitation have a positive correlation with all the three types of cereal (greater than 0 .3).

Population is positively highly correlated with sorghum (0.938), maize (0.895), and rice (0,851). It means that population accounted for about 88% of the variability of sorghum, 80% of the variability of maize and 72% of the variability of rice. Although positive, the correlation of precipitation with cereals is moderate, sorghum (0.528), maize (0.496), and rice (0.537). Precipitation explained the variability of sorghum at about 28%, the one of maize at about 24%, and account for 28% of the variability of rice.

The two predictive variables are both positively correlated with the cereals but population accounted for more than precipitation in their variability. The Normal Probability Plots do not present points with major deviations from the lines of normality, and those in the scatterplots have a rectangular distribution.

The R Square shows that the two predictive variables, population and precipitation, explained the production of sorghum at about 90.2%, maize at 81.8%, and rice paddy at 76.3%. Only 9.8% of sorghum, 18.2% of maize, and 23.7% are explained by other factors. Sig in Anova gives us 0.000 (< 0.5) as the value for all the three dependent variables. So, there is a statistical significance for this model; it accurately predicts the outcome. The standardized coefficients let us know that population contributed respectively at about 87, 83, and 76% to the production of sorghum, maize, and rice paddy. Precipitation's contribution was about 16, 15, and 22%, respectively.

As we see, the population with Coefficient Sig 0.000 for all the cereals has made a unique and statistically significant contribution to the prediction of sorghum, maize, and rice. Likewise, precipitation having a Sig value 0.016 with sorghum, 0.103 with maize and 0.036 with rice has made a statistically unique contribution to the prediction.

Table 14. Cereals' Statistical Characteristics

Predictive Variables	Hypotheses	Dependent Variables			Conclusion
		Sorghum	Maize	Rice paddy	
	R Square	0.902	0.818	0.763	Major Explanation
	Normality	No Major Deviation	No Major Deviation	No Major Deviation	Normal Distribution
	Anova	0.000	0.000	0.000	Accurate Prediction
Population	Correlation	0.938	0.895	0.851	Positive Significant
	r^2 (%)	88	80	72	
	Standardized Coef	0.87	0.833	0.759	Stronger Effect
	Coefficient Sig	0.000	0.000	0.000	Statistically Sig. Contrib
Precipitation	Correlation	0.528	0.496	0.537	Positive Moderate
	r^2 (%)	28	24	28	
	Standardized Coef	0.164	0.147	0.219	Lower Effect
	Coefficient Sig	0.016	0.103	0.036	Statistically Sig. Contrib

Population accounted for 88% of the variability of sorghum, 80% of the variability of maize and 72% of the variability of rice. Precipitation explained the variability of sorghum at about 28%, the one of maize at about 24%, and account for 28% of the variability of rice.

4.6.2. Commercial and Industrial Crops Multiple Linear Regression Analysis

Based on the information in table 15 summarizing all the statistical information on commercial and industrial crops, population is positively and very lowly correlated with cotton (0.001), highly correlated with sugar cane (0.914), and negatively (although moderately) correlated with tobacco (-0.516). So, the contribution of the population in the variability of cotton was insignificant. On the contrary, it contributed at about 83% to the variability of sugar cane and 26% to the variability of tobacco.

The correlation of precipitation with cotton is low (0.226), moderate with sugar cane (0.398), and very low with tobacco (0.074). Thus, precipitation accounted for about 5% of

the variability of cotton, 16% of the variability of sugar cane, and 0.5% of the variability of tobacco.

The points in the Normal Probability Plot do not have a major deviation from the line of normality and those in the scatterplot show a rectangular distribution. R Square shows us how much of the variance of cotton, sugar cane, and tobacco is explained by the variability of population and precipitation.

The predictive variables, population and precipitation, explained the production of cotton lint at about 62%, sugar cane at 83.5%, and tobacco at 37%. Therefore other factors explained cotton lint at 38%, sugar cane at 16.5%, and tobacco at about 63%. Significant values in Anova are 0.398 for cotton, 0.000 for sugar cane, and 0.001 for tobacco. We notice that all those values are less than the critical value (0.5).

The standardized coefficients let us know that population counted for 11.3% in the variability of cotton lint, 90.6% in the variability of sugar cane, and 66.4% in the variability of tobacco. Meanwhile, precipitation contributed at 27, 1.8, and 35% to the variability of cotton lint, sugar cane, and tobacco respectively.

The coefficients sig table below gives us the significant value between our predictive and dependent variables. Population with Sig 0.572, greater than 0.5, did not make a significant unique contribution to the prediction of cotton lint. In contrary, its contribution is significant and unique to the prediction of sugar cane and tobacco for it has sig 0.000 for those two dependent variables. Precipitation, having Sig value 0.178 for cotton lint and 0.0038 for tobacco, both of them less than 0.5, made a statistically unique contribution to the prediction of those two crops. In opposition, with Sig value 0.830, precipitation did not make a statistically unique contribution to the prediction of sugar cane.

Table 15. Commercial and Industrial Crops' Statistical Characteristics

Predictive Variables	Hypotheses	Dependent Variables			Conclusion
		Cotton Lint	Sugar Cane	Tobacco	
	R Square	0.62	0.835	0.369	Maj. & Mod.Explanation
	Normality	No Major Deviation	No Major Deviation	No Major Deviation	Normal Distribution
	Anova	0.398	0.000	0.001	Accurate Prediction
Population	Correlation	0.001	0.914	-0.516	Pos., Neg., Insig, Mod. & Sig
	r2 (%)	0.0001	83.53	26.62	
	Standardized Coef	-0.113	0.906	-0.664	Insig. Mod. & Strong Effect
	Coefficient Sig	0.572	0.000	0.000	Statistically Sig. Insig. Contrib.
Precipitation	Correlation	0.226	0.398	0.074	Positive Moderate & Low
	r2 (%)	5	16	0.5	
	Standardized Coef	0.273	0.018	0.353	Low to Mod. Effect
	Coefficient Sig	0.178	0.83	0.038	Statistically Sig.& Insig. Contrib

4.6.3. Livestock Multiple Linear Regression Analysis

Population is positively moderate to highly correlated with all the livestock dependent variables as shown in table 16. It contributed 50 % in the variability of sheep, more than 95% in the variability of goats, and more than 93% in the variability of cattle.

The correlation of precipitation with livestock, although positive, is moderate. Precipitation explained the variability of sheep at about 18%, the one of goats at about 25%, and accounted for more than 16% of the variability of cattle. The dots in the Normal Probability Plot reasonably line close to the line of best fit and those in the scatterplot show a rectangular distribution.

The R Square informs us how much of the variance of sheep, goats, and cattle is explained by the variability of population and precipitation.

Population and precipitation explained the production of sheep at 72.6%, goat at 98%, and cattle at 96.7%. Therefore, other factors explained the variability of sheep at 27.4%, and the ones of goats and cattle at only 2% and 3.3%, respectively.

Significant values in Anova are 0.000 for all the dependent variables (sheep, goat, and cattle). We notice that all those values are less than the critical value (0.5). Consequently, we say that the model accurately predicts the variability of livestock; there is a statistical significance for this model.

The standardized coefficients let us know that population counted for 64.5.3% in the variability of sheep, 92.9% in the variability of goats, and 96.7.4% in the variability of cattle. Precipitation had contributed at 15.8, 11.2, and 1.4% to the variability of sheep, goats, and cattle, respectively.

Thus, population made a strong contribution in explaining the production of goats and cattle; its contribution is moderate in explaining sheep variability. Precipitation, on the other hand, had an insignificant contribution in explaining cattle variability; it had, however, lowly contributed to the sheep and goats' variability.

The standard coefficients Sig give us the significant values for our predictive and dependent variables. Population, with Sig 0.000, less than 0.5, made a statistically significant unique contribution to the prediction for all the livestock types. On the contrary, precipitation made a statistically significant and unique contribution to the prediction sheep and goat with Sig 0.270 and 0.010, respectively. However, with Sig 0.989 (greater than 0.5), precipitation had not made a statistically unique contribution to the prediction of cattle.

Table 16. Livestock's Statistical Characteristics

Predictive Variables	Hypotheses	Dependent Variables			Conclusion
		Sheep	Goat	Cattle	
	R Square	0.726	0.98	0.967	Major Explanation
	Normality	No Major Deviation	No Major Deviation	No Major Deviation	Normal Distribution
	Anova	0.000	0.000	0.000	Accurate Prediction
Population	Correlation	0.711	0.975	0.967	Positive Mod. & Significant
	r2 (%)	50	95	93	
	Standardized Coef	0.645	0.929	0.967	Mod. & Strong Effect
	Coefficient Sig	0.000	0.000	0.000	Statistically Sig. Contrib.
Precipitation	Correlation	0.429	0.501	0.406	Positive Moderate
	r2 (%)	18	25	16	
	Standardized Coef	0.158	0.112	0.014	Low Effect
	Coefficient Sig	0.27	0.01	0.989	Statistically Sig.& Insig. Contrib

CHAPTER 5

DISCUSSION

5.1 Atmospheric Parameters

The study on global rainfall showed that the driest years are in the 1980s; the wettest years are in the late 1990s and 2000s. The precipitation trend increased from 1980 (28.5 mm) to 2012 (33.5 mm). The precipitation annual cycle shows that the area of study received its maximum precipitation from April to October. This study confirmed some previous studies including the study by the UNEP (2012) which indicated that annual to decadal variations in rainfall over the Sahel are large, with a quasi-80 – year cycle of wetter and drier periods; the 1950s and early 1960s was a wet period, followed by a decline in rainfall that reached its peak in the early 1970s and 1980s. Since the droughts incidents, rainfall has been increasing. Jury (2012) also confirmed the return to wet conditions over Africa.

The current study showed through the stations data that rainfall distribution in Chad followed the West Africa precipitation pattern, presenting a gradient from the south to the north. The rainy season starts in May/June and ends in September/October with maximum rainfall occurring during June to September. The finding from the station data is close to and confirms the conclusions of Funk et al. (2012) which stated that Chad receives rainfall totals of more than 500 mm between June and September.

It is also found, through the krigging interpolation, that precipitation followed a gradient south-north and did not follow the line of normal distribution. It was positively skewed and approximately symmetric with a west – east direction. The highest precipitation occurred between 8˚N and 9˚N, and the lowest from 13˚N to 14.5 ˚N.

Precipitation is highly and positively correlated with all the cloud fractions. The correlation is higher with daytime and nightime cloud fraction but the amount of nightime cloud fraction was greater than the others. As would be expected, cloud amounts in wetter years were greater than those in dryer years.

Specific humidity and precipitation had almost the same pattern. The specific humidity at 850 hPa or Q850 (ITCZ) was higher in wetter year than in dryer ones. Also, the specific humidity at 500 hPa or Q500 (AEJ) was greater for all the wetter months compared to the dryer months. According to UNEP (2012), the annual cycle of relative humidity closely follows the rainfall cycle, ranging from about 30% in the peak dry season to 80% during the summer monsoon. This study also confirms the statement made by Nicholson (2009): "In the context of the role of moisture, it is interesting to note that the vapor content can higher in wet years than in dryer years, even those contrasting in the intensity of the rainbelt."

It is theoretically expected that the low level southerwerly flow should be higher during the wetter years to bring moisture from the Atlantic Ocean to the continent, but this study shows that wind speeds at 850 hPa were lower in wetter years than in dryer years. While this was surprising result, it is supported by the suggestion of Nicholson (2009) that much of the moisture in the monsoon layer is recycled water deriving from local evaporation over the continent, rather than transported from the Atlantic Ocean. Consequently, the precipitation regime over West Africa is controlled by atmospheric dynamics rather than low-level moisture.

It is also observed in this study that the specific humidity was higher in wetter years than in dryer years despite the fact that the wind speeds presented an inverse situation (wind speeds were lower in wetter years than in dryer years). This situation confirms once again the

conclusion made by Nicholson (2009) stating that much of the moisture in the monsoon layer is recycled water deriving from local evaporation over the continent, rather than transport from Atlantic.

Aerosols serve as cloud condensation nuclei (CCN) and so have considerable effect on cloud properties and the initiation of precipitation. As a result of their radiative and CCN activities, large amount of aerosols have been reported to both decrease and increase rainfall. On the one side, natural tropical clouds with low CCN concentrations rain out rapidly to mature into long-lived clouds. On the other side, heavily polluted clouds evaporate much of their water before precipitation can occur (Rosenfeld et al., 2008). On the contrary, a significant relationship between AOD and cloud fractions was found by Yi, Yang, Bowman, & Xiaodon (2012) using MODIS operational and Deep Blue algorithm products to examine the relationship of AOD with cloud properties and precipitation in both the satellite data and a GCM simulation. Also, Grandey et al. (2012) found strong relationships between retrieved cloud fractions and AOD in Aqua-MODIS satellite data. They demonstrated that the negative cloud fraction – AOD relations in the tropic are primarily due to wet scavenging by convective precipitation; these results demonstrate the important contribution of wet scavenging to aerosol-cloud interactions.

This study used atmospheric observations data over the Sahel for a 12-year-period (from 2000 to 2012) and found that AOD had negative and insignificant relationship with cloud fractions. In addition, this study found that AOD and precipitation had a significant inverse relationship. This is consistent with the results of Hui, Cook, Ravi, Fuentes, & D'Odorico (2008) on dust-rainfall feedbacks in the West African Sahel, which found that there was a significant inverse relationship between rainfall amounts and aerosols. Yi et al. (2012)

showed that model simulation tends to produce stronger correlations between AOD and precipitation than the satellite observations. Their study also showed that precipitation reduction by AOD occur over the equatorial regions and over land and that precipitation increases when AOD increases in extra-tropical oceans. The smoke/soot aerosols from biomass burning is a possible reason for the stronger negative relationship between AOD and precipitation. Yi et al. (2012) also found that in the Sahara region, dust aerosols act to increase precipitation while in the Sahel, smoke/soot aerosols decrease precipitation. Aerosol distribution, in the focus area of the current study, is highly skewed with an almost southwest – northeast direction. The annual cycle shows that the highest amount of aerosol in March, which might be the result of bush fire practiced in some localities of that region by farmers in preparation for their farming activities during the following rainy season. The lowest AOD amount occurs in August when precipitation peaks. AOD in wetter years was higher than in dryer years from June to August but lower in September.

The study of ambient temperature in the area of study revealed an inverse relationship between precipitation and temperature. The years/months when temperatures were higher corresponded to the years/months of lower precipitation and vice versa. So, 2009, with higher temperatures was a relatively dry year, and 2012, with lower temperatures was a relatively wet year. August had the lowest temperatures and the highest precipitation in the annual cycle. Temperature data had an inverse gradient compared to precipitation. The highest temperatures occurred in the northern parts of the area of study while the lowest temperatures occurred in the south. Its distribution was negatively and moderately skewed with a west – east direction. The temperature is higher in dryer years compared to the wetter years. These results are consistent with those of UNEP (2012) that found in the Sahel an average annual

temperature (of where) about 27 to 30 ˚C varying from between roughly 25˚C in December to roughly 32˚C in April.

5.2. Land Parameters

Through the annual cycle, total evapotranspiration, soil moisture, and precipitation progressively increased in value from January, reached their peaks in August and then gradually decreased through December. All three variables are positively correlated.

Total Evapotranspiration followed the pattern of precipitation with which they are positively and considerably correlated. The higher the rainfall, the higher the evapotranspiration. Its distribution was approximately symmetric. Its amounts in both dryer and wetter years increase from June to September with its maximum in August. Wetter years had higher evapotranspiration except for June with a null value and September where dryer years had a greater amount.

Soil moisture also presented an approximately symmetric distribution with a south – north gradient following the precipitation gradient. Except for June, all the wetter months had higher soil moisture than the dryer ones. This finding is consistent with the result of Fahnbulleh, Lakhankar, and Seo (2009) who stated that during the rainy season, the tropical zones experience higher rainfall and soil moisture is at its peak. During the dry season, the soil moisture levels drastically decline below the average value. However, for some regions in Africa, this pattern is not consistent for the soil moisture of some areas such as Northern and Eastern Africa is below the expected value regardless of the time of year (season).

NDVI also followed the precipitation pattern. The NDVI is higher where precipitation is higher, and lower where precipitation is lower.

- The highest NDVI range, 0.7 - 0.8, mostly spread in the southeast and had its peak about 9.5 ^{0}N and 23 and 24˚E in 2002, then increased in width from 18 to 24˚E in 2012;
- The lowest NDVI range, 0.1 - 0.2, was from about 14 to 14.5˚N in 2002, then did not exist in 2012. This is an indication that the northern part of the Sahel was greener in 2012 than it was in 2002, suggesting an increase in biomass over that ten-year-period.

This conclusion is supported by UNEP (2012), where absolute vegetation growth was determined to have increased (green) in the Sahel since the droughts of 1980. However, that study (UNEP, 2012) also indicated that vegetation has not recovered to its full potential since the rainfall started to increase after the droughts of 1980s. It showed that the annual cycles of rainfall, temperature and evapotranspiration all follow the annual oscillation of the ITCZ as it moves between the northern and southern hemispheres. Rainfall over the Sahel is highest in the summer, as are temperature and evapotranspiration. The examination of NDVI values during dryer and wetter periods suggests that the NDVI in Chad is a function of precipitation. During the rainy season, the lower NDVI values were in June whereas the higher values were in September. The NDVI values are higher in the south in both wetter and dryer years. The findings in this study on soil moisture and the NDVI are consistent with the previous results reported by Musyimi (2011), which showed that, in the transition zone between the Sahara desert and the equatorial zone, the NDVI and soil moisture increase from the south to the north.

5.2.1. Land Use Land Cover Analysis and Trends

For this study, five LULC classes were defined using Landsat satellite data for 1986, 2003, and 2013. These classes include water bodies, wetland, bare soils, forest-savanna-steppe, and grassland-farmland.

The findings from the LULC analysis revealed that there is a considerable decrease in forest cover from 1986 (23.06%) to present (7.39%). This might be due to the human pressure from farming activities and fuel wood demand, as farmland and grassland have increased since 1986 (0.38 to 32.15%). Wetland decreased from 1986 (14.12%) to 2003 (0.875%), then increased from 2003 to 2013 (2.78%). The increase of grassland and wetland might be explained by the increase of rainfall in these later years. Bare soils increased from 1986 (62.25%) to 2003 (77.84%), probably due to the decrease of wetland and forest-savanna-steppe, then decreased from 2003 to 2013 (48.3%), probably due to the increase of wetland and grassland-farmland linked to the increase of precipitation. Water bodies increased from 0.2 % (1986) to 0.62% (2003), then decreased to 0.49 (2013).

The rate of change analysis shows the following situations for the five classes:

- Forest cover is decreasing almost at the same rate from 1986 (-3.81%) to present; even though that decrease has dropped off since 2003 (-3%)
- Bare soils increased from 1986 to 2003 (1.5%) then decreased in 2013 (-3.18). Wetland decreased from 1986 to 2003 then had a relative recovery in the 2010s.
- Water bodies and grassland-farmland increased since 1986 but the rate slows down around 2010s.

We can conclude that there are two driving forces: human activities and precipitation causing forest-savanna-steppe, grassland, wetland and bare soils changes.

The continuous dimunition of forest cover might be due to persistent pressures exercised by increasing population and livestock in the area.

5.3. Socio-economic Data

Population, agricultural area, agricultural, commercial, and industrial, and livestock productions data were retrieved from the FAO Statistics web portal for the 31 year-period from 1980 to 2011. Their analyses provides the following information:

Population and Agricultural Land Trends: This information shows that population of Chad increased from 4,554,000 million in 1980 to 11,525,000 million in 2011. During this period, agricultural land also increased from 48,150,000 to 49,932,000 hectares. The Pearson correlation between population and agricultural land is positive and moderate (0.412). This suggests that increasing population is one of the major derivers of the expansion in agricultural land area in Chad over the last three decades.

Agricultural Production: Rice paddy, sorghum, and maize production are the three cereals whose trends were analyzed in this study. The production pattern of the cereals follows the precipitation pattern. Almost all lower quantities of the three cereals correspond to lower values of precipitation and almost all their higher quantities correspond to higher values of precipitation (figure 47). According to Funk et al. (2012), human and animal pressures on a degraded ecosystem, combined with limited agricultural development, have led to low levels of national food production.

Commercial and Industrial Production: Cotton, sugar cane, and tobacco are some of the main commercial and industrial crops in Chad. All of the commercial and industrial crops followed the precipitation, except sugar cane. Their higher production years correspond

almost identically to the years of higher precipitation (figure 48). The case of sugar cane might be explained by the fact that it is mainly an irrigated crop.

Livestock: Cattle, sheep, and goats are also very important sources of protein in Chad. This study revealed that, in contrast to the crops, livestock is less sensible to the inter-annual and intra-annual rainfall variations. Except for the severe drought of the 1980s, the livestock trend shows an almost exponential growth despite the fluctuations in rainfall. However, the recovery was very slow after the 1980s drought (figure 49).

5.4. Multiple Linear Regression Analysis

The multiple linear regression (MLR) was used to model the relationship between the socio-economic data considered in this study. Population and precipitation were considered as predictive or independent variables. The data such as cereals, commercial and industrial crops, and livestock were considered as dependent variables or outcome. The purpose is to figure out which of the independent variables (population and precipitation) contributed the most in the variability of the dependent variables (cereals, commercial and industrial crops, and livestock).

The relationship between the predictive variables, population and precipitation, is indicated by a correlation coefficient of 0.419. The value of tolerance for both population and precipitation is 0.824 (less than 1) while both population and precipitation have a variance inflexion factor (VIF) of 1.213 (much less than 10). Thus, both of these statistical analyses demonstrate that there is no multicollinearity; consequently, the model can accurately predict the outcome and provide accurate contribution of individual predictor.

5.4.1. Cereals Multiple Linear Regression Analysis

Population and precipitation are both positively correlated with the cereals but population accounted for more in their variabilities. The distribution of cereals is normal.

R Square shows that the two predictive variables, population and precipitation, explained the production of sorghum at about 90.2%, maize at 81.8%, and rice paddies at 76.3%. Sig in Anova shows that there is a statistical significance for this model; it accurately predicts the outcome. The standardized coefficients show that population made the strongest contribution in explaining the production of all the three cereals; the contribution of precipitation was much less.

In conclusion, the two predictive variables accounted for a unique and statistically significant contribution to the prediction of sorghum, maize, and rice. The fact that population accounted more than precipitation in the variability of cereals might be due to two reasons:

- The growing population with high density is expanding the agricultural land and practicing farming activities even in dry and cold seasons, the case of a *Sorghum durra* or *Sorghum caudatum* called “Berebere” in Chad, that is grown from October to December/January
- Increase in irrigated agriculture that is taking place with rice as the main crop but also maize in the river plains.

5.4.2. Commercial and Industrial Crops Multiple Linear Regression Analysis

Ultimately, population accounted more than precipitation in the variability of sugar cane and tobacco. But precipitation contributed more than population in the variability of cotton. The lower contribution of precipitation to the variability of sugar cane might be explained by

the fact that sugar cane is mainly irrigated. The distribution of commercial and industrial samples is normal. Through R Square, population and precipitation explained the production of cotton lint at about 62%, sugar cane at 83.5%, and tobacco at 37%. Significant values in Anova shows that the model accurately predicts the variability of our commercial and industrial crops; there is a statistical significance for this model.

Population made the strongest and moderate contribution in explaining the production of sugar cane and tobacco, respectively; its contribution is low in explaining cotton lint variability. Precipitation had an insignificant contribution in explaining sugar cane variability; however, moderately contributed to the cotton lint and tobacco variability.

5.4.3. Livestock Multiple Linear Regression Analysis

Both of our predictive variables are positively correlated with the livestock types, but the correlation is higher with population than with precipitation, and consequently, population contributed more than precipitation in the variability of livestock. Livestock samples are normally distributed. Population and precipitation explained the production of sheep at 72.6%, goat at 98%, and cattle at 96.7%. Significant values in Anova shows that the model accurately predicts the variability of livestock; there is a statistical significance for this model. Population was more of a factor in explaining the production of livestock than precipitation.

These findings are similar to those of Bourn and Wint (1994) whose multiple regression analyses confirmed the close association between livestock biomass and the presence of people. They found that cultivation and rural habitation were the primary predictors of livestock distribution. Rainfall was of secondary importance. They also indicated that similar trends were evident for disaggregated cattle and population of small ruminants. Their

regression analysis revealed that habitation accounted for 60% of the variance in seasonal mean livestock biomass, with rainfall accounting for 7%. The present study found that population accounted for at least 50 % in the variability of sheep, more than 95% in the variability of goats, and more than 93% in the variability of cattle. Precipitation accounted for 18% of variability of sheep, 25% of the one of goats, and 16% of the variability of cattle.

CHAPTER 6

CONCLUSION

This study used an integrated approach to investigate drivers and impacts of environmental change from the 1980s to 2012 using geospatial and statistical analyses of atmospheric, climate, land use land cover, and socio-economic data. The atmospheric and climate data were obtained from the NASA Giovanni web-portal for an area covering all of Southern Chad and extending to the neighboring countries of Cameroon, Central African Republic, Niger, Nigeria, and Sudan.

Agricultural productivity country summary data for Chad was obtained from the Food and Agriculture Organization (FAO) of the United Nations. Landsat imagery was used for deriving land use and land cover information focusing on the transition areas, ecologically sensitive and especially vulnerable to changes in climate variables, between the desert in the Northern Chad and the Sahel/Savanna areas to the South. Other data sets were also obtained.

The study on rainfall showed that precipitation presented a gradient south-north and did not follow a line of normal distribution. The driest years were in the 1980s; the wettest years were in the late 1990s and 2000s. The rainy season started in April/May and ended in September/October with maximum rainfall occurring from June to September. The stations data analysis indicate that rainfall distribution in Chad followed the precipitation pattern. This confirms previous studies done by some authors that also showed evidence for a return to wet conditions over the Sahelian Africa during recent years (Jury, 2012).

The geostatistical analysis demonstrated that there are south – north gradients of atmospheric and land parameters. Precipitation and temperature are the two factors that guide the distribution of other parameters.

The composite analysis revealed specific forces contributing to the years of higher and lower precipitation. Cloud amount, specific humidity, and aerosol optical depth are higher during wetter years than during dryer years. Wind speed and surface air temperature, on the contrary, are lower during wetter years than during dryer years. NDVI and soil moisture values are greater in wetter than in dryer years. The correlation study showed that precipitation, soil, NDVI, and evapotranspiration are highly positively correlated. They are, on the other hand negatively moderate to highly correlated with surface air temperature.

The findings about wind speeds and humidity confirm the suggestion previously done by Nicholson (2009) that the precipitation patterns over West Africa are controlled by atmospheric dynamics rather than low-level moisture; much of the moisture in the monsoon layer is recycled water deriving from local evaporation over the continent, rather than transport from Atlantic.

This study demonstrated that Aerosol Optical Depth has an apparent west – east distribution and had a negative and insignificant relationship with cloud fractions. This contradicts Grandey et al. (2012) who showed a strong relationships between retrieved cloud fractions and AOD. It was also shown in this study that the AOD and precipitation presented significant inverse relationship. This conforms to a previous finding of a significant inverse relationship between rainfall amounts and aerosols (Hui et al., 2008). In addition, it supports the view that in the Sahara region, dust aerosols act to increase precipitation while in the Sahel, smoke/soot aerosols decrease precipitation (Yi et al., 2012).

The analysis of temperature revealed an inverse relationship as well an inverse gradient between temperature and precipitation. The highest temperatures were found in the north and during the dryer years, with the lowest in the south and during the wetter years. August had

the lowest temperatures and the highest precipitation in the annual cycle. This finding is consistent with those of UNEP (2012) that found an average annual temperature about 27 to 30 ˚C varying from between roughly 25˚C in December to roughly 32˚C in April.

Evapotranspiration, soil moisture, and NDVI had positive and significant correlation and also with precipitation. All of them had higher values in the south and lower values in the north, indicating that they follow the pattern of precipitation. The higher the rainfall, the higher the evapotranspiration, the soil moisture and the NDVI. This finding is consistent with that of Fahnbulleh, Lakhankar, and Seo (2009) who stated that during the rainy season, the tropical zones experience higher rainfall and that soil moisture is at its peak. Futhermore, Musyimi (2011) found that, in the transition zone between the Sahara desert and the equatorial zone, the NDVI and soil moisture increase from the south to the north.

The land use land cover analysis tells us that the forest-savanna-steppe areas are under continuous pressure; they have been decreasing since 1986. Farmlands and grasslands are increasing; while bodies of water first decreased then increased meagerly. The continuous dimunition of forest cover might be due to persistent pressures for development exercised by increasing numbers of population and livestock in the area.

This study also investigated the relationship between agricultural productivity and changing patterns of population and rainfall. Population of Chad has been an exponential increase from 1980 to 2012 while precipitation has been recovering following periods of droughts in the 1970s and 1980s. All the crops' (cereals, commercial, and industrial) production follow the rainfall except for sugar cane. The livestock trend shows an almost exponential growth despite the rainfall variability meaning it is less sensitive to the inter-annual variability of rainfall.

The multiple linear regression analysis has shown a positive correlation between precipitation and crops such as sorghum, maize, and rice and livestock such as sheep, goat, and cattle, but most of those dependent variables such as cereals and livestock are more correlated with population than with precipitation. This is consistent with the finding of Bourn and Wint (1994) who confirmed the close association between livestock biomass and the presence of people. They concluded that cultivation and rural habitation were the primary predictors of livestock distribution and that rainfall was of secondary importance.

Annexes: Accuracy Assessment Tables

Accuracy Report 1986

Class name	Reference Totals	Classified Totals	Number Correct	Producer's Accuracy (%)	User's Accuracy (%)	Kappa
Water bodies	30	28	22	73.33	78.57	1
Forest/Sav/Steppe	50	48	45	90.00	93.75	1
Grassland/Farmland	24	22	20	83.33	90.91	1
Wetland	31	40	28	90.32	70.00	1
Bare soils	121	118	115	95.04	97.46	1
Totals	256	256	230	(Column)	(row)	

Overvall Classification Accuracy: 89.84%

A. Accuracy Assessment 1986

Accuracy Report 2003

Class name	Reference Totals	Classified Totals	Number Correct	Producer's Accuracy (%)	User's Accuracy (%)	Kappa
Water bodies	22	26	19	86.36	73.08	1
Forest/Sav/Steppe	33	42	31	93.94	73.81	1
Grassland/Farmland	28	29	25	89.29	86.21	1
Wetland	36	34	31	86.11	91.18	1
Bare soils	137	125	120	87.59	96.00	1
Totals	256	256	226	(column)	(row)	

Overvall Classification Accuracy: 88.28%

B. Accuracy Assessment 2003

Accuracy Report 2013

Class name	Reference Totals	Classified Totals	Number Correct	Producer's Accuracy (%)	User's Accuracy (%)	Kappa
Water bodies	24	21	21	87.50	100.00	1
Forest/Sav/Steppe	26	30	24	92.31	80.00	0.8286
Grassland/Farmland	93	92	80	86.02	86.96	0.9659
Wetland	26	26	26	100.00	100.00	1
Bare soils	87	87	85	97.70	97.70	0.9652
Totals	256	256	236	(column)	(row)	

Overvall Classification Accuracy: 92.18%

C. Accuracy Assessment 2013

REFERENCES

Awa, D. N., Ndjoya, A., Mopate Logtene, Y., Ndomadji, J. A., Onana, J., Osongwed-Awa, A., … Maho, A. (2002). Livestock production systems in the semi-arid savannah of the Central African sub-region. Actes du colloque, 27-31 mai 2002, Garoua, Cameroun Cirad, Montpellier, France. [Accessed on March 25th, 2014 at http://hal.archives-ouvertes.fr/docs/00/13/79/77/PDF/T306Awa2.pdf]

Barrios, S., Bertinelli, L., & Strobl, E. (2010). Trends in rainfall and economic growth in Africa: A neglected cause of the African growth tragedy. *The Review of Economics and Statistics*, 92(2): 350-366. [Accessed on July 15th, 2013 at http://www.mitpressjournals.org/doi/pdfplus/10.1162/rest.2010.11212]

Bourn, D. & Wint, W. (1994). Livestock, land use and agricultural intensification in sub-Saharan Africa. Pastoral Development Network. [Accessed on Mars 27th, 2014 at http://www.academia.edu/4996734/LIVESTOCK_LAND_USE_AND_AGRICULTURAL_INTENSIFICATION_IN_SUB-SAHARAN_AFRICA]

Bulmer, M. G., (1979). Principles of Statistics. New York, NY: Dover Publications. [Accessed on February 4th, 2014 http://bobweigel.net/csi763/images/Bulmer_Principles_of_Statistics_1979_all.pdf].

Coe, M. T. & Foley, A. (2001). Human and natural impacts of the water resources of the Lake Chad Basin. *Journal of Geophysical Research, 106*, No. D4, 3349-3356 [Accessed on May 23rd, 2014 at http://onlinelibrary.wiley.com/doi/10.1029/2000JD900587/pdf]

Conway, D. & Schipper E. L. F. (2011). Adaptation to climate change in Africa: Challenges and opportunities identified from Ethiopia. *Global Environmental*

Change, 21, 227-237. [Accessed on February 15th, 2013 at http://adaptationandwfgd.wikispaces.com/file/view/8.+Conway+%26+Schipper+2011+Adaptation+to+climate+change+in+Africa+-+challenges+%26+opportunities+in+Ethiopia.pdf]

Darden, R. L. (2011). Clean water act jurisdiction: What about isolated wetlands? Building Strong. [Accessed on August 21st, 2013 at https://www.dnr.sc.gov/marine/NERR/present/isolatedwetlands/USACOEIsolatedWetlandsJurisdiction.pdf]

Edet, A, Ukpong, A. J, & Ekwere, A. S. (2011). A statistical tool for predicting the impact of climate variability on groundwater resources in cross River State, Southeastern Nigeria. *Africa Geoscience Review, 18*, 109-119.

Fahnbulleh, G., Lakhankar, T., & Seo, D. (2009). Soil moisture and droughts in Africa. [Accessed on May 26th, 2014 at http://crest.ccny.cuny.edu/reu/mainframe/ckfinder/userfiles/files/Gilbert_Fahnbulleh_Paper_1.pdf]

Funk, C., Rowland, J., Adoum, A., Eilerts, G., & White, L. (2012). A climate trend analysis of Chad. U.S. Department of the Interior, U.S. Geological Survey, Fact Sheet 2012–3070, June 2012. [Accessed on February 6th, 2014 at http://pubs.usgs.gov/fs/2012/3070/FS2012-3070.pdf]

Gasse, F. (2006). Climate and hydrological changes in tropical Africa during the past million years. *C. R. Palevol 5* (2006) 35–43. [Accessed on February 16th, 2013 at http://www.sciencedirect.com/science/article/pii/S1631068305001107#]

Grandey, B. S, Stier P., & Wagner, T. M. (2012). Investigating relationships between aerosol optical depth and cloud fraction using satellite, aerosol reanalysis and general circulation model data. *Atmos. Chem. Phys. Discuss., 12*, 30805–30823. [Accessed on March 23rd, 2014 at http://www.readcube.com/articles/10.5194/acpd-12-30805-2012]

Griffith, J. A., Martinko, E. A., Whistler, J. L., & Price, K. P. (2002). Interrelationships among landscapes, NDVI, and stream water quality in the U.S. Central Plains. *Ecological Applications, 12(6),* 1702–1718. [Accessed on July 30th, 2013 at http://cpcb.ku.edu/media/uploads/work/griffith_ecological_applications.pdf]

Gruber, A. & Levizani, V. (2008). Assessment of global precipitation products. A project of the World Climate Research Programme. Energy and Water Cycle Experiment (GEWEX) Radiation Panel WCRP-128, WMO/TD-No. 1430 [Accessed on July 28th, 2013 at http://www.gewex.org/reports/2008AssessmentGlobalPrecipReport.pdf]

Haas, E. M., Bartholome, E., Lambin, E. F., & Vanacker, V. (2011). Remotely sensed surface water extent as an indicator of short-term changes in ecohydrological processes in sub-Saharan western Africa. *Remote Sensing of Environment,* 115, 3436-3445. [Accessed on February 15th, 2013 at http://www.sciencedirect.com/science/article/pii/S0034425711002896#]

Harrison, G. P., & Whittington, H. W. (2001). Impact of climate change on hydropower investment. Hydropower in the new millennium, 4th International Conference on Hydropower Development, Bergen Norway, June 2001, 257-261.

Hou, G., Zhang, H., & Wang, Y. (2011). Vegetation dynamics and its relationship with climatic factors in the Changbai Mountain Natural Reserve. *J. Mt. Sci., 8*, 865–875.

[Accessed on July 30th, 2013 at http://download.springer.com/static/pdf/5/art%253A10.1007%252Fs11629-011-2206-4.pdf?auth66=1404359370_f8dbf422aa3f23bece8b821150ed4880&ext=.pdf]

Hui, W. J., Cook, B. I., Ravi, S., Fuentes, J. D., & D'Odorico, P. (2008). Dust-rainfall feedbacks in the West African Sahel. *Water Resources Research, 44*, W05202. [Accessed on May 1st, 2014 at http://people.virginia.edu/~pd6v/Publications_files/2008WRR-Hui-Dust-Rainfall1.pdf]

IPCC (Intergovernmental Panel on Climate Change) (2001). Impacts, Adaptation, and Vulnerability, Contribution of Working Group II to the Third Report of IPCC. Cambridge University Press, Cambridge, UK. [Accessed on February 15th, 2013 at https://ipcc.ch/ipccreports/tar/wg2/pdf/wg2TARfrontmatter.pdf]

Jury, M. (2013). A return to wet conditions over Africa: 1995–2010. *Theor Appl Climatol.*, 111, 471–481.

Kundzewicz, Z.W., Mata, L.J., Arnell, N.W., Doll, P., Kabat, P., Jimenez, B. …Shiklomanov I.A. (2007). Freshwater Resources and their Management. Climate Change 2007: Impacts, Adaptation and Vulnerability. Contribution of Working Group II to the Fourth Assessment Report of the Intergovernmental Panel on Climate Change, Parry, M.L., Canziani, O.F., Palutikof, J.P., van der Linden P.J. & Hanson, C.E., Eds., Cambridge University Press, Cambridge, UK, 173-210. [Accessed on February 17th, 2013 at https://www.ipcc.ch/pdf/assessment-report/ar4/wg2/ar4-wg2-chapter3.pdf]

Lambin, E. F, Geist, H. J., & Lepers, E. (2003). Dynamics of land-use and land-cover change in tropical regions. *Annual Review of Environment and Resources,* 28, 205-241. [Accessed on May 27th, 2013 at http://www.globalrestorationnetwork.org/uploads/files/LiteratureAttachments/93_dynamics-of-land-use-and-land-cover-change-in-tropical-regions.pdf]

Laux, P., Kunstmann, H., & Bardossy, A. (2008). Predicting the regional onset of the rainy season in West Africa, *International Journal of Climatology*, 28(3), 329-342. [Accessed on July 16th, 2013 at http://onlinelibrary.wiley.com/doi/10.1002/joc.1542/pdf]

Lebel, T., Diedhiou, A., & Laurent, H. (2003). Seasonal cycle and inter-annual variability of the sahelian rainfall at hydrological scales. *Journal of Geophysical Research,* 108 No. D8, 8389. [Accessed on July 15th, 2013 at http://onlinelibrary.wiley.com/doi/10.1029/2001JD001580/pdf]

Lele, M.I. & Lamb, P.J. (2010). Variability of the Intertropical Front (ITF) and rainfall over the West African Sudan – Sahel Zone. *Journal of Climate*, 23, 3984-4004. [Accessed on July 15th, 2013 at http://journals.ametsoc.org/doi/pdf/10.1175/2010JCLI3277.1]

Lloyd, A. S. (2008). Using NASA's Giovanni Web Portal to access and Visualize satellite-based earth science data in the classroom. Teaching with the New Geoscience Tools: Visualizations, Models and Online Data. Amherst, MA, 10-12 February. [Accessed on September 13th, 2013 at http://irina.eas.gatech.edu/EAS6145_Spring2011/Giovanni-tutorial.pdf]

Magadza, C. (1996). Climate change: Some likely multiple impacts in southern Africa. *NATO ASI Series, 137,* 449-486. Climate change and world food security. Ed. By Downing T.E, Springer-Verlag Berlin Heidelberg 1996 [Accessed on May 27th, 2014 at http://link.springer.com/chapter/10.1007%2F978-3-642-61086-8_17#page-2]

Masters, W. A., & Wiebe, K. D. (2000). Climate and Agricultural Productivity. *Center for International Development phone*, *617*(496), 7100. [Accessed on May 6th, 2014 at http://scholar.google.com/scholar?cluster=5557861976270729116&hl=en&as_sdt=0,26&sciodt=0,26]

McSweeney, C., New, M., & Lizcano, G. (2010). The UNDP climate change country profiles. Chad: Reports. [Accessed on April 29th, 2014 at http://www.geog.ox.ac.uk/research/climate/projects/undp-cp/index.html?country=Chad&d1=Reports]

Mercier, F., Cazenave, A., & Maheu, C. (2002). Inter-annual lake level fluctuations (1993-1999) in Africa from Topex/Poseidon: Connections with ocean-atmosphere interactions over the Indian Ocean. *Global and Planetary Change*, 32, 141-163. [Accessed on February 15th, 2013 at http://www.sciencedirect.com/science/article/pii/S0921818101001394#]

Molders, N. (2012). Land-use land-cover changes. Impact on climate and air quality. Atmospheric and Oceanographic Sciences Library, 44, 1-10. [Accessed on July 15th, 2013 http://www.springer.com/earth+sciences+and+geography/atmospheric+sciences/book/978-94-007-1526-4]

Musyini, Z. (2011). Temporal relationship between remotely sensed soil moisture and the NDVI over Africa: Potential for Drought Early Warning. Enschede, The Netherlands, March, 2011. [Accessed on May 6th, 2014 at http://www.itc.nl/library/papers_2011/msc/nrm/musyimi.pdf]

Nicholson, S.E. (2013). The West African Sahel: A review of recent studies on the rainfall regime and its inter-annual variability. *ISRN Meteorology*, 2013, ID 453521.

Nicholson, S.E. (2009). A revised picture of the structure of the "monsoon" and land ITCZ over West Africa," *Climate Dynamics*, 32, no. 7-8, 1155–1171. [Accessed on April 13th, 2014 at http://download.springer.com/static/pdf/597/art%253A10.1007%252Fs00382-008-0514-3.pdf?auth66=1404444048_3b44f79d8f41f03e80867acee1f63c23&ext=.pdf]

Ojo, O., Oni, F., & Ogunkunle, O. (2003). Implications of climatic variability and climate change on water resources availability and water resources management in West Africa. *IAHS-AISH Publication*, 280, 37-47.

Oki, T. & Kanae, S. (2006). Global hydrological cycles and world water resources. *Science, 313,* 1068. [Accessed on sept. 4th, 2013 at http://bprc.osu.edu/hydro/publications/OkiKanae_GlobalHydro_Science.pdf]

Okonkwo, C. & Demoz, B. (2014). Identifying anthropogenic 'hotspots' and management of water resources in Lake Chad Basin using GIS. *Journal of Natural Resources Policy Research*, DOI: 10.1080/19390459.2014.920581. [Accessed on May 23rd, 2014 at https://www.researchgate.net/publication/262560201_Identifying_anthropogenic_hotspots_and_management_of_water_resources_in_Lake_Chad_Basin_using_GIS]

Peyrille, P., Lafore, J.P., & Redelsperger, J.L. (2007). An idealized two-dimensional framework to study the West African Monsoon - Part I: Validation and key controlling factors. *Journal of the Atmospheric Sciences*, 64, No. 8, 2765–2782. [Accessed on July 15th, 2013 at http://journals.ametsoc.org/doi/full/10.1175/JAS3919.1]

Pielke, R.A., Avissar, R., Raupach, M., Dolman, A.J., Zeng, X., & Denning, A.S. (1998). Interactions between the atmosphere and terrestrial ecosystems: Influence on weather and climate. *Global Change Biology*, 4, 461-475. [Accessed on May 6th, 2014 at http://www.cnr.berkeley.edu/biometlab/espm298/Piekle%20et%20al%201998%20GCB.pdf]

Pyke, C.R. & Andelman, S.J. (2007). Land use and land cover tools for climate adaptation. *Climatic Change,* 80, 239-251. [Accessed on May 6th, 2014 at http://crest.ccny.cuny.edu/reu/mainframe/ckfinder/userfiles/files/Gilbert_Fahnbulleh_Paper_1.pdf]

Rosenfeld, D., Lohmann, U., Raga, G.B., O'Dowd, C.D., Kulmala, M., Fuzzi, S., … Andreae, M.O. (2008). Flood or drought: How do aerosols affect precipitation? *Science*, 321, 1309-1313. [Accessed on May 1st, 2014 at http://www.nuigalway.ie/ccaps/documents/05.09.08_flood_or_drought_science.pdf]

Sultan, B. & Janicot, S. (2003). The West African monsoon dynamics. Part II: The "Pre-Onset" and the "Onset" of the summer monsoon. *American Meteorological Society*, 16, 3407-3427. [Accessed on May 26th, 2014 at http://www.lodyc.jussieu.fr/~bslod/JCLI2.pdf]

Sultan, B. & Janicot, S. (2000). Abrupt shift of the ITCZ over West Africa and intra-seasonal variability. *Geophysical Research Letters*, 27, No.20, 3353-3356. [Accessed on May 26th, 2014 at http://onlinelibrary.wiley.com/doi/10.1029/1999GL011285/pdf]

Taylor, C.M., Lambin, E.F., Stephenne, N, Harding, R.J., & Essery, R.L.H. (2002). The influence of land use change on climate in the Sahel. *Journal of Climate*, 15, 3615-3629. [Accessed on May 2nd, 2014 at http://iri.columbia.edu/~alesall/ouagaCILSS/articles/taylor_jcli2002.pdf]

Thorncroft, C. & Hodges, K. (2001). African easterly wave variability and its relationship to Atlantic tropical cyclone activity. *Journal of Climate Volume*, 14, No. 6, 1166–1179. [Accessed on May 26th, 2014 at http://citeseerx.ist.psu.edu/viewdoc/download;jsessionid=08A43F9B2AA23459F5F3795D5F5EFAF2?doi=10.1.1.207.9644&rep=rep1&type=pdf]

Thorncroft, C.D, Nguyen, H., Zhang, C., & Peyrille, P. (2011). Annual cycle of the West African monsoon: Regional circulations and associated water vapor transport. *Quarterly Journal of the Royal Meteorological Society*, 137, no. 654, 129–147. [Accessed on February 17th, 2013 at http://onlinelibrary.wiley.com/doi/10.1002/qj.728/pdf]

UNEP (2012). Sahel atlas of changing landscape: Tracing trends and variations in vegetation cover and soil condition. United Nations Environment Programme, Nairobi. [Accessed on February 4th, 2014 at http://www.unep.org/dewa/Portals/67/pdf/Sahel_Atlas_lowres.pdf]

UNFCCC (2006). United Nations Framework Convention on Climate Change: Impacts, vulnerabilities and adaptation in developing countries. [Accessed on March 10th, 2013 at http://unfccc.int/resource/docs/publications/impacts.pdf]

USGS (2005). Global Visualization (GloVis) Viewer. Fact sheet 2005-3118. [Accessed on Sept. 4th, 2013 at http://pubs.er.usgs.gov/djvu/FS/2005_3118.pdf]

Ventrice, M.J., Thorncroft, C.D., & Roundy, P.E. (2011). The madden-julian oscillation's influence on african easterly waves and downstream tropical cyclo-genesis. *Monthly Weather Review*, 139, 2704–2722. [Accessed on July 15th, 2013 at http://www.atmos.albany.edu/daes/atmclasses/atm305/Ventrice-et-al-2011.pdf]

Vereecken, H., Huisman, J.A., Bogena, H., Vanderborght, J., Vrugt, J.A, & Hopmans, J.W. (2008). On the Value of Soil Moisture Measurements in Vadose Zone Hydrology: A review. *Water Resources Research*, 44. [Accessed on July 16th, 2013 at http://onlinelibrary.wiley.com/doi/10.1029/2008WR006829/pdf]

Washington, R., Bouet, C., Cautenet, G, Mackenzie, E., Ashpole I., Engelstaedter, S., Lizcano, G., Henderson, G.M., Schepanski, K., & Tegen I. (2009). Dust as a tipping element: The Bodele Depression, Chad. Potsdam Institute for Climate Impact Research, Germany. *PNAS*, 106, No. 49, 20465-20571. [Accessed on April 29th, 2014 at http://www.pnas.org/content/early/2009/07/17/0711850106.full.pdf+html]

William, C.J.R. & Kniveton, D. R. (2011). African climate and climate change. Physical social, and political perspectives. *Advances in Global Change Research*, 43. [Accessed on May 27th, 2013 at http://download.springer.com/static/pdf/668/bfm%253A978-90-481-3842-5%252F1.pdf?auth66=1404495657_f2686f174cdb87becaa217e07c9883ff&ext=.pdf]

Wu, R., Chen, J., & Wen Z. (2013). Precipitation - surface temperature relationship in the IPCC CMIP5 Models. *Advances in Atmospheric Sciences*, 30, No. 3, 766–778. [Accessed on July 15th, 2013 at http://download.springer.com/static/pdf/293/art%253A10.1007%252Fs00376-012-2130-8.pdf?auth66=1404496054_f9c0571e10d7e0faef595882b1bbc153&ext=.pdf]

Yang Z., Wang J., Ichoku C., Hyer E., & Zeng J. (2013). Mesoscale Modeling and satellite observation of transport and mixing of smoke and dust particles over northern sub-Saharan African region, J. Geophys. Res. Atmos., 118, 12,139–12,157, doi:10.1002/2013JD020644. [Accessed on May 26th, 2014 at http://www.geosciences.unl.edu/~jwang/docs/publication/paper_pdf/2013/Yang_final_print_smallsize.pdf]

Yi, B., Yang, P., Bowman, K.P., & Xiaodon, L. (2012). Aerosol-Cloud-Precipitation Relationships from Satellite Observations and Global Climate Model Simulations. *Journal of Applied Remote Sensing*, 6. [Accessed on March 21st, 2014 at http://geotest.tamu.edu/userfiles/229/Yi_et_al_2012.pdf]

Zhang, C., Woodworth, P., & Gu, G. (2006). The seasonal cycle in the lower troposphere over West Africa from sounding observations. *Quarterly Journal of the Royal Meteorological Society*, 132, no. 621, 2559–2582. [Accessed on July 16th, 2013 at http://onlinelibrary.wiley.com/doi/10.1256/qj.06.23/pdf]

Website sources

ERDAS IMAGINE 2013 What's New? Intergraph. [Accessed on August 30th, 2013 at http://geospatial.intergraph.com/Libraries/Tech_Docs/ERDAS_IMAGINE_2013_What_s_New.sflb.ashx]

ESRI Introduction to ArcGIS 10.1. ArcNews Spring 2012 [Accessed on August 30th, 2013 at http://www.esri.com/news/arcnews/spring12articles/introducing-arcgis-101.html]

ESRI ArcGIS 9 Using ArcGIS Geostatistical Analyst. Copyright 2001, 2003. [Accessed on August 30th, 2013 at http://webhelp.esri.com/arcgisdesktop/9.3/pdf/Geostatistical_Analyst_Tutorial.pdf]

F.A.O (1998) Crop Evapotranspiration – Guide for Computing Crop Water Requirements. FAO Corporation Repository. [Accessed on March 15th, 2014 at http://www.fao.org/docrep/x0490e/x0490e04.htm#weather parameters].

FAO (1990). Forest Resources Assessment 1990. Survey of tropical Forest Cover and Study of Change Processes. FAO Forestry Paper 130. [Accessed on March 22nd, 2014 at http://www.fao.org/docrep/007/w0015e/W0015E03.htm]

FAOSTAT. [Accessed on May 2nd, 2013 at http://faostat3.fao.org/faostat-gateway/go/to/download/O/*/E]

Global Visualization (GloVis) Viewer. [Accessed on January 13th, 2014 at from http://glovis.usgs.gov/]

IBM 2012 IBM SPSS Statistics 21 Core System User's Guide. [Accessed on August 30th, 2013 at https://www.google.com/#q=IBM+2012+IBM+SPSS+Statistics+21+Core+System+User%E2%80%99s+Guide]

IBM 2012 Software Business Analytics IBM SPSS Statistics [[Accessed on August 30th, 2013 at www-01.ibm.com/software/analytics/spss/products/statistics]

PRD, (2013) World Population Data Sheet. Population Reference Bureau. [Accessed on March 10th, 2014 at www.prb.org]

GES DISC 2013-2014. Goddard Earth Sciences Data and Information Services Center "The data used in this effort were acquired as part of the activities of NASA's Science Mission Directorate, and are archived and distributed by the Goddard Earth Sciences (GES) Data and Information Services Center (DISC)". http://disc.sci.gsfc.nasa.gov/giovanni

Video sources

TheRMUoHP Biostatistics Resource Channel May 2nd, 2013. How to Use SPSS: Standard Multiple Regression. [Accessed on March 20th, 2014 at http://www.youtube.com/watch?v=f8n3Kt9cvSI]